DOT/FAA/TC-26/16

Federal Aviation Administration
William J. Hughes Technical Center
for Advanced Aerospace
Aviation Research Division
Atlantic City International Airport
New Jersey 08405

National Airport Pavement Test Facility Construction Cycle 9

Volume 4—Cement-Treated Permeable Base Test

April 2026

Final Report

U.S. Department of Transportation
Federal Aviation Administration

NOTICE

Technical Report Documentation Page

1. Report No.	2. Government Accession No.	3. Recipient's Catalog No.
DOT/FAA/TC-26/16		

4. Title and Subtitle	5. Report Date
NATIONAL AIRPORT PAVEMENT TEST FACILITY CONSTRUCTION CYCLE 9 VOLUME 4—CEMENT-TREATED PERMEABLE BASE TEST	April 2026
	6. Performing Organization Code ANG-E262

7. Author(s)	8. Performing Organization Report No.
Hasan Kazmee*, Scott Murrell*, Lia Ricalde*, Timothy Parsons*, Ebenezer Duah*, David R. Brill and Daniel I. Offenbacker	7

9. Performing Organization Name and Address		10. Work Unit No. (TRAIS)
U.S. Department of Transportation Federal Aviation Administration Airport Pavement R&D Section William J. Hughes Technical Center for Advanced Aerospace Atlantic City International Airport, NJ 08405	*ARA, Inc 2628 Fire Road Suite 300 Egg Harbor Twp, NJ 08234	11. Contract or Grant No. 692M15-21-D-00004

12. Sponsoring Agency Name and Address	13. Type of Report and Period Covered
U.S. Department of Transportation Federal Aviation Administration Airport Engineering Division 800 Independence Ave., SW Washington, D.C. 20591	Final Report
	14. Sponsoring Agency Code AAS-100

15. Supplementary Notes

The Federal Aviation Administration Aviation Research Division COR was Murphy Flynn.

16. Abstract

Construction Cycle 9 (CC9) was the ninth in a series of full-scale airport pavement tests performed at FAA's National Airport Pavement Test Facility (NAPTF), the fifth involving flexible pavements. It contained four test areas: Fatigue, Geosynthetics, Cement-Treated Permeable Base (CTPB), and Overload. This report addresses the CTPB test area, which consisted of two test items with the same flexible pavement structure except for different base course materials. Test item LFS-4N had a CTPB base, while control test item LFC-4S had a conventional crushed aggregate (FAA Item P-209) base. These test items were subjected to equal simulated full-scale aircraft traffic using the NAPTF test vehicle. The goal of this test was to assess the feasibility of using a CTPB layer in a standard flexible pavement structure. Data were collected through laboratory and in situ testing, visual evaluation, and embedded pavement sensors. Embedded sensors included asphalt strain gauges, thermocouples, earth pressure cells, coil sensors, and moisture sensors. Performance was tracked by monitoring surface upheaval, rutting, and surface cracking. Key performance and sensor data were compared to an earlier test, the Construction Cycle 7 (CC7) asphalt-treated permeable base (ATPB) test item at the NAPTF. Both in-place and laboratory characterization results indicated CTPB materials had substantially higher stiffness than traditional crushed aggregate bases. Cracking and surface upheaval were lower in the CTPB test item compared to the control test item. Structural performance of CTPB under full-scale traffic may be characterized as intermediate between a standard high-quality aggregate base (P-209) and a fully bound material (P-403).

17. Key Words	18. Distribution Statement
National Airport Pavement Test Facility, NAPTF, Construction Cycle 9, CC9, Cement-treated permeable base	This document is available to the U.S. public through the National Technical Information Service (NTIS), Springfield, Virginia 22161. This document is also available from the Federal Aviation Administration William J. Hughes Technical Center for Advanced Aerospace at actlibrary.tc.faa.gov.

19. Security Classif. (of this report)	20. Security Classif. (of this page)	21. No. of Pages	22. Price
Unclassified	Unclassified	95	

TABLE OF CONTENTS

LIST OF FIGURES

LIST OF TABLES

LIST OF SYMBOLS AND ACRONYMS

μ	Mean value
σ	Standard deviation
θ_v	Volumetric moisture content
M_r	Resilient modulus
2D	Two duals in tandem (four-wheel)
3D	Three duals in tandem (six-wheel)
AC	Advisory Circular
ASG	Asphalt strain gauge
ATPB	Asphalt-treated permeable base
AUPP	Area under pavement profile
CBR	California bearing ratio
CC	Construction cycle
CC7	Construction cycle 7
CC9	Construction cycle 9
cd	Crack density
CS	Coil sensor
CTPB	Cement-treated permeable base
D	Dual (two-wheel)
FAA	Federal Aviation Administration
FAARFIELD	FAA Rigid and Flexible Iterative Elastic Layered Design
GPR	Ground-penetrating radar
HMA	Hot mix asphalt
HWD	Heavy weight deflectometer
ksi	kilopound per square in.
LEAF	Layered elastic analysis
LiDAR	Light detection and radar
LSG	Longitudinal strain gauge
LWD	Lightweight deflectometer
MDD	Multi-depth deflectometer
MR	Modified research
MS	Moisture sensor
NAPTF	National Airport Pavement Test Facility
NDT	Nondestructive testing
NGPML	NextGen Pavement Materials Laboratory
PC	Pressure cell
pcf	Pounds per cubic ft
PG	Performance grade
PSE	Physical straightedge
psi	Pounds per square in.
PSPA	Portable Seismic Properties Analyzer
TSG	Transverse strain gauge
VSE	Virtual straightedge
VUC	Virtual upheaval calculator

EXECUTIVE SUMMARY

From 2020 to 2024, the Federal Aviation Administration (FAA) executed a series of full-scale traffic tests on flexible airport pavements at the National Airport Pavement Test Facility (NAPTF), designated Construction Cycle 9 (CC9). Within CC9, the Cement-Treated Permeable Base (CTPB) test was designed to test the feasibility of using CTPB in lieu of standard crushed aggregate base (FAA Item P-209) in airport flexible pavements. This report specifically addresses two test items within CC9: LFS-4N and LFC-4S. LFS-4N followed standard FAA design for flexible pavements but used a CTPB layer under the asphalt surface. The control test item (LFC-4S) had similar materials and thickness but used a standard P-209 base. Both test items were subjected to equal simulated full-scale aircraft traffic. The goal of the test was to quantify any significant differences in performance of the CTPB test item relative to the control test item.

Historically, the FAA has avoided using CTPB in flexible airport pavement structures because of the susceptibility of asphalt surfaces to reflective cracking. However, the most recent revision to Advisory Circular (AC) 150/5370-10, *Standards for Specifying Construction of Airfields*, states that Stabilized Drainable Base Course (designated Item P-307) can be used as a stabilized base course under both flexible and rigid pavements and may be stabilized with either asphalt or cement. The intention of this research was to obtain full-scale test data for standard flexible pavements including CTPB and to determine properties of CTPB layers for use in standard FAA thickness designs. This research complements a previous full-scale test of flexible pavement including asphalt-treated permeable base (ATPB) conducted under NAPTF Construction Cycle 7 (CC7).

This report covers data collection and analysis from the construction, pre-traffic, and traffic testing phases. During the construction phase, materials were carefully characterized through laboratory and in situ testing. During traffic, data were acquired from regular visual surveys, nondestructive testing (NDT), and embedded pavement sensors. Embedded sensors (asphalt strain gauges, thermocouples, earth pressure cells, inductive coil sensors, and moisture sensors) were located in various layers to enable researchers to analyze the effect of the different base materials on pavement responses to load. Researchers quantified test item performance using indicators such as surface upheaval, rutting, and crack density (CD). Key performance and sensor data were compared to the CC7 (ATPB) test item. Both CD and surface upheaval were lower in the CTPB test item than in the control test item. From an analysis of relative performance under full-scale traffic, CTPB may be characterized as intermediate between a standard high-quality aggregate base (P-209) and a fully bound material (P-403). This report includes recommendations for material characterization of P-307 (CTPB) for thickness design of flexible pavements using the FAA software FAA Rigid and Flexible Iterative Elastic Layered Design (FAARFIELD).

1. INTRODUCTION

Cement-treated permeable base (CTPB) layers have been researched and successfully employed for rapidly removing water from within the pavement structure (Hall et al., 2005) while providing additional load-distribution capacity for flexible pavements. CTPB uses the cement paste to eliminate the rutting susceptibility of open-graded base course material caused by poor stability (Liang, 2007). Historically, the Federal Aviation Administration (FAA) did not recommend the use of CTPB as a stabilized base under flexible pavements due to its susceptibility to reflective cracking (FAA, 2018). However, the most recent revision to FAA Advisory Circular (AC) 150/5370-10H, *Standards for Specifying Construction of Airfields*, states that Stabilized Drainable Base Course (designated Item P-307) can be used as a stabilized base course under both flexible and rigid pavements and may be stabilized with either asphalt or cement (FAA, 2018). Given the lack of historical experience, it is unknown if existing CTPB construction specifications and structural design properties intended for rigid pavements are suitable for use with flexible pavements.

The Construction Cycle 9 (CC9) CPTB Test at the National Airport Pavement Test Facility (NAPTF) was intended to address this research gap. The NAPTF, located on the campus of the FAA William J. Hughes Technical Center for Advanced Aerospace approximately 9 miles west of Atlantic City, New Jersey, is a unique enclosed facility for full-scale testing of airport pavements. Under CC9, the FAA conducted full-scale tests to generate performance data on CTPB-stabilized structures and to identify adequate design and construction parameters for flexible airfield pavements with CTPB. The CC9 CTPB test items were constructed in 2019 and tested to failure between April 2021 and October 2022. CC9 was the ninth in a series of full-scale tests performed at the NAPTF since it opened in 1999, and the fifth involving flexible pavements. A previous series of flexible pavement tests at the NAPTF, Construction Cycle 7 (CC7) included an asphalt-treated permeable base (ATPB) test item, and the current test was intended to obtain similar structural performance data on CTPB.

In practice, the thickness design of a permeable base, whether CTPB or ATPB, may be governed by its drainage capacity rather than by structural requirements. Both CC7 and CC9 tests were limited to investigating the structural performance of permeable base layers under simulated aircraft traffic. The CTPB materials used in CC9 were designed to meet the permeability standards of Item P-307, but otherwise no attempt was made to test the water removal function. Hydraulic requirements of permeable bases including CTPB are covered under FAA AC 150/5320-5D, *Airport Drainage Design*.

1.1 OBJECTIVE AND SCOPE

The main objective of the CC9 CTPB test was to quantify the performance of P-307 CTPB course relative to P-209 standard base course in flexible pavement structures. The secondary objective was to compare the CTPB test results to similar full-scale traffic tests in CC7 involving a P-407 ATPB course test item.

1.2 NATIONAL AIRPORT PAVEMENT TEST FACILITY TERMINOLOGY

1.2.1 Test Terminology

The following sections define terms and phrases commonly used at the NAPTF.

Construction Cycle (CC). CC refers to the overall test project including design, construction, traffic testing, post-traffic testing, data collection, data analysis, and final demolition. Each CC is developed with specific test objectives in mind. Typically, a CC is dedicated to either rigid or flexible pavement testing.

Test Area. Each CC is divided into multiple test areas as required by the test objectives. Dividing the test pavement into test areas allows the FAA to conduct multiple experiments simultaneously. A test area can be made up of one or more test items.

Transition Area. Transition areas separate the test items in the longitudinal direction, avoiding abrupt changes in layer thickness at test item boundaries. Transition areas are of sufficient length to allow vehicle start-up and shutdown while maintaining a constant speed and load over the test items themselves.

Test Item. A test item is a unit of pavement within the test area characterized by a unique combination of pavement structure and test traffic. For CC9, each test area was divided into two test items, designated north and south, on the corresponding sides of the facility centerline. Each test item is designated by an identifier consisting of three letters, followed by a dash and two additional characters.

- The first letter corresponds to the strength of the subgrade (L = low strength, M = medium strength, H = high strength).
- The second letter corresponds to the type of pavement structure (F = flexible, R = rigid).
- The third letter corresponds to the type of base (S = stabilized, C = conventional/unstabilized, G = slab-on-grade/no base).
- The last two characters give the sequential numbering of the test item, and whether it is on the north (N) or south (S) side of the centerline.

As an example, in this report the designation LFS-4N refers to the north test item of Test Area 4 that is built on a low-strength subgrade (L), using a flexible (F) pavement, with an aggregate (i.e., conventional) (C) base course. Test items are numbered from west to east.

Wander Pattern. The National Airport Pavement Test Vehicle (NAPTV), depicted in Figure 1, executes a wander pattern consisting of a repeated sequence of 66 passes arranged in 9 longitudinal tracks. The lateral spacing between adjacent tracks is 10.25 in. The NAPTF wander pattern is designed to approximate a normal lateral distribution of aircraft traffic with a standard deviation from centerline equal to 30.54 in.

Figure 1. National Airport Pavement Test Vehicle

1.2.2 Work Item Modifiers

In general, NAPTF test items follow the material and construction standards in FAA AC 150/5370-10H (FAA, 2018). However, research objectives may require deviation from some aspects of the standard. To indicate that the construction specification is altered, work items are modified with the following designations: M = Modified, R = Research, MR = Modified Research. Material items listed below are modified from the standard FAA specifications.

- P-152MR Subgrade: Work Item P-152MR is a prepared subgrade composed of soil that provides the specified design California bearing ratio (CBR) values for test items constructed on low-strength subgrades. The subgrade material is prepared in the excavated bed of the NAPTF or the FAA Subgrade Processing building in accordance with the project specifications.

- P-209MR Crushed Aggregate Base Course: Work Item P-209MR is a base course composed of crushed aggregate.

- P-307MR CTPB Course: Work Item P-307MR is an open-graded drainable base composed of mineral aggregate, cement, and water. See Appendix E for the modified specification.

- P-401MR Asphalt Mix Pavement Surface Course: Work Item P-401MR is a hot mix asphalt (HMA) pavement course composed of mineral aggregate and asphalt binder mixed in a central mixing plant, placed on a prepared base or stabilized course, and compacted. It can be used for multiple pavement courses but is typically used as a surface course.

2. DESIGN AND CONSTRUCTION OF TEST AREAS

CC9 was built on the west end of the NAPTF building. All test areas were built on clay subgrade with a nominal CBR of 5 (low strength, L). The CC9 CTPB test area consisted of two test items, designated LFS-4N and LFC-4S, as shown in Figure 2. Locations within the test area are identified by stations (STA) and offset left (north) or right (south) of the centerline, in ft. The CTPB test items were constructed between STA 1+80 and 2+25. Allowing for 3-ft. shoulders, the center of traffic for test item LFS-4N was at lateral offset -15 ft, and the center of traffic for the test item LFC-4S was at +15 ft. As shown in Figure 2, each test item was 33 ft wide by 45 ft long, with 15-ft transition areas separating the test items.

Figure 3 shows cross-sections of the pavement structures. The two test items had identical pavement layer structures except for the base layer material. Test item LFS-4N had a CTPB base (Item P-307MR), and test item LFC-4S had a standard crushed aggregate base (Item P-209MR). Both test items had approximately 5-in.-thick asphalt surface (Item P-401MR) and approximately 29-in.-thick granular subbase. As shown in Figure 4, and as discussed in Volume 3 of this report series addressing the Geosynthetic Test (Kazmee et al., 2026b), test item LFC-4S served as the control for both the CTPB test and the Geosynthetics test.

The instrumentation layout was designed considering traffic wander. As discussed in Section 1.2.1, the traffic followed a defined wander pattern giving an approximately normal lateral distribution. The center positions of the north and south carriages, as shown in Figure 1, were set at transverse offsets -15 ft and +15 ft, respectively. Those center offsets were assigned to wander track 0. At the outermost wander positions (tracks -4 and +4), the outer wheels of the load modules could traverse 5.662 ft north and south of center offsets. For example, the outer wheels of LFS-4N operated between -9.338 and -20.662 ft. Areas outside these limits were considered un-trafficked. Further details on the wander pattern are presented in Section 4.

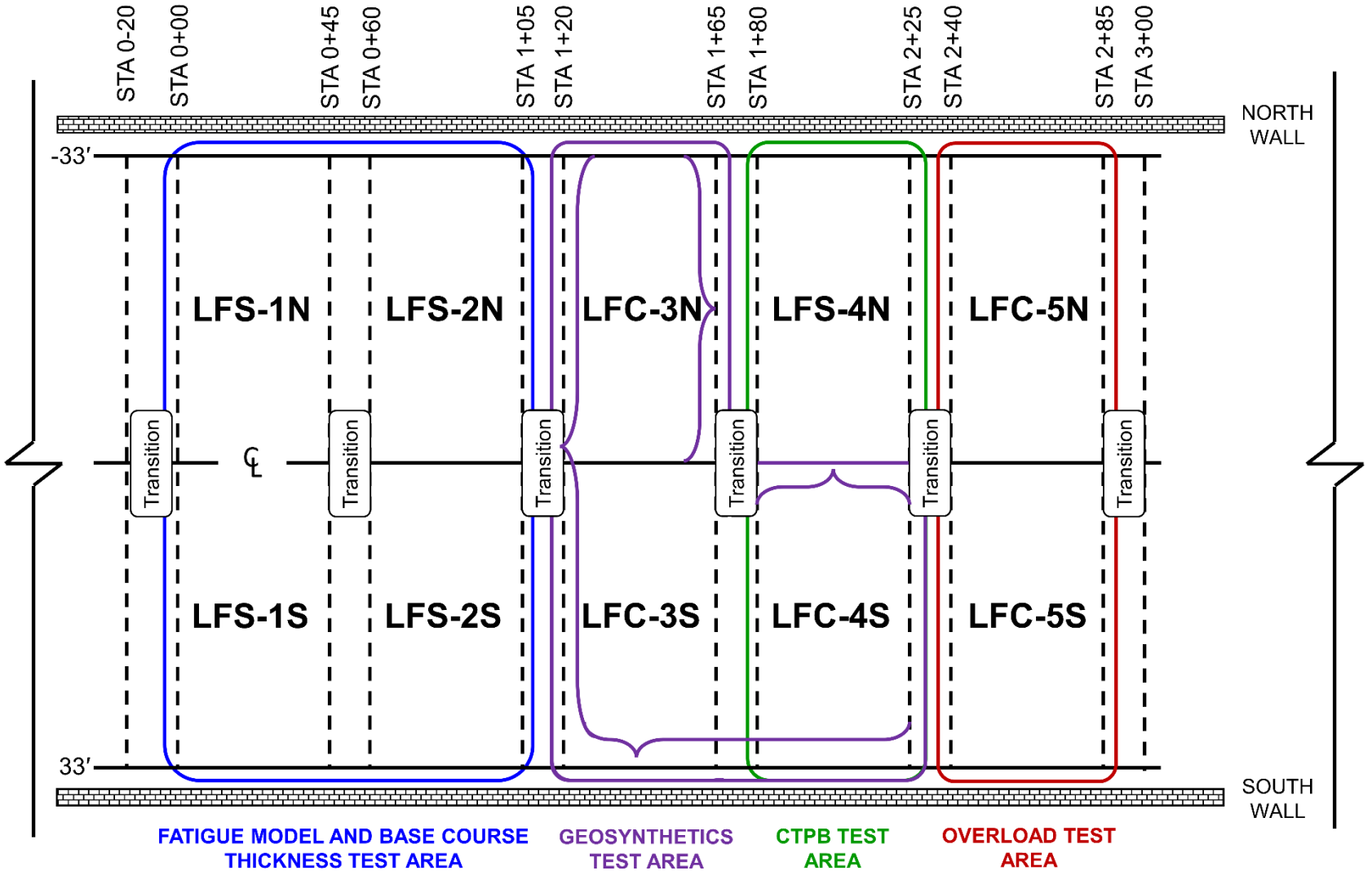

Figure 2. Plan View of the Construction Cycle 9 Test Areas and Items

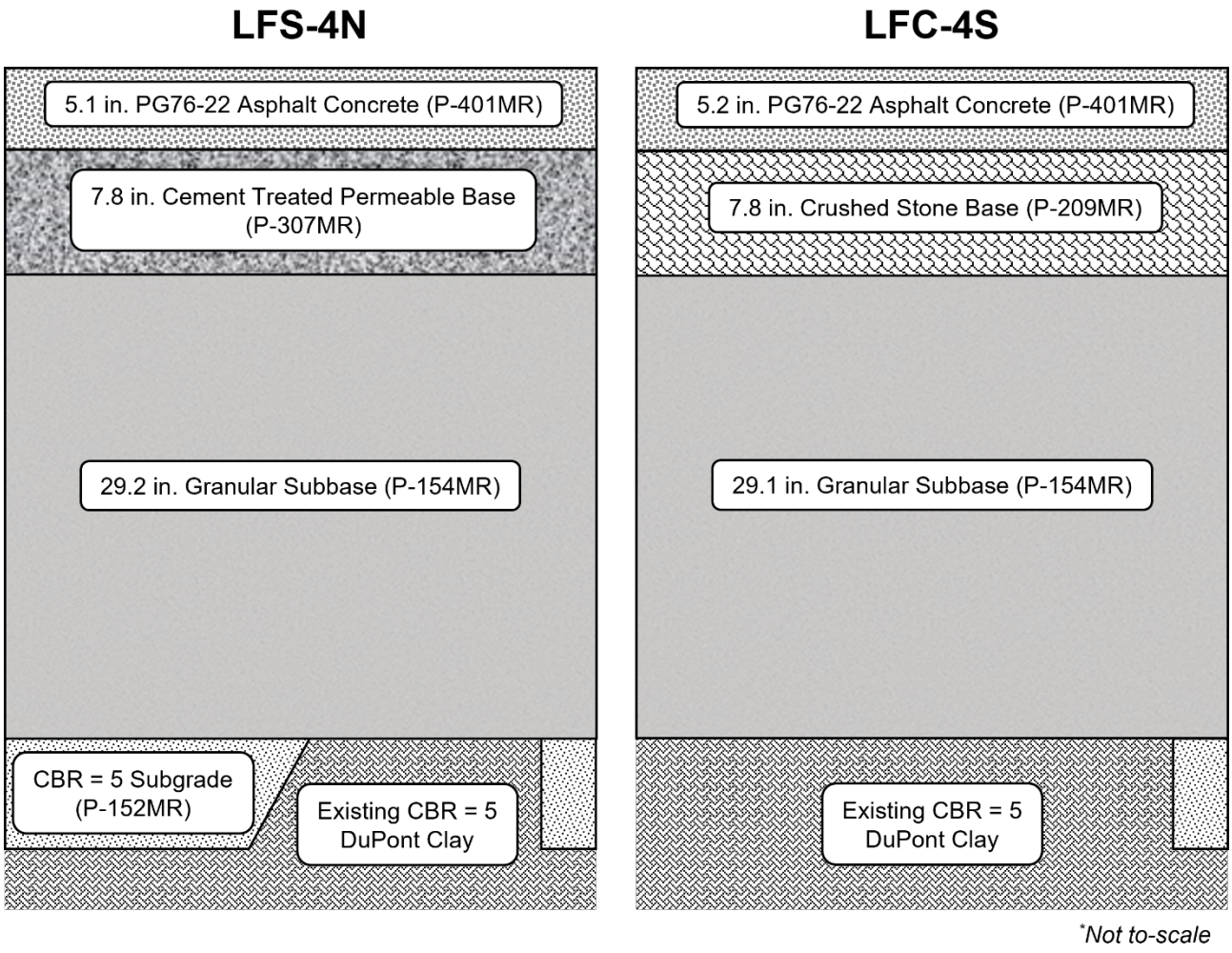

Figure 3. Pavement Structural Cross-Sections of CTPB Test Items

2.1 REVIEW OF CONSTRUCTION QUALITY CONTROL AND ASSURANCE

2.1.1 Placement and Compaction of Subgrade (P-152MR)

The CC9 subgrade (P-152MR) consisted of two clay materials. The upper subgrade is Dupont Clay, classified by the Unified Soil Classification system as a high-plasticity clay (CH) with a plastic limit of 19 and liquid limit of 56. Approximately 5 ft below the surface of Dupont Clay is County Sand and Stone Clay originally placed during CC1 construction. County Sand and Stone clay may be classified as either MH or CH per the original NAPTF pavement design report (Hall, 1998). Both materials were sourced from the Delaware Bay area, approximately 40 miles west of the NAPTF. The upper subgrade material was either reprocessed (tilled, spread/shifted, recompacted) in situ to meet the required grade at the target CBR, or new Dupont Clay was added and processed in situ to the target CBR. All new subgrade material was sourced from the subgrade stockpile stored at the FAA subgrade processing facility yard adjacent to the NAPTF.

As shown in Figure 3, LFS-4N incorporated an area of P-152 fill from the stockpile. This fill added complexity to achieving a uniform strength subgrade and achieving a consistent subgrade for LFS-

4N and LFC-4S was difficult. Additional details pertaining to the prepared subgrade placement can be found in Tomlinson et al. (2022).

2.1.2 Placement and Compaction of Subbase Course (P-154MR)

The subbase was a carbonate-based manufactured sand placed in lifts ranging from 5 to 10 in. for all layers. Steel drum rollers were used to compact each lift. Compaction was performed in both longitudinal and transverse directions throughout the test items. A nuclear density gauge was used to determine density and moisture content at depths that did not exceed the lift thickness. Measurements were made at two random locations in each test item, and the average of those values had to meet or exceed the target dry density of 138.3 pounds per cubic ft (pcf), with a moisture content between 2% and 6%. In establishing these criteria, the target density corresponded to the maximum density on the modified Proctor curve at 6% moisture content. A maximum of 6% moisture content was chosen because that was the highest value for which no drain-down was observed during laboratory testing.

2.1.3 Placement and Compaction of Base Course (P-307MR and P-209MR)

The base course material for test item LFS-4N was a CTPB conforming to Item P-307MR (see specification in Appendix E). In preparation for placing this material in the NAPTF, the contractor placed three test strips. The first test strip was intended for the contractor to become familiar with the materials and to obtain experience, which was then used to estimate the roll-down of the material (about 1 inch per 8 in. of material).

The second test strip was performed in the contractor's yard and attended by FAA personnel. Wooden forms were sprayed with form oil and installed on a 17-ft-wide and 20-ft-long grid with a height of 9 in. A form-riding triple roller paver was set on the forms, and the CTPB material (P-307MR) was delivered in ready-mix concrete trucks. P-307MR was discharged directly into the forms and spread using rakes and other hand tools. Loose materials higher than the 9-in. height of the formwork were scraped off with rakes. The form-riding triple roller paver compacted the P-307MR without vibration in tandem with the ready-mix trucks progressing towards the end of the formed area. As the tires of the ready-mix truck cleared the form limits, a final form was quickly installed, and the remaining P-307MR was discharged. The 9-in.-thick forms consisted of a 1-in.-thick board at the top, which was removed once the form-riding triple roller paver passed the formed limits, ensuring a preliminary smooth surface. In total, three passes were made with the form-riding triple roller paver on the P-307MR to compact the material down to 8 in. No cracks were observed in the aggregate.

The third and final test strip was placed in a yard adjacent to Building 207 at the Technical Center, approximately 1,000 ft from the NAPTF (Figure 4). The wooden forms from the first test strip were reused. The 8-in.-tall rectangular wooden forms had braces every 1 ft and were placed flush along a stretched stringline. Concrete forming stakes (3/4-in. steel) were driven into the ground to brace the prefabricated wooden forms. These stakes were spaced at 4 ft. Wooden wedges were placed between the stakes and the forms to ensure contact between the two items. Contractors installed 1-in. × 4-in. lumber on top of the forms, increasing the total height of the forms to 9 in. The area dimensions of the test strip were 17×45 ft. Jersey barriers were placed approximately 2 ft from the forms to simulate the foundation wall at the NAPTF during placement. During material placement,

the form-riding triple-roller paver made six passes to bring the material flush with the top of the form.

Figure 4. Removing Forms from the Third CTPB Test Strip, October 11, 2019

CTPB was placed at the NAPTF in two placements, on October 18 and 25, 2019. Forms were set up for the first placement from STA 1+73 to 2+33 at offsets of -12.5 to -28.5 ft (negative offsets are measured north of the facility centerline). During the second placement, the contractor repositioned and installed the forms along the centerline. The surface of the subbase was dampened before the placement of CTPB materials. Deviating from the practice during construction of the third test strip, the contractor used a ¾-in. board on top of the formwork rather than the previously used 1-in. board. The FAA approved this measure considering the stiffer foundation support available from the CC9 granular subbase compared to the outdoor yard.

After the forms were removed, the contractor used a laser scanner to generate grade and thickness maps for acceptance. The acceptance criterion for grade was that no single point could deviate more than 1/2 in. from the design grade on a 5-×5-ft grid. A 12-ft straightedge was used to verify the smoothness criterion in both longitudinal and transverse directions. The acceptance criterion for smoothness was that at least 85% of the tested area must not deviate more than 3/8 in. from a 12-ft straightedge. Characterization tests were performed on the surface after 7 days and 28 days of curing. Additional details on the placement, compaction, and acceptance of the CTPB material can be found in Tomlinson et al. (2022).

The crushed aggregate base material (P-209MR) for control test item LFC-4S was a blend of three diabase granular materials sourced from Birdsboro Quarry in Skippack, Pennsylvania. The base was

placed in lifts of 4 to 8 in. Steel drum rollers were used to compact each lift. A nuclear density gauge was used to determine density and moisture content. Two random locations were selected in each test item for acceptance testing, and the average of those values was required to meet or exceed the target dry density of 151.3 pcf, with a moisture content between 1.5% and 5.5%. The target density corresponded to the maximum density on the modified proctor curve. A maximum of 5.5% moisture content was chosen because that was the highest value where no drain-down was observed during laboratory testing.

2.1.4 Placement and Compaction of Asphalt Concrete (P-401MR)

The asphalt mixture conformed to the FAA P-401MR specification as presented in Tomlinson et al. (2022). The nominal maximum aggregate size was 0.75 in. Table 1 lists the complete gradation. A Performance Grade (PG) 76-22 asphalt binder was used with a binder content of 5% (by total mixture weight). The asphalt layer was placed in two lifts. A nuclear density gauge was used to monitor compaction of the test area during compaction. For the first lift, the asphalt was paved and compacted using a static roller. Rollers were used in static mode to protect the instrumentation embedded in the asphalt layer. For the second lift, two rollers were operated in vibratory mode until density was achieved as indicated by the nuclear gauge. A final roller pass in static mode removed any roller marks.

Table 1. P-401MR Aggregate Gradation

Sieve Designation	Contractor Provided Percent Passing, %	Percent Passing Band, %
1 in. (25 mm)	100.0	100
3/4 in. (19 mm)	97.1	90–100
1/2 in. (12.5 mm)	84.0	68–88
3/8 in. (9.5 mm)	74.4	60–82
No. 4 (4.75 mm)	52.0	45–67
No. 8 (2.38 mm)	36.0	32–54
No. 16 (1.19 mm)	25.2	22–44
No. 30 (600 µm)	17.8	15–35
No. 50 (300 µm)	11.4	9–25
No. 100 (150 µm)	7.2	6–18
No. 200 (75 µm)	4.0	3–6

2.2 IN-PLACE TESTING FOR CONSTRUCTION UNIFORMITY

Detailed test results for material acceptance and characterization are available in Tomlinson et al. (2022), Appendices D and E. This section summarizes certain characterization test data pertinent to construction uniformity. During the period of testing, the NAPTF NextGen Pavement Materials Laboratory was closed for several months due to the COVID-19 health emergency, and various laboratory tests were delayed.

Light Weight Deflectometer (LWD) modulus values were determined from Boussinesq's half-space equation (Mooney & Miller, 2009). The stress distribution factors listed in Table 2 are those

recommended by Bilodeau and Doré (2014), assuming Poisson's ratios and LWD plate radii are as listed in Table 2.

$$E = \frac{f \times (1-\nu^2) \times \sigma_0 \times a}{d_0} \quad (1)$$

where:

E = LWD modulus
f = stress distribution factor
ν = Poisson's ratio
σ_0 = contact stress
a = plate radius
d_0 = center deflection

Table 2. Properties and Assumptions for the Determination of LWD Modulus

Layer	Poisson's Ratio	Stress Distribution Factor	Plate Radius (in.)
Subgrade	0.4	4/3	5.9
Granular subbase	0.35	8/3	5.9
Crushed aggregate base	0.35	8/3	3.0

2.2.1 Subgrade (P-152MR)

Table 3 lists material properties tested on the subgrade. Figure 5 plots in situ CBR for the CTPB test area. Subgrade CBR values were within acceptable tolerance (±1% of the target CBR 5%). Figure 6 plots subgrade shear strength from vane shear tests.

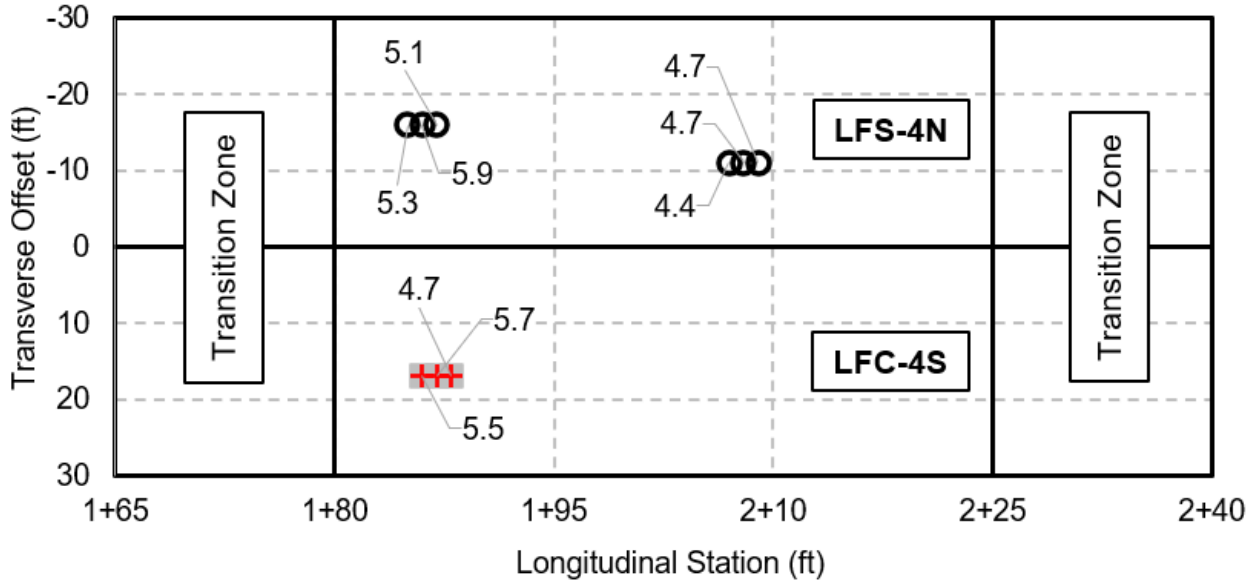

Figure 5. Summary of CC9 Subgrade CBR Values in CTPB Test Items

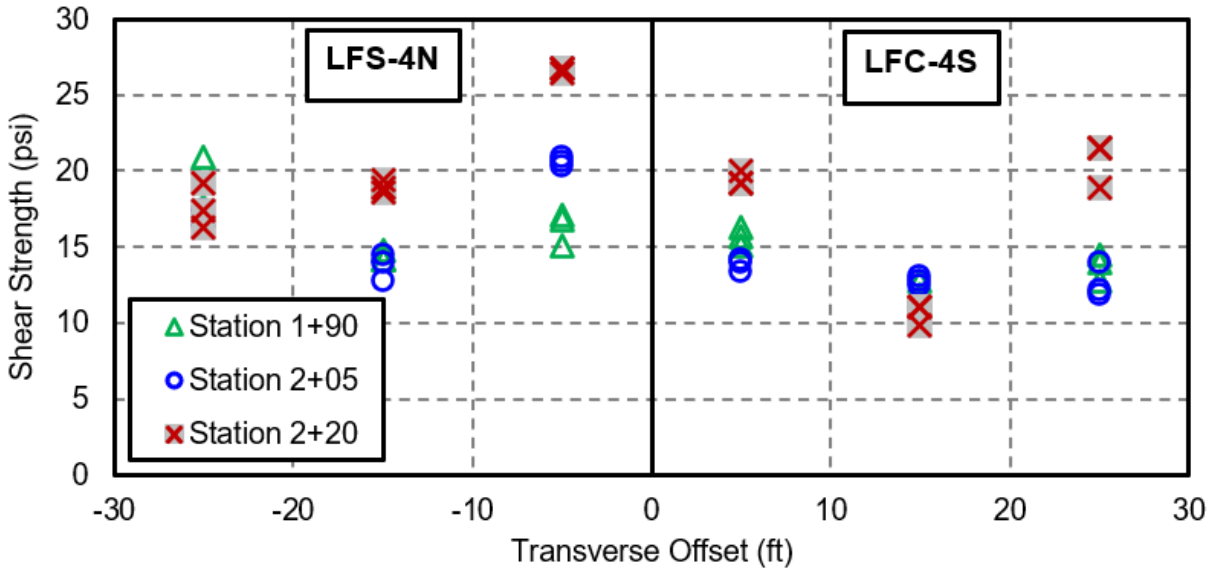

Figure 6. As-Built Subgrade Shear Strength in CTPB Test Items Measured with Vane Shear Tests

2.2.1.1 Light Weight Deflectometer Modulus

Subgrade stiffness was measured with LWD equipment. LWD modulus values for test items LFS-4N and LFC-4S are plotted against the contact stresses in Figure 7(a) and (b), respectively. Generally, moduli for LFS-4N were higher than for LFC-4S. The LWD modulus values were plotted against the contact stresses to evaluate the stress dependency of fine-grained soils. As expected for low-strength clay soil, the modulus values exhibited stress-softening behavior, decreasing with increasing contact stress.

Table 3. Summary of In-Place Characterization of Clay Subgrade

Test Item	**LFS-4N**			**LFC-4S**		
Properties	**μ**	**σ**	**COV (%)**	**μ**	**σ**	**COV (%)**
CBR (%)	5.4	0.4	7.7	5.3	0.5	10
MC (%)	24	N/A	N/A	27.1	N/A	N/A
In situ dry density (pcf)	99.4	N/A	N/A	95.5	N/A	N/A
Shear strength (psi)	18.2	3.8	21.1	14.6	3.4	23.1
LWD modulus (ksi)	7.6	2.8	37.3	4.7	3.4	72.1
Seismic modulus (ksi)	22.4	4.5	19.9	15.9	2.3	14.4
GeoGauge modulus (ksi)	14	3	21.2	11.6	2.4	20.5

μ = Mean value, σ = Standard deviation, COV = Coefficient of variation, pcf = pounds per cubic ft, psi = pounds per square in., ksi = kilopound per square in.

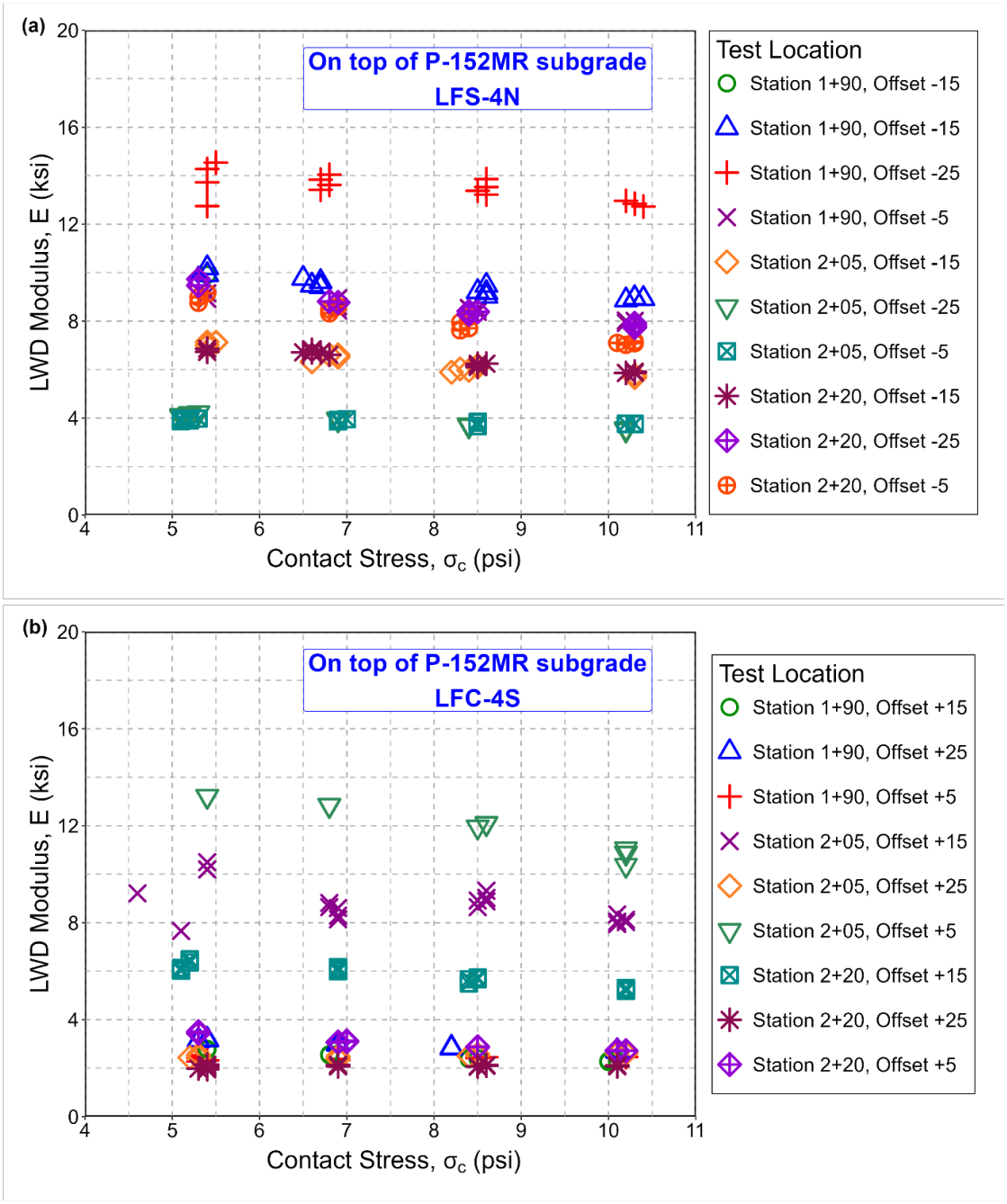

Figure 7. As-Built Subgrade Modulus in CTPB Test Items Measured with LWD

2.2.1.2 Seismic Modulus

Seismic moduli of the subgrade layers were measured using the Dual-Portable Seismic Properties Analyzer (D-PSPA) device (Nazarian et al., 1993). Seismic moduli of the subgrade layers measured parallel and perpendicular to the direction of traffic are presented along with the transverse offsets for LFS-4N and LFC-4S in Figure 8(a) and (b), respectively. As with the LWD modulus, the

subgrade seismic modulus was generally higher for LFS-4N than for LFC-4S in both directions. As shown in Figure 8, there was considerable variation in recorded D-PSPA modulus, with values ranging from as low as 12 kilopound per square in. (ksi) at the center of LFC-4S to more than 25 ksi at several locations.

2.2.1.3 GeoGauge Modulus

Figure 9 plots GeoGauge modulus values against transverse offset. GeoGauge moduli showed high variation for both test items. Moreover, for both test items the variation was greater at points along the center of the test item (offsets ±15 ft) than at points along the outside offsets (±5 ft and ±25 ft from centerline). Considering the outside offsets only, the average geogrid modulus was significantly higher for LFS-4N than for LFC-4S.

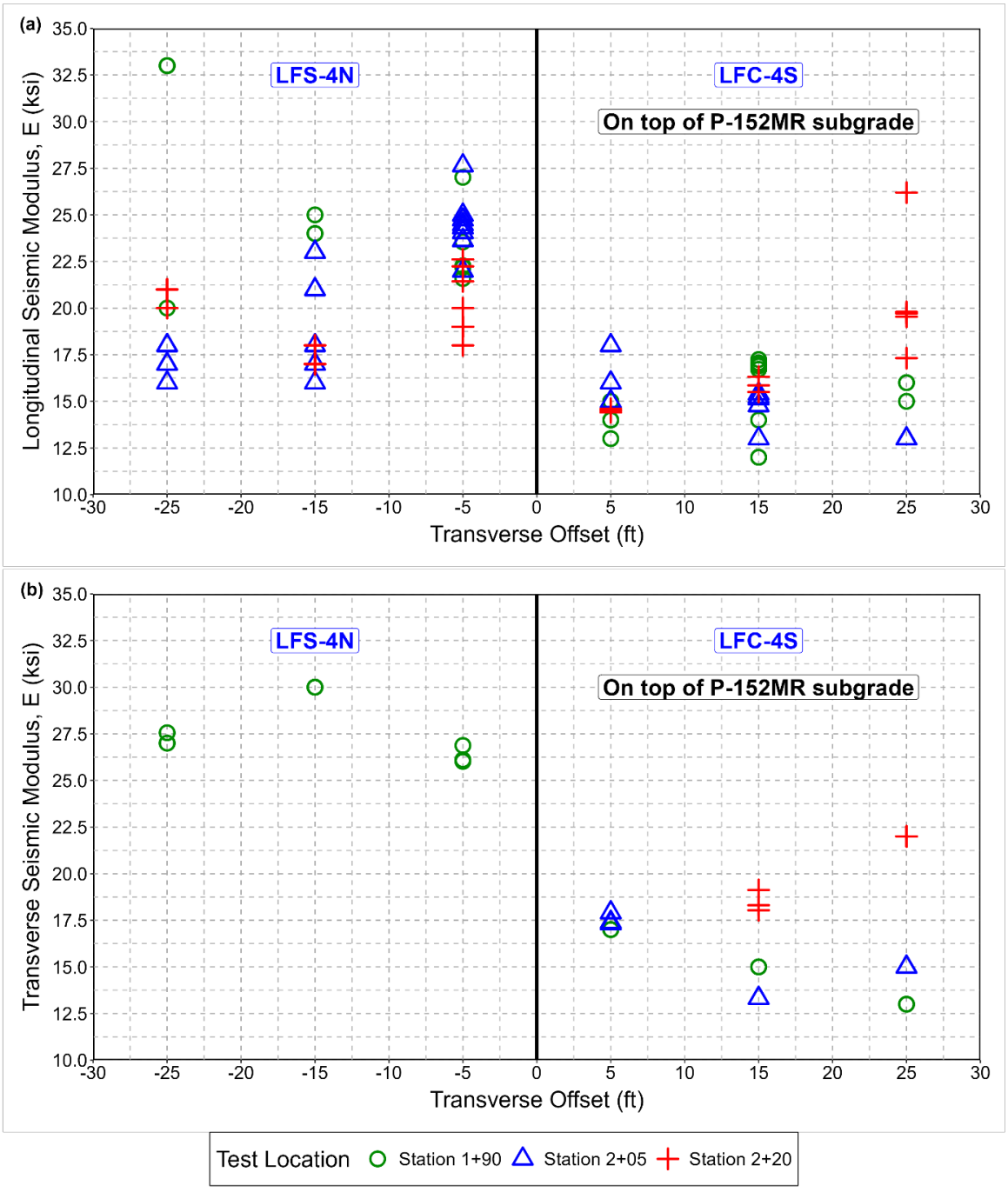

Figure 8. As-Built Subgrade Seismic Modulus in CTPB Test Items Measured with D-PSPA

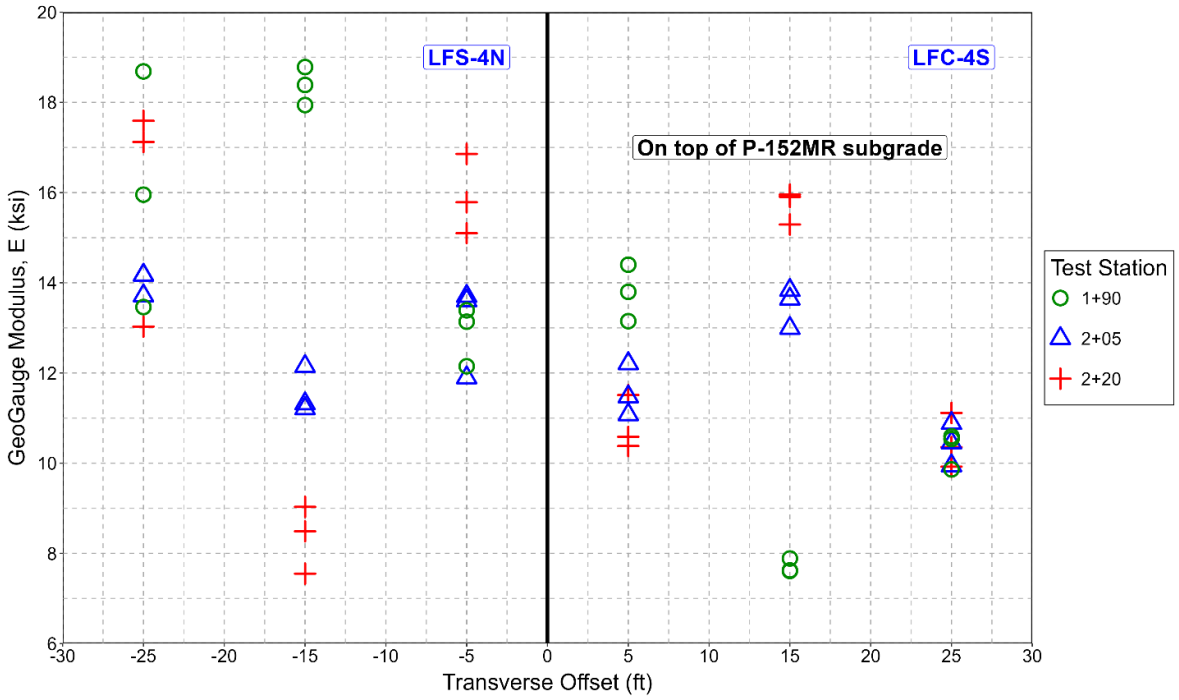

Figure 9. As-Built Subgrade Modulus in CTPB Test Items Measured with GeoGauge

2.2.2 Subbase Course (P-154MR)

Table 4 lists summary statistics for five material properties measured on the granular subbase. Seismic modulus values measured with the D-PSPA device were on average about four times higher than moduli from LWD and GeoGauge. Measured dry densities and mean LWD moduli were similar for both test items.

Table 4. Summary of In-Place Characterization of Granular Subbase

Test Item	**LFS-4N**			**LFC-4S**		
Properties	**μ**	**σ**	**COV (%)**	**μ**	**σ**	**COV (%)**
Nuclear gauge density (pcf)	138.7	N/A	N/A	138.9	N/A	N/A
Nuclear gauge M.C. (%)	3.4	N/A	N/A	4.2	N/A	N/A
LWD modulus (ksi)	17.1	2.2	12.9	17.3	1.8	10.3
Seismic modulus (ksi)	64.9	7.4	11.5	74.8	8.3	11.1
GeoGauge modulus (ksi)	16.6	2.1	12.9	17.3	1.3	7.7

μ = Mean value, σ = Standard deviation, COV = Coefficient of variation, ksi = kilopound per square in.

Figure 10 plots the LWD modulus at top of subbase against the corresponding LWD plate contact stresses. Figure 11 plots top-of-subbase seismic moduli (D-PSPA) against the transverse offset for all three test items. Figure 12 plots top-of-subbase GeoGauge moduli against the transverse offset. The overall distribution of modulus values was similar for the two test items. Modulus values plotted against the contact stresses (Figure 10) substantiate the expected stress-hardening behavior

of the granular subbase. In both test items, modulus magnitude increased, and the variation in modulus decreased, with increasing contact stresses.

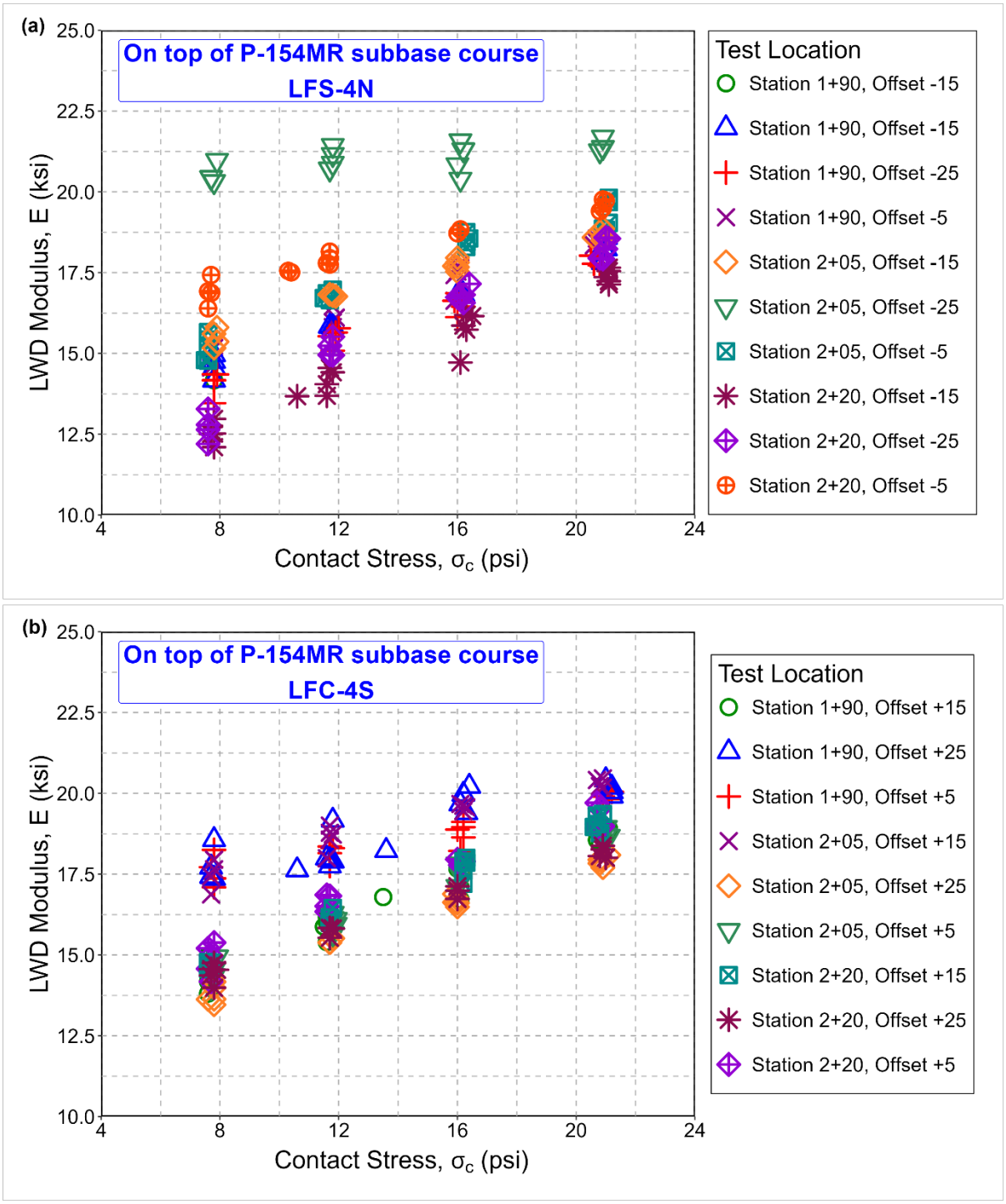

Figure 10. As-Built Subbase Modulus in CTPB Test Items Measured with LWD

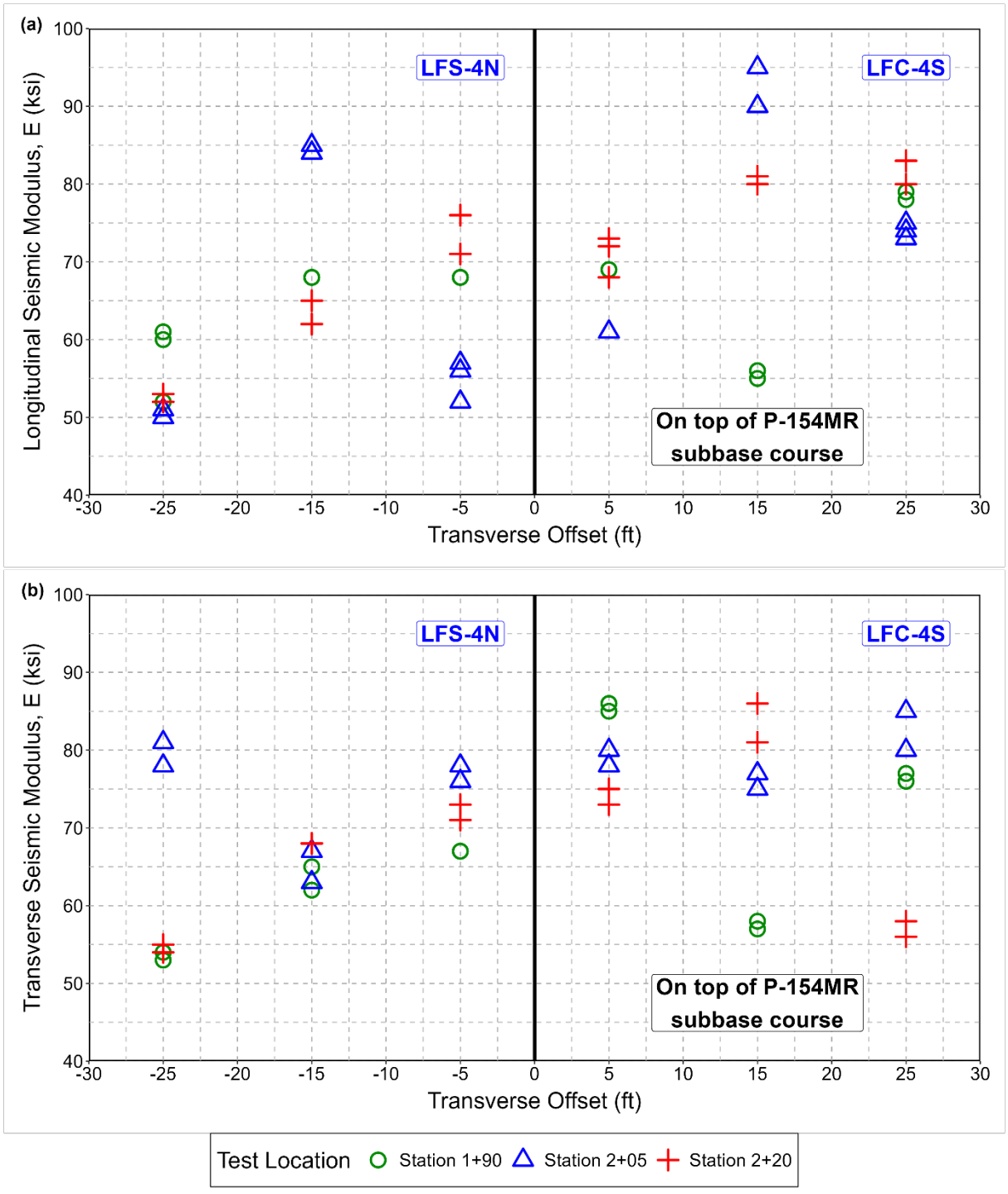

Figure 11. As-Built Subbase Seismic Modulus in CTPB Test Items Measured with D-PSPA

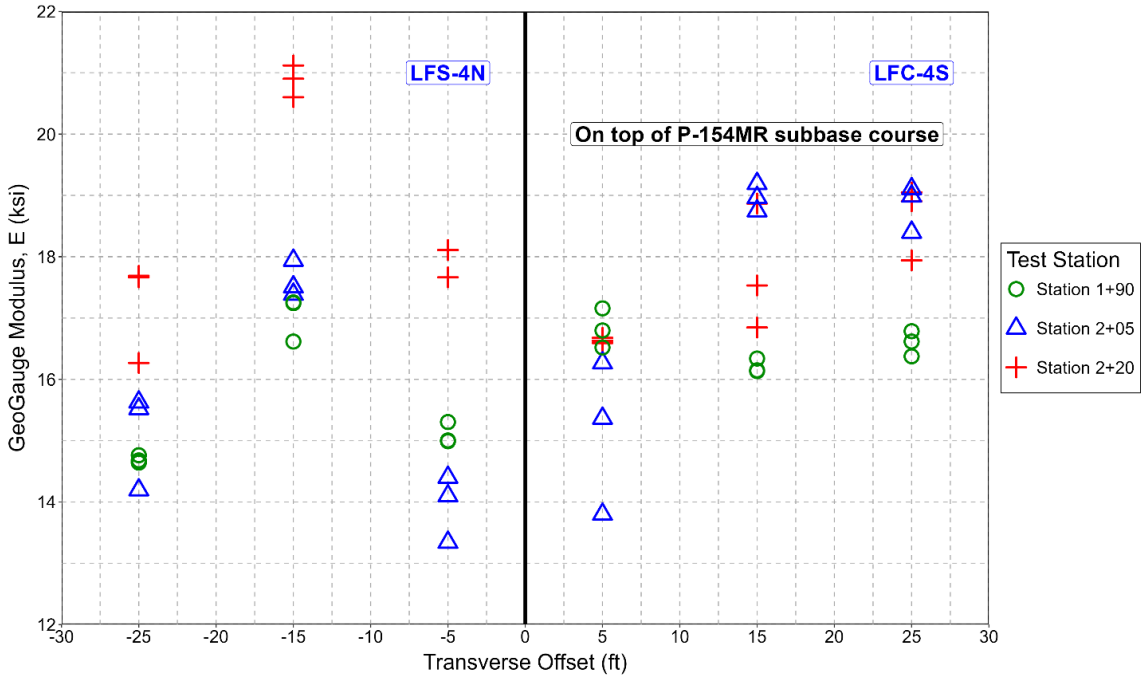

Figure 12. As-Built Subbase Modulus in Fatigue Test Items Measured with GeoGauge

2.2.3 Base Course (P-209 MR and P-307MR)

Table 5 lists summary statistics for P-209MR crushed aggregate base course material properties as placed in test item LFC-3S. Compared to Table 4, the LWD modulus at the surface of LFC-4S increased due to the addition of the crushed aggregate base. However, both seismic (D-PSPA) and GeoGauge moduli decreased slightly.

Table 6 lists summary statistics for P-307MR CTPB material properties. The material attained a 28-day flexural strength of 330 pounds per square in. (psi), approximately a 3.5% increase over the 7-day strength. Both 7-day compressive strength and coefficient of permeability exceeded the upper limits set by the P-307MR specification (Appendix E). The FAA waived these upper limit requirements when accepting the material.

Table 5. In-Place Characterization of Crushed Aggregate Base Course (P-209MR)

Property	Mean μ	Standard Deviation σ	COV (%)
Nuclear gauge density (pcf)	152.4	N/A	N/A
Nuclear gauge MC (%)	2.0	N/A	N/A
LWD modulus (ksi)	29.2	3.0	10.3
Seismic modulus (ksi)	67.6	11.0	16.3
GeoGauge modulus (ksi)	14.1	1.6	11.4

μ = Mean value, σ = Standard deviation, COV = Coefficient of variation, pcf = pounds per cubic ft, ksi = kilopound per square in.

Table 6. Material Characterization of CTPB (P-307MR)

Property	Mean μ	Standard Deviation σ	COV (%)
7-day Compressive strength[1] (psi)	1441	354	24.6
Coefficient of permeability (ft/day)	3871	N/A	N/A
7-day LWD modulus (ksi)	306.3	69.8	22.8
7-day Compressive strength[2] (psi)	1068.9	345.0	32.3
7-day Flexural strength (psi)	318.9	57.5	18.0
28-day LWD modulus (ksi)	309.3	33.0	10.7
28-day Compressive strength[3] (psi)	1118.3	318.2	28.5
28-day Flexural strength (psi)	330	55.2	16.7

[1]Cylinders were consolidated using the method described in ASTM C31.
[2]Cylinders were consolidated using the method described in ASTM C1688 and finished with a strike-off plate.
μ = Mean value, σ = Standard deviation, COV = Coefficient of variation, psi = pounds per square in., ksi = kilopound per square in.

Figure 13 plots LWD field modulus at the top of the base against contact stress and LWD drop location. Figure 13(a) and (b) show the 7-day LWD moduli for the two placement lots of the CTPB. Figure 13(c) shows 28-day LWD data for the CTPB. For comparison to CTPB, Figure 13(d) shows the LWD modulus of crushed aggregate base (P-209MR) versus contact stress. In contrast to the conventional crushed aggregate bases, the CTPB shows little or no change in modulus values with respect to the contact stresses (i.e., it is neither a stress-hardening nor stress-softening material.) The LWD modulus of CTPB was approximately 10 times that of crushed aggregate base.

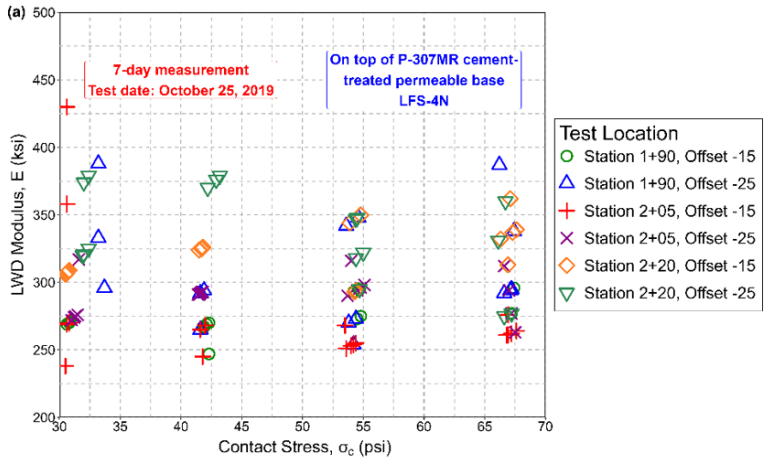

(a) CTPB Modulus, 7-day (1st Placement, LFS-4N)

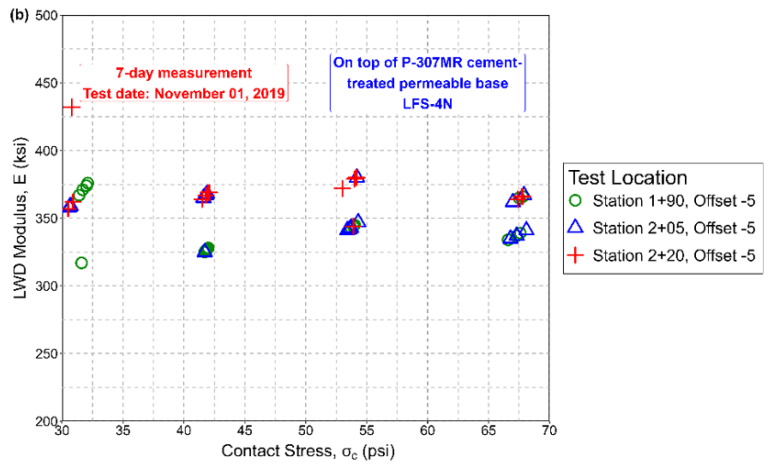

(b) CTPB Modulus, 7-day (2nd Placement, LFS-4N)

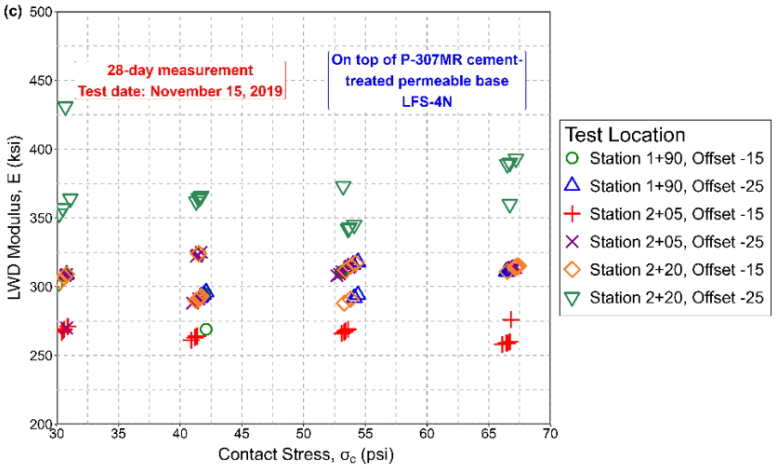

(c) CTPB Modulus, 28-day (LFS-4N)

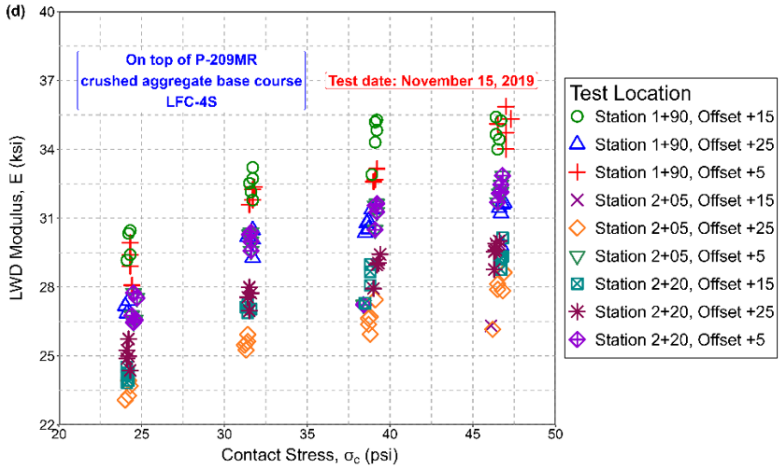

(d) Crushed Aggregate Base Course Modulus (LFC-4S)

Figure 13. As-Built Base Modulus in CTPB Test Items from LWD

2.2.4 Asphalt Concrete (P-401MR)

Table 7 summarizes the Quality Assurance/Quality Control (QA/QC) results for the asphalt concrete surface layer. Mat and joint densities were measured in situ with the nuclear gauge. Air voids were determined in the laboratory from extracted asphalt concrete cores. Seismic modulus values were measured directly on the surface using PSPA, and (as expected) were higher than the average elastic moduli backcalculated from HWD tests.

Table 7. In-Place Characterization of P-401 Asphalt Layer

Test Item	**LFS-4N**			**LFC-4S**		
Properties	**μ**	**σ**	**COV (%)**	**μ**	**σ**	**COV (%)**
Mat Density (%)	98.1	N/A	N/A	95.6	N/A	N/A
Joint Density (%)	95.6	N/A	N/A	91.2	N/A	N/A
Lab Air Voids (%)	4.1	N/A	N/A	4.1	N/A	N/A
Seismic Modulus (ksi)	3,337	104.3	3.1	3,063	221.2	7.2
Elastic Modulus (ksi)	1,194	161.2	13.5	1,494	230.8	15.5

μ = Mean value, σ = Standard deviation, COV = Coefficient of variation, pcf = pounds per cubic ft, psi = pounds per square in., ksi = kilopound per square in.

2.3 REVIEW OF INSTRUMENTATION

Embedded sensors included asphalt strain gauges (ASGs), coil sensors (CSs), pressure cells (PCs), moisture sensors, and thermocouples. Details of the installation are found in Tomlinson et al. (2022). Figure 14 and Figure 15 show the sensor layout for the CC9 CTPB test area. Appendix A lists sensor locations for each test item.

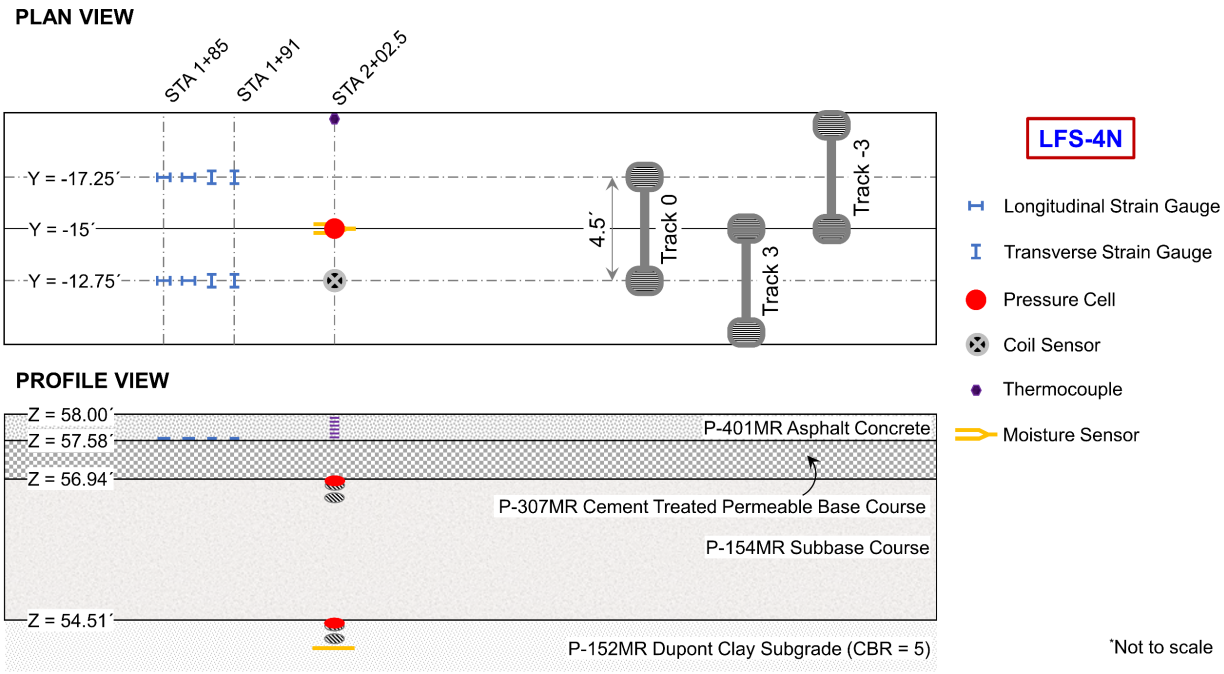

Figure 14. Layout of Instrumentation in CTPB LFS-4N

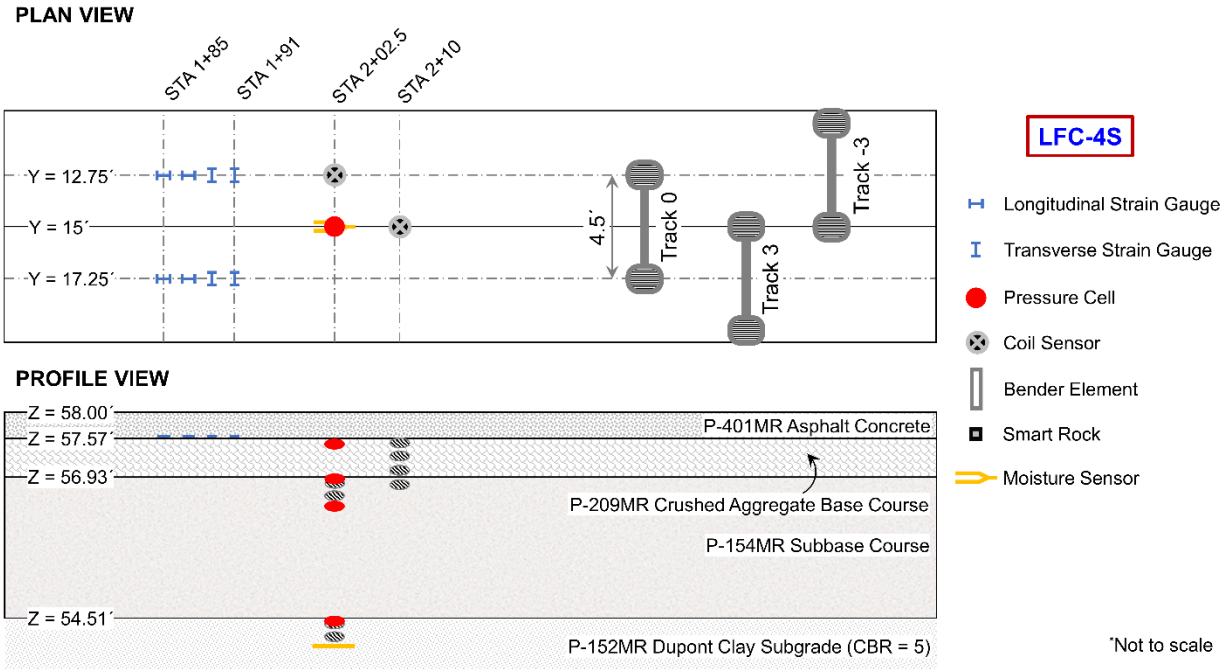

Figure 15. Layout of Instrumentation in CTPB Test Item LFC-4S

2.3.1 Asphalt Strain Gages

Four longitudinal and four transverse strain gauges were installed in each test item to monitor the tensile strain at the bottom of the asphalt concrete layer. Strain gauges were positioned at offsets from the centerline such that they received maximum wheel loads for Track 0 of the wander pattern.

2.3.2 Pressure Cells

CTPB test items had a total of six PCs—two in LFS-4N and four in LFC-4S. Each test item had one PC at the top of the subbase and one at the top of the subgrade to monitor compressive stress. Test item LFC-4S had two additional PCs, at the top of the crushed aggregate base, and 6 in. below the top of the subbase. All PCs were installed at an offset ±15 ft from the centerline, placing them at the center of the traffic area within each test item. Due to the dual-wheel configuration of the load modules, they received maximum loads for Tracks +3 and -3 of the wander pattern.

2.3.3 Coil Sensors

Paired induction CSs, spaced at approximately 3 in., were installed near the top of the granular subbase and subgrade to measure vertical deformation and strain in those layers. A "short stack" of three pairs was placed in the P-209MR base layer at zero offset (15 ft) to determine the permanent deformation in the base course of test item LFC-4S. No parallel stack was installed in LFS-4N due to the incompatibility of the sensor with the CTPB material.

The induction coil-based strain measurement system (known as ε-mu, an acronym for strain (ε) measuring unit) has been used extensively to monitor permanent deformation and strain in pavement subsurface layers. The system was originally developed by Selig and Grangaard (1970). The data acquisition process was later automated by Dawson (1994).

2.3.4 Static Sensors

A thermocouple tree consisting of six temperature probes was installed in the asphalt concrete layer of LFS-4N. A single moisture sensor was installed in the subgrade in each test item to monitor the influence of moisture on subgrade stress and strength under traffic.

3. LABORATORY MATERIAL CHARACTERIZATION

The FAA NextGen Pavement Materials Laboratory (NGPML) performed a range of laboratory tests on material samples from CC9. Tests performed under the CC9 material characterization testing program included:

- Moisture-density relations for granular materials
- Resilient modulus (M_r) of subgrade and granular materials
- Shear strength of granular materials
- Dynamic modulus of asphalt concrete
- Rutting susceptibility test results for asphalt concrete mixes

The NGPML performed M_r tests on CTPB core samples (Gemini & GDIT, 2019). The tests were questionable due to the difficulty of attaching Linear Variable Differential Transformers to the samples but gave repeatable results. Average M_r was in the range about 180 to 600 ksi, depending on the state of confinement. These values are generally consistent with the field data from Section 2.2.3. Based on the combination of M_r test results with in-situ LWD material characterization, a default value of 300,000 psi for CTPB, with a range of 200,000 to 400,000 psi, is reasonable for design. For laboratory characterization of the other pavement layers, *NAPTF CC9, Volume 3—Geosynthetic Test* provides a summary of the tests performed and the results (Kazmee et al., 2026b).

4. TRAFFIC TESTS ON CTPB TEST ITEMS

4.1 PRE-TRAFFIC TESTS

4.1.1 Slow-Roll Response Tests

The slow-roll response test was executed November 6–20, 2020, on the CTPB test items LFS-4N and LFC-4S. Pavement responses (stresses, strains, and deflections) were recorded for the following gear configurations: S, D, Two Duals in Tandem (2D), and Three Duals in Tandem (3D). The response test variable matrix was as follows:

- Vehicle speed (mph): 0.5, 1.6, 2.5
- Gear offset from centerline (ft): ±8.25, ±10.50, ±12.75, ±15.00, ±17.25, ±19.50
- Wheel Loads (lb): 12,000, 24,000, 36,000
- Tire Pressure: 255 psi
- Passes: 2 passes for each wheel load at each offset (one forward, one return).

Sensor functionality was assessed under various loads and speeds. Observations from the slow-roll response tests are discussed in the traffic testing summary report (CC9 Technical Report Vol. 1) (Kazmee et al., 2026a). Table 8 lists the operational status of all dynamic sensors in CTPB test items at the end of the slow-roll test. (Refer to Appendix A for sensor locations). As shown in Table 8, most of the sensors survived, except the four longitudinal ASGs in LFS-4N.

CS responses were evaluated for pairs of adjacent sensors (e.g., CS-LFS4N-1/2 is the response of paired sensors CS-LFS4N-1 and CS-LFS4N-2). All CS pairs in CTPB test items were operational at the start of the test, but the quality of the data varied. As discussed in *NAPTF CC9, Volume 1—Traffic Test Summary* of this report series, significant postprocessing of the CS response data was necessary to extract meaningful data (Kazmee, et al. 2026a).

Table 8. Status of Dynamic Sensors Following Slow-Roll Test (November 20, 2020)

Test Item LFS-4N		Test Item LFC-3S	
Sensor	Status	Sensor	Status
CS-LFS4N-1/2	OK	CS-LFC4S-1/2	OK
CS-LFS4N-3/4	OK	CS-LFC4S-3/4	OK
LSG-LFS4N-1	Failing	CS-LFC4S-5/6	OK
LSG-LFS4N-2	Failing	CS-LFC4S-6/7	OK
LSG-LFS4N-3	Failed	CS-LFC4S-7/8	OK
LSG-LFS4N-4	Failed	LSG-LFC4S-1	OK
PC-LFS4N-1	OK	LSG-LFC4S-2	OK
PC-LFC4N-2	OK	LSG-LFC4S-3	OK
TSG-LFS4N-1	OK	LSG-LFC4S-4	OK
TSG-LFS4N-2	OK	PC-LFC4S-1	OK
TSG-LFS4N-3	OK	PC-LFC4S-2	OK
TSG-LFS4N-4	OK	PC-LFC4S-3	OK
-	-	PC-LFC4S-4	OK
-	-	TSG-LFC4S-1	OK
-	-	TSG-LFC4S-2	OK
-	-	TSG-LFC4S-3	Failing
-	-	TSG-LFC4S-4	OK

TSG = Transverse strain gauge; LSG = Longitudinal strain gauge

Although Table 8 shows all four transverse strain gauges (TSGs) in LFS-4N as operational, the responses from these sensors were generally noisier than those from the four TSGs in LFC-4S (see Figure 16). The response from both sets of TSGs was characterized by a significant difference between the starting and ending strain (the unrecovered part). Therefore, the magnitude of peak asphalt strain depends on whether it is calculated with reference to the starting strain value (offset left) or ending strain value (offset right) for the pass. Figure 16 and Figure 17 show examples of ASG slow-roll test data. In Figure 17, the peak strains are relative to the "offset right" and may be considered to represent recovered strain. Figure 17 shows the general trend where, as expected, increasing wheel load and decreasing vehicle speed both correspond to increasing peak tensile strain in the bottom of the asphalt layer. For the same load conditions, the strain magnitudes are much lower for LFS-4N (on CTPB) than for LFC-3S (standard base). In contrast to LFC-4S (Figure 17(b)), LFS-4N showed little or no sensitivity of the asphalt peak strain to vehicle speed, especially at higher wheel loads (Figure 17(d)).

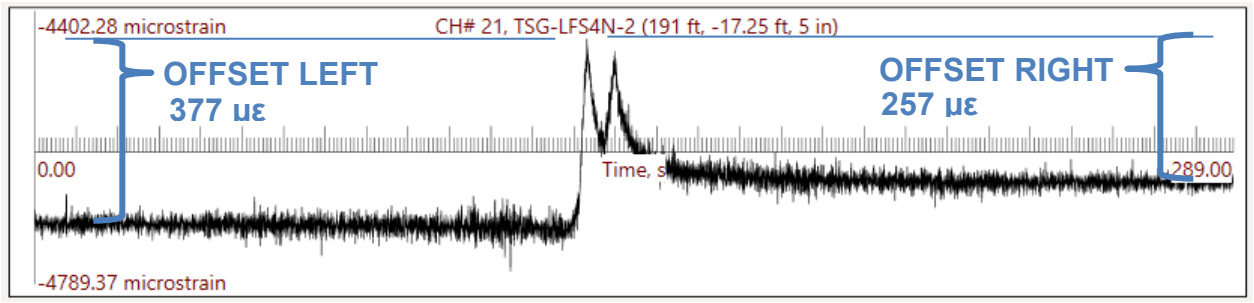

(a) TSG-LFS-4N-2

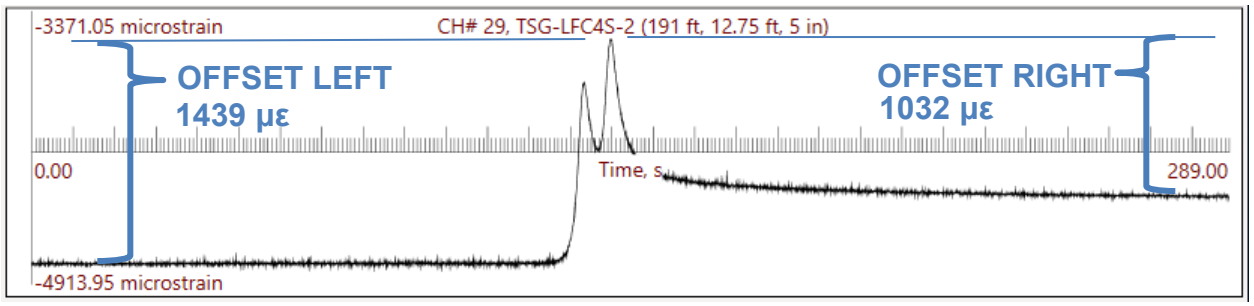

(b) TSG-LFC-4S-2

Figure 16. Slow-Roll TSG Responses (2D gear, 36,000 lb/wheel, 5 mph), Test Conducted November 17, 2022

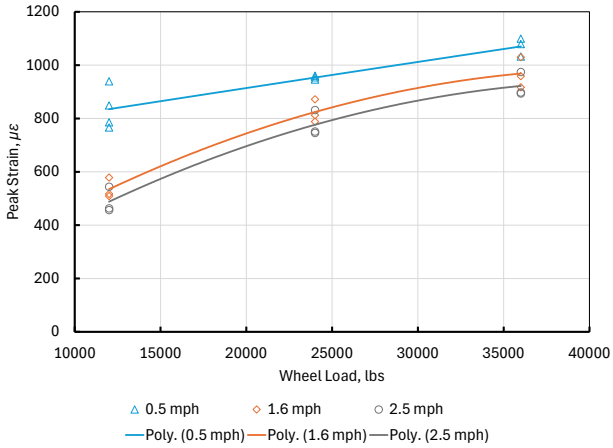

(a) LFC-4S – TSG Strain versus Wheel Load

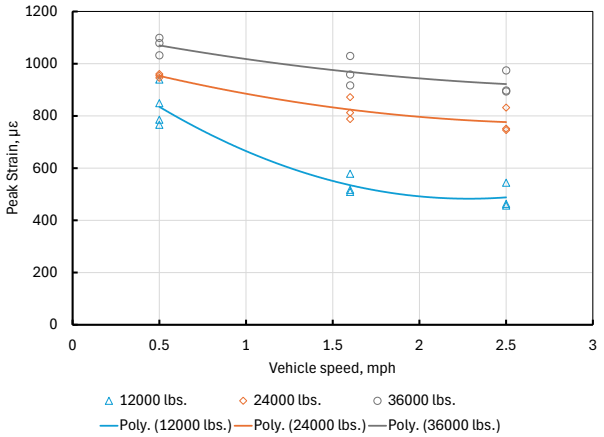

(b) LFC-4S – TSG Strain versus Vehicle Speed

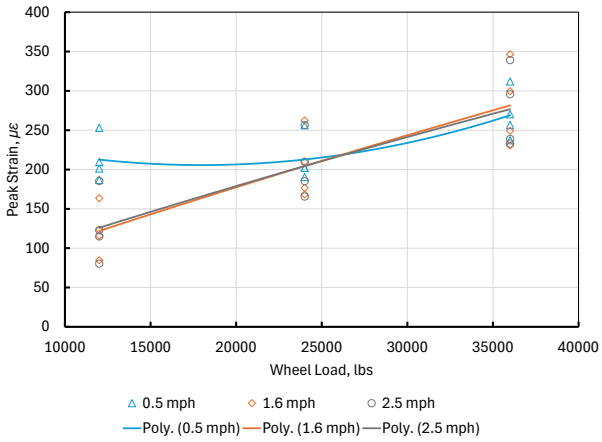

(c) LFS-4N – TSG Strain versus Wheel Load

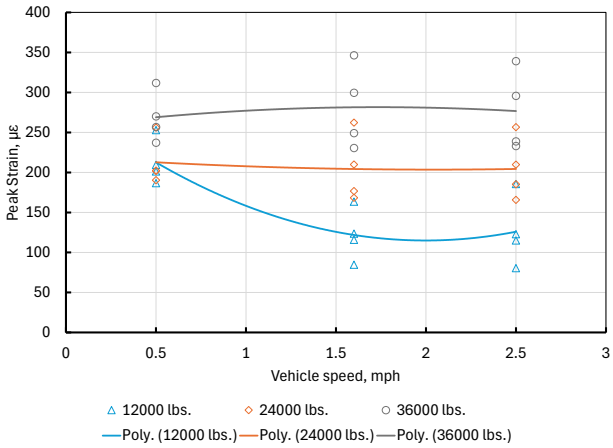

(d) LFS-4N – TSG Strain versus Vehicle Speed

Figure 17. Peak Strains from TSG in CTPB Test Items, Slow-Roll Test

4.1.2 Proof Roll

A proof-roll sequence was applied using the carriage positions in Table 9 and Figure 18. As expected, the magnitudes of peak stresses and strains decreased with increasing lateral distance between the embedded sensor and loading wheel. Proof-rolling used a D gear at 20,000 lb per wheel.

Table 9. Carriage Positions for Each Pass of Proof Roll

Pass Sequence	Direction	Carriage Centerline Location (ft)	
		North	South
1	W–E	-19.34	2.68
2	E–W	-19.34	2.68
3	W–E	-18.507	3.513
4	E–W	-18.507	3.513
5	W–E	-17.674	4.346
6	E–W	-17.674	4.346
7	W–E	-16.841	5.179
8	E–W	-16.841	5.179
9	W–E	-16.008	6.012
10	E–W	-16.008	6.012
11	W–E	-15.175	6.845
12	E–W	-15.175	6.845
13	W–E	-14.342	7.678
14	E–W	-14.342	7.678
15	W–E	-13.509	8.511
16	E–W	-13.509	8.511
17	W–E	-12.676	9.344
18	E–W	-12.676	9.344
19	W–E	-11.843	10.177
20	E–W	-11.843	10.177
21	W–E	-11.01	11.01
22	E–W	-11.01	11.01
23	W–E	-10.177	11.843
24	E–W	-10.177	11.843
25	W–E	-9.344	12.676
26	E–W	-9.344	12.676
27	W–E	-8.511	13.509
28	E–W	-8.511	13.509
29	W–E	-7.678	14.342
30	E–W	-7.678	14.342
31	W–E	-6.845	15.175
32	E–W	-6.845	15.175
33	W–E	-6.012	16.008
34	E–W	-6.012	16.008
35	W–E	-5.179	16.841
36	E–W	-5.179	16.841
37	W–E	-4.346	17.674
38	E–W	-4.346	17.674
39	W–E	-3.513	18.507
40	E–W	-3.513	18.507
41	W–E	-2.68	19.34
42	E–W	-2.68	19.34

W = West, E = East

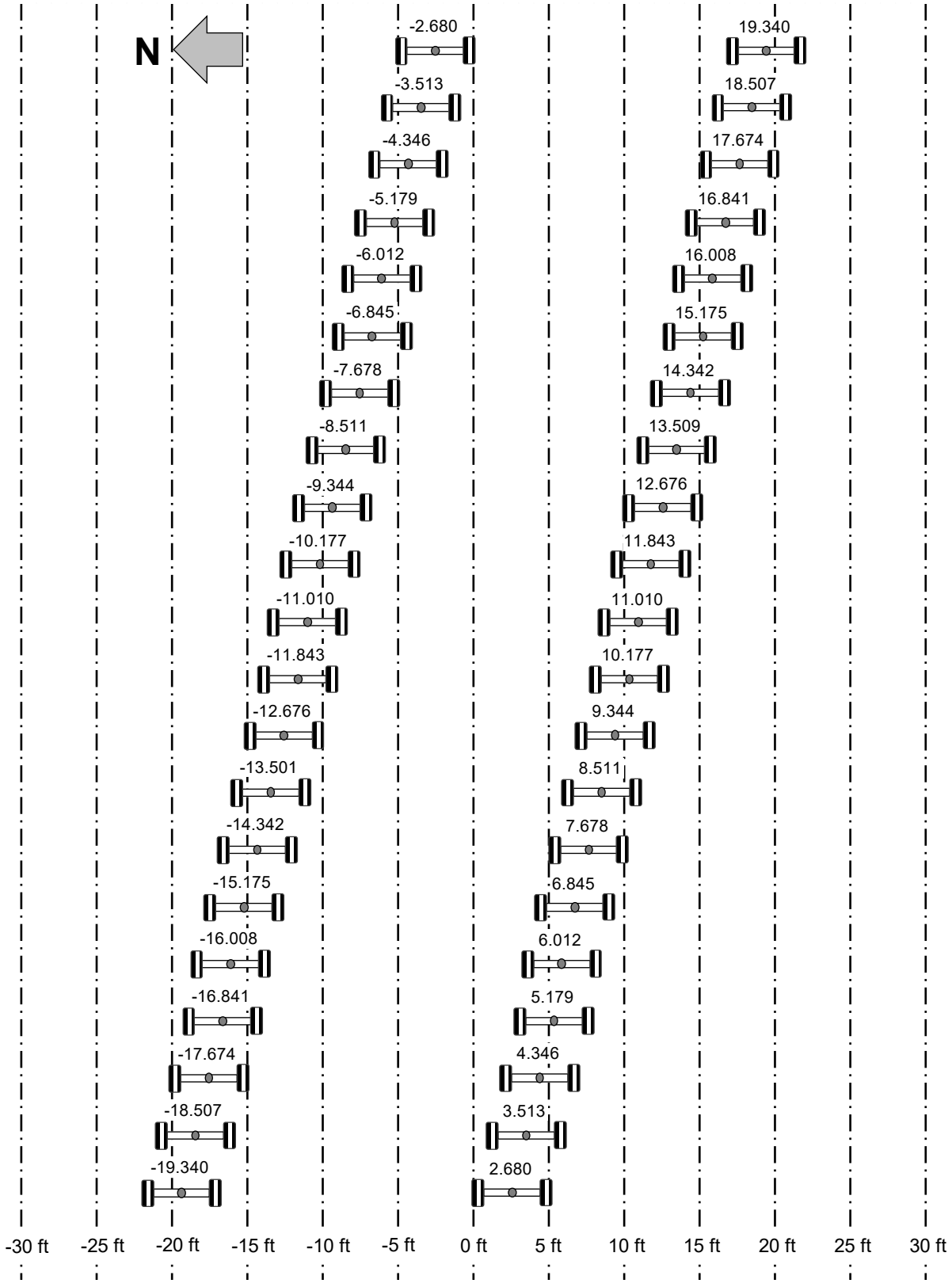

Figure 18. Carriage Positions for Each Pass of Proof Roll

4.2 TRAFFIC TESTING AND MONITORING

4.2.1 Wander Pattern

The wander pattern consisted of 66 passes arranged in 9 wheel tracks, as shown in Table 10 and Figure 19. Passes were in both directions, west-to-east (odd) and east-to west (even). The even-numbered (return) pass was always along the same track as the preceding odd-numbered pass, but in the opposite direction. The complete wander pattern is listed in Table 11.

Table 10. Construction Cycle 9 Traffic Wander Wheel Track Locations

Track No.	Carriage Centerline Location, ft	
	North	South
-4	-18.412	11.588
-3	-17.559	12.441
-2	-16.706	13.294
-1	-15.853	14.147
0	-15.000	15.000
1	-14.147	15.853
2	-13.294	16.706
3	-12.441	17.559
4	-11.588	18.412

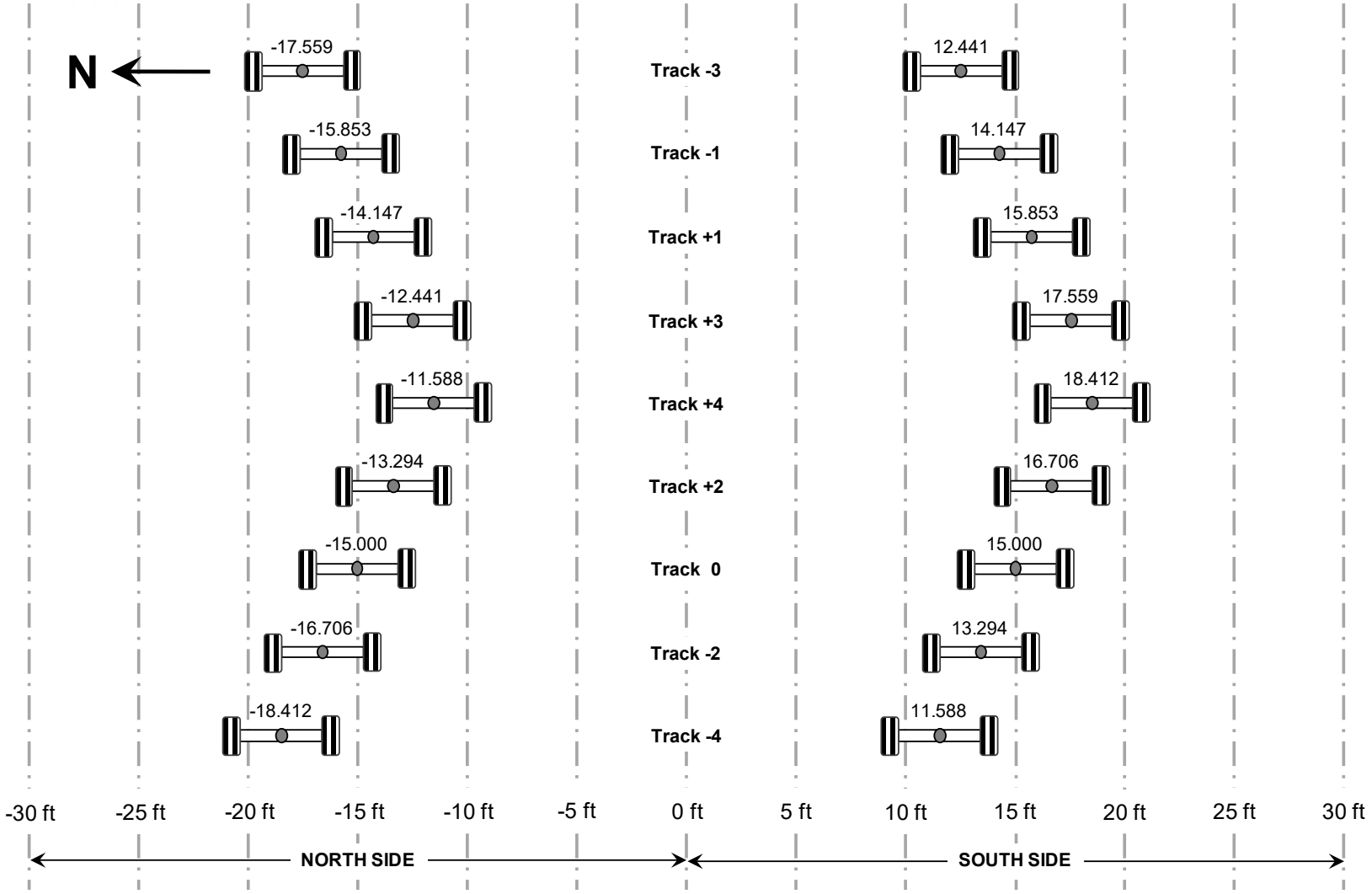

Figure 19. Construction Cycle 9 Traffic Wander Wheel Tracks

Table 11. Cconstruction Cycle 9 Complete Wander Sequence

Pass Sequence	Direction	Track No.	Carriage Centerline Location (ft)	
			North	South
1	W–E	-4	-18.412	11.588
2	E–W	-4	-18.412	11.588
3	W–E	-2	-16.706	13.294
4	E–W	-2	-16.706	13.294
5	W–E	0	-15.000	15.000
6	E–W	0	-15.000	15.000
7	W–E	2	-13.294	16.706
8	E–W	2	-13.294	16.706
9	W–E	4	-11.588	18.412
10	E–W	4	-11.588	18.412
11	W–E	3	-12.441	17.559
12	E–W	3	-12.441	17.559
13	W–E	1	-14.147	15.853
14	E–W	1	-14.147	15.853
15	W–E	-1	-15.853	14.147
16	E–W	-1	-15.853	14.147
17	W–E	-3	-17.559	12.441
18	E–W	-3	-17.559	12.441
19	W–E	-4	-18.412	11.588
20	E–W	-4	-18.412	11.588
21	W–E	-2	-16.706	13.294
22	E–W	-2	-16.706	13.294
23	W–E	0	-15.000	15.000
24	E–W	0	-15.000	15.000
25	W–E	2	-13.294	16.706
26	E–W	2	-13.294	16.706
27	W–E	4	-11.588	18.412
28	E–W	4	-11.588	18.412
29	W–E	3	-12.441	17.559
30	E–W	3	-12.441	17.559
31	W–E	1	-14.147	15.853
32	E–W	1	-14.147	15.853
33	W–E	-1	-15.853	14.147
34	E–W	-1	-15.853	14.147
35	W–E	-3	-17.559	12.441
36	E–W	-3	-17.559	12.441
37	W–E	3	-12.441	17.559
38	E–W	3	-12.441	17.559
39	W–E	1	-14.147	15.853
40	E–W	1	-14.147	15.853
41	W–E	-1	-15.853	14.147
42	E–W	-1	-15.853	14.147
43	W–E	-3	-17.559	12.441
44	E–W	-3	-17.559	12.441
45	W–E	-2	-16.706	13.294
46	E–W	-2	-16.706	13.294
47	W–E	0	-15.000	15.000
48	E–W	0	-15.000	15.000
49	W–E	2	-13.294	16.706
50	E–W	2	-13.294	16.706
51	W–E	-2	-16.706	13.294
52	E–W	-2	-16.706	13.294
53	W–E	0	-15.000	15.000
54	E–W	0	-15.000	15.000
55	W–E	2	-13.294	16.706
56	E–W	2	-13.294	16.706
57	W–E	1	-14.147	15.853
58	E–W	1	-14.147	15.853
59	W–E	-1	-15.853	14.147
60	E–W	-1	-15.853	14.147
61	W–E	1	-14.147	15.853
62	E–W	1	-14.147	15.853
63	W–E	-1	-15.853	14.147
64	E–W	-1	-15.853	14.147
65	W–E	0	-15.000	15.000
66	E–W	0	-15.000	15.000

W = West, E = East

4.2.2 Failure Criteria

Ahlvin et al. (1971) defined failure as the earlier of:

(i) Surface upheaval of the pavement adjacent to the traffic wander exceeded 1 in. or
(ii) Surface cracking so severe that the pavement no longer remained waterproof.

The same failure criteria were adopted in all preceding flexible pavement construction cycles.

4.2.3 Traffic History

Table 12 lists the key events during CC9 trafficking with dates. Traffic on the CTPB test items, LFS-4N and LFC-3S, is highlighted in yellow. For all passes, the NAPTV was configured as a 3D gear with a wheel load of 58,000 lb and nominal tire pressure of 255 psi.

Table 12. Key Events During CC9 Trafficking

Dates	Passes on Test Items			Load Description
	LFS-1/2	LFC-3/4	LFC-5	
4/5/2021–6/3/2021	5,544	5,544	0	Traffic test items 1–4
7/1/2021	0	0	66	1st Overload LFC-5N
7/1/2021–7/28/2021	0	0	5,478	Traffic LFC-5 only
8/2/2021–10/14/2021	7,066	7,066	7,066	Traffic all test items
10/15/2021–2/21/2022	0	0	0	Vehicle down for maintenance
2/22/2022–3/28/2022	3,956	3,956	3,956	Resume traffic all test items
3/29/2022	0	0	66	2nd overload LFC-5N
3/29/2022–10/5/2022	24,354	24,354	24,288	Traffic all test items
10/12/2022	0	0	396	3rd overload LFC-5N
10/13/2022–12/21/2022	0	0	15,312	Traffic LFC-5 only
1/3/2023–3/29/2023	13,728	0	0	Traffic test items LFS-1/2
1/25/2024–4/2/2024	20,460	0	0	Traffic test items LFS-1/2
Total	75,108	40,920	56,628	

4.2.4 Routine Monitoring and Testing

4.2.4.1 Dynamic Responses

Dynamic responses are sensor responses triggered by an NAPTV pass. Dynamic responses included:

- Horizontal strains (bottom of HMA layer)
- Permanent deformations using coil sensors
- Vertical stresses from pressure cells

4.2.4.2 Static Responses

Sensor responses were collected hourly. Static sensor responses included temperature and moisture data. Subgrade moisture sensors (MSs) record volumetric moisture content. Volumetric moisture content θ_v measured with the embedded gauges may be converted to gravimetric moisture content using the formula:

$$w = \theta_v \times \frac{\rho_{water}}{\rho_{soil}} \quad (2)$$

where:

w = gravimetric moisture content,
ρ_{water} = density of water, and
ρ_{soil} = laboratory-determined dry density of subgrade soil.

4.2.4.3 Manual Distress Survey

Visual distress surveys were performed daily in accordance with ASTM D5340 (ASTM, 2020), after each day's traffic. In addition to the standard survey data, technicians marked and measured very fine cracks (i.e., those that would be disregarded in a standard condition survey). All cracks were marked on the surface, and the beginning and end coordinates of the cracks were recorded to track their progression. Appendix C presents logs of observed cracks for the two test items that constitute the CTPB test. The inspector prepared detailed reference maps for each inspection, in which the cracks were color-coded, identifying the date first observed and the associated number of passes. Thus, new crack initiation and propagation of existing cracks were tracked using the color-coded maps. Appendix D contains distress maps for both test items.

4.2.4.4 Straightedge Rut Measurement

To monitor the accumulation of surface ruts, transverse surface profiles were measured with a 16-ft straightedge in accordance with ASTM E1703 (ASTM, 2015). The maximum rut depth value along the full length of the beam was measured with a dial gauge and recorded. This measurement was performed at two stations within each test item. Ruts were measured at the end of each trafficking day.

4.2.4.5 Portable Seismic Properties Analyzer and Heavy Weight Deflectometer Test

HWD and PSPA tests were conducted at two-week intervals during testing to monitor structural changes. HWD testing was conducted with a four-drop loading sequence beginning with a nominal 36,000-lb seating load, followed by 12,000-lb, 24,000-lb, and 36,000-lb (nominal) loads. Deflection basin parameters were normalized to the 36,000-lb load level. HWD tests were conducted at two stations and three lateral offsets (±5 ft, ±15 ft, ±25 ft) in each test item. Tests at the ±15-ft offset location represented the center of traffic, while the other offsets were in the non-trafficked areas.

4.2.4.6 Three-Dimensional Laser Scanning

Three-dimensional laser scanning using a Leica ScanStation P20 was used to track the relative change in surface elevations over time. Light Detection and Ranging (LiDAR) scans were conducted prior to trafficking and during trafficking at a regular interval to track changes in surface elevation with traffic. For each measurement set, a proprietary design and documentation software (AutoCAD® 3D) was used to generate the Cartesian coordinates from the random three-dimensional-point cloud elevations. The resulting 1-in. regularly spaced coordinates were then input into a C# programming language-based software (named SurfaceD) to compute a three-dimensional surface map, transverse profiles, and surface upheaval magnitudes.

4.2.5 Routine Performance Measurements

4.2.5.1 Crack Growth

Crack maps developed during the manual distress survey were reviewed to track the first appearance and progress of cracks. Surface distresses included longitudinal cracks in the trafficked area that later developed into alligator cracks. For each test item, lengths of individual cracks and areas of alligator cracks were carefully measured and recorded in a schematic as they appeared.

4.2.5.2 Crack Density

Crack density (CD) is a metric for damage quantification and is defined as the portion of pavement surface that is occupied by distresses. A grid of uniform elements or units was established for each test item. If any portion of a unit is distressed, the entire unit area is considered distressed. The CD area is determined by counting the number of units exhibiting distresses. Therefore, the accuracy of CD increases with the number of discrete units within the area of interest. Crack measurements with an adequately small unit size can ensure a true representation of the distressed surface. Following CC7 practices (Garg et al., 2020), the CDs of CC9 test items were computed using 1×1-ft unit size in the traffic area only.

5. TEST RESULTS AND DISCUSSION

This chapter covers the following topics:

- Section 5.1 discusses surface distresses: surface upheaval, surface rutting, and cracking.
- Section 5.2 discusses dynamic sensor responses: ASG, PC, and CS.
- Section 5.3 discusses results from nondestructive testing (NDT).

5.1 SURFACE DISTRESS MONITORING

5.1.1 Upheaval and Rutting

Surface upheaval outside of the trafficked area greater than approximately 1 in. is a key indicator of structural failure (Section 4.2.2). Figure 20 plots the development of upheaval in both test items at two stations, STA 1+95 and STA 2+10. In Figure 20, the maximum upheavals were

computed from transverse profile data using a software procedure called Virtual Upheaval Calculator (VUC). VUC computed upheaval relative to a baseline (pre-traffic) profile, where both profiles (current and baseline) were extracted from three-dimensional laser surveys of the pavement surface (Section 4.2.4.6). Details of the VUC procedure are found in Mazzotta et al. (2024).

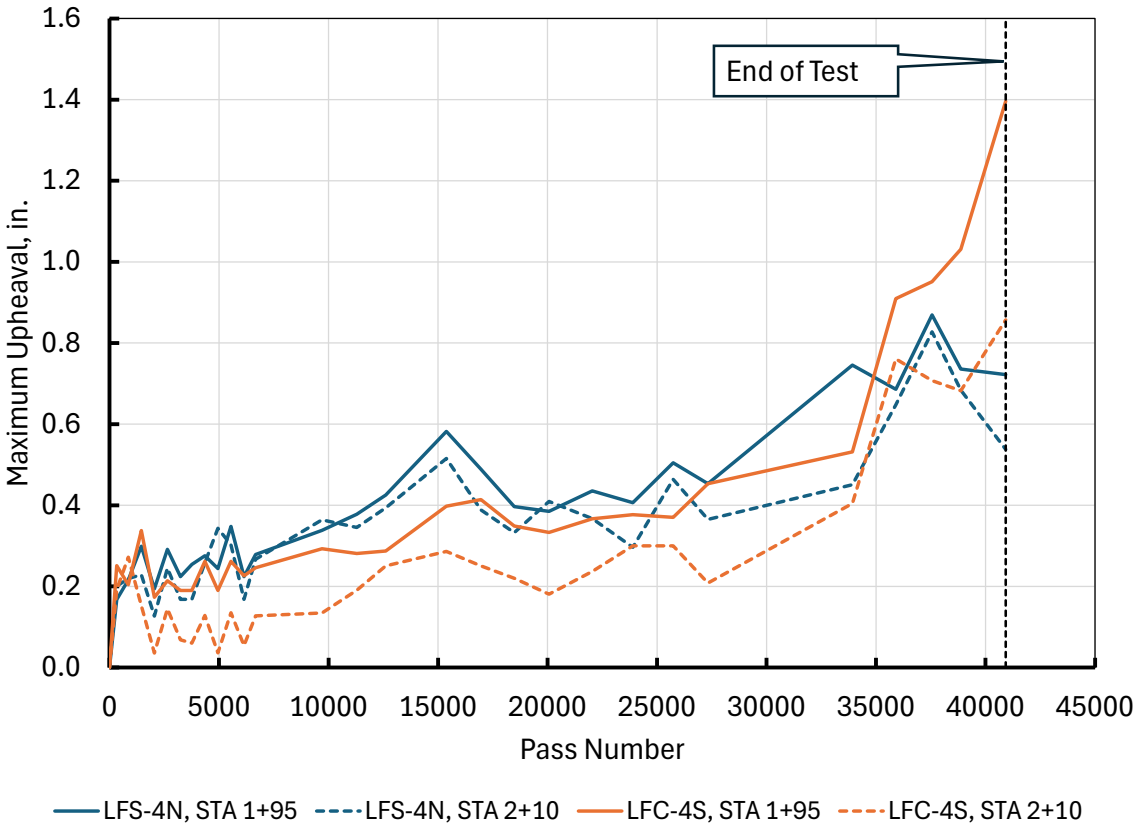

Figure 20. Maximum Upheaval from VUC in CTPB Test Items

Appendix B lists the surface upheaval data for the CTPB test items. As shown in Figure 20, test item LFC-4S failed according to the technical criterion (i) in Section 4.2.2, passing the 1-in. threshold at STA 1+95 after approximately 38,000 passes. Test item LFS-4N did not fail according to this criterion. However, Figure 20 shows that for most of the test, the upheaval in LFS-4N tracked closely with LFC-4S, and the final upheaval (~ 0.8 in.) near the failure criterion. Complicating the analysis, small variations in computed upheaval (less than about 0.25 in.) may be due to nonstructural factors including lateral displacement of the asphalt surface material under wandered traffic, surface macrotexture, and inherent limitations of the VUC procedure, and do not necessarily reflect true structural layer damage. Figure 21 shows the extent of deformation in test item LFS-4N at the end of the test.

Figure 21. Deformed Surface of the CTPB Test Item After 40,920 Passes (November 3, 2022)

Another key measure of structural performance is straightedge rutting. CC9 rut depths were (a) measured physically using a 16-ft physical straightedge (PSE), and (b) computed from transverse profile data using a 16-ft virtual straightedge (VSE) computer program. The transverse profiles were extracted from three-dimensional laser surveys (Section 4.2.4.6). For comparison, Figure 22 plots both types of rut data against traffic passes and against time for the two CTPB test items. Mazzotta et al. (2024) gives a full description of the rut depth determination. Mazzotta et al. (2024) noted that "typically, the VSE values are higher than PSE, which is reasonable since the straightedge operator must physically search for the maximum rut depth location and may not find it, while the VSE program can find the absolute maximum rut depth location automatically." Note that both PSE and VSE rut depths are determined from the current profile geometry alone and, unlike computed upheaval values, are not relative to a baseline condition. Thus, straightedge rut depths at the start of the test are small but nonzero, reflecting the fact that the initial transverse profiles were not perfectly flat. Figure 22 shows very little difference in rut accumulation between the two test items. The CTPB did not improve rutting performance compared to the standard base. Figure 22(a) and (b) appear to show a three-phase progression of rutting: initial rutting up to 12,500 passes, followed by an extended period of stability, then the beginning of failure. However, a closer look at Figure 22(c) and Figure 22(d) suggests that the periods of significant rutting are associated with higher ambient temperatures in the NAPTF during the summer months.

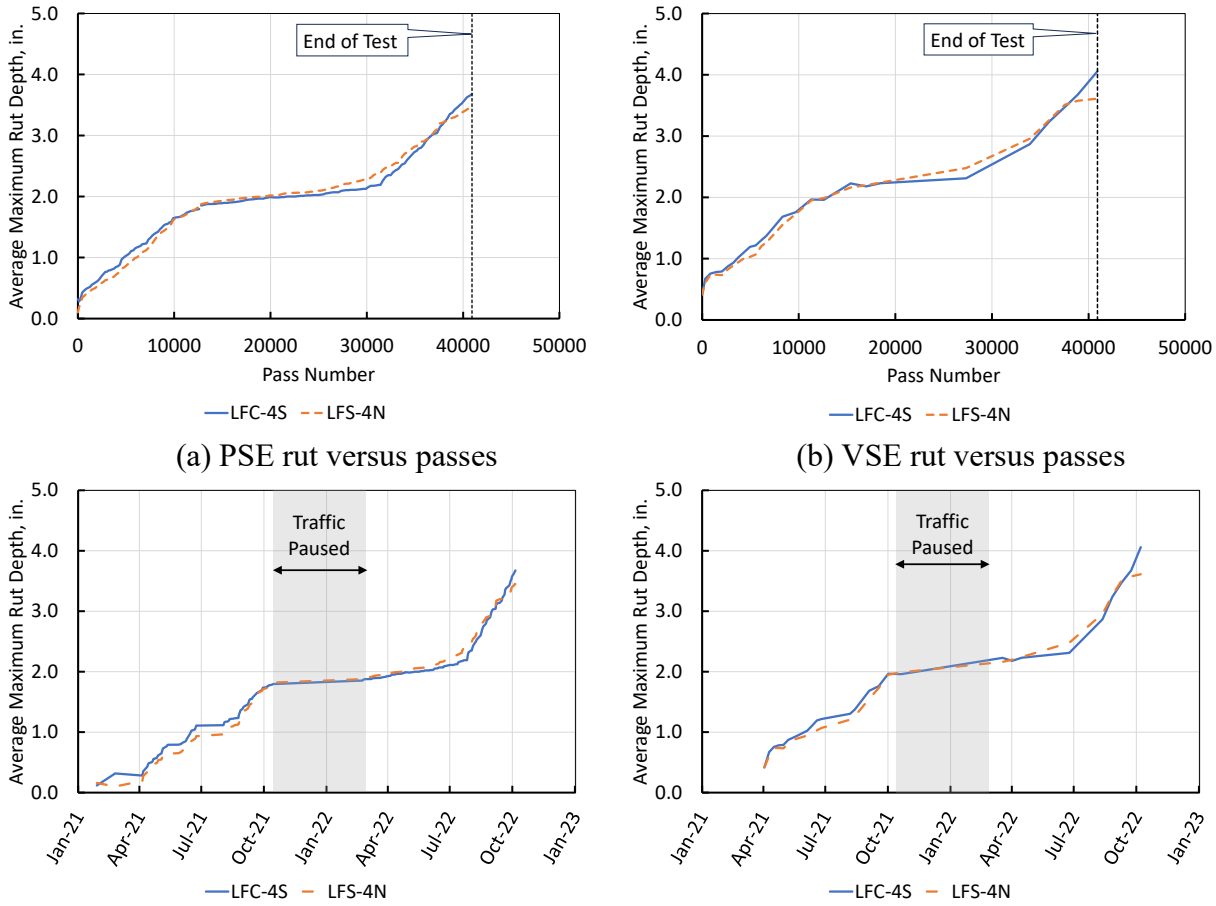

(a) PSE rut versus passes

(b) VSE rut versus passes

(c) PSE rut versus time

(d) VSE rut versus time

Figure 22. Straightedge Rut Depth in CTPB Test Items
(Values plotted are averages of rut depths determined at STA 1+95 and STA 2+10.)

5.1.2 Cracking

Engineers performed regular visual surveys on the test items to track surface distresses. Data acquired from visual surveys were added to crack maps (Appendix D). Using the distress mapping data, engineers calculated cracking areas and CD for the three test items. Following the procedure in Section 4.2.5, the test item surface was divided into 1-ft squares. Because each test item is 30×45 ft, there are 1,350 squares. To calculate CD, a square was considered damaged if at least one marked crack impinged on it. Table 13 summarizes the CD data by test item. Figure 23 shows the relationship between traffic and CD. The data are well-fitted by a four-parameter generalized logistic trend line, also known as a Richards model, of the following form:

$$\mathrm{CD} = \frac{a}{\left(1+exp(b-c\times N)\right)^{(1/d)}} \tag{3}$$

where N is the pass number, and a, b, c, and d are parameters, as given in Table 14.

Table 13. Surface Cracking Data from Crack Maps

Date	Pass No.	Cracked Area, SF		CD, Percent	
		LFC-4S	LFS-4N	LFC-4S	LFS-4N
04/22/2022	19470	76	2	5.63	0.15
04/29/2022	20064	90	9	6.67	0.67
05/05/2022	21120	132	16	9.78	1.19
05/27/2022	23826	160	20	11.85	1.48
06/15/2022	26532	171	20	12.67	1.48
07/01/2022	28314	202	23	14.96	1.70
07/22/2022	31218	205	25	15.19	1.85
08/11/2022	33924	209	25	15.48	1.85
08/26/2022	35904	212	28	15.70	2.07
09/22/2022	38874	245	30	18.15	2.22
10/07/2022	40722	255	31	18.89	2.30

Table 14. Parameters for Generalized Logistic Growth Model (Equation 3)

Parameter	LFC-4S	LFS-4N
a	1.82E+01	2.14E+00
b	9.63E-01	2.57E+00
c	1.65E-04	2.31E-04
d	1.00E-01	1.00E-01

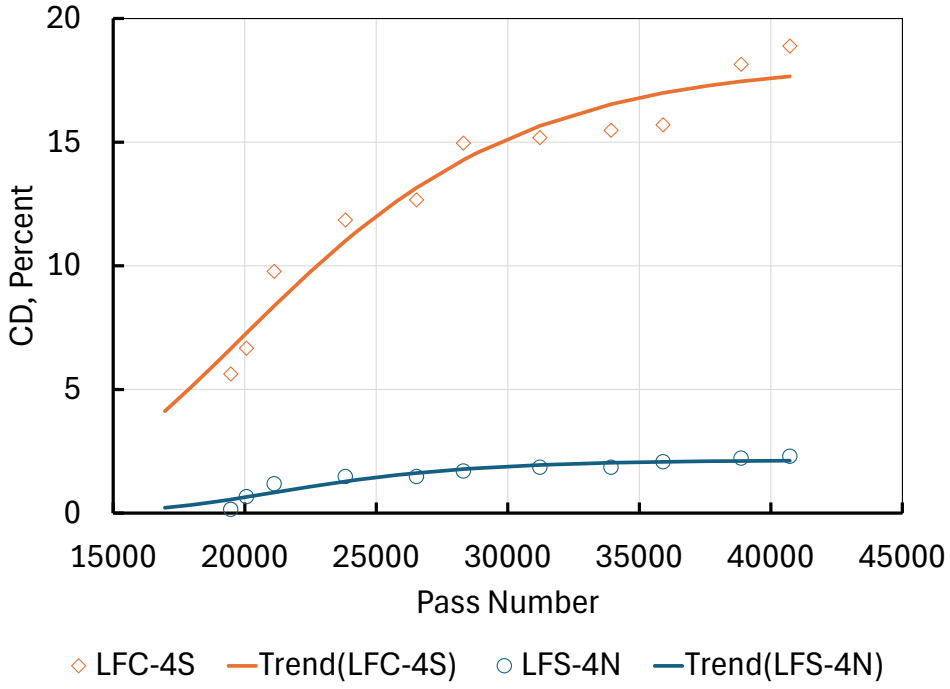

Figure 23. Variation of Crack Densities with Traffic in Test Items LFS-4N and LFC-4S

Figure 23 shows that crack growth was much higher in LFC-4S (control) than in LFS-4N (CTPB). The logistical model (Equation 3) that fits the available CD data has a mathematical upper bound represented by the parameter *a*. However, this does not mean that even larger values of CD would not be possible with additional traffic. Due to the definition of CD and the fact that the trafficked area of the test item covered approximately 12 ft of the 30-ft width, the natural upper limit of CD is about 12/30, or 40% (assuming that every 1-ft square in the traffic area has a visible crack). As shown in Section 6, CD values approaching 35% were observed in CC7 test items.

5.2 SENSOR RESPONSES

5.2.1 Asphalt Strain

Figure 24 and Figure 25 plot peak load-induced tensile strains from the start of the test up to 8,000 passes, at which point most of the sensors had failed due to large surface deformations. Graphs (a) and (c) show peak strain versus passes for longitudinal strain gauges (LSGs) and TSGs respectively, while graphs (b) and (d) plot peak strain against asphalt temperature. All temperature readings were taken at T-LFS-4N-6 and represent the hourly reading closest to the timestamp on the strain gage reading. For both test items, the peak longitudinal strain magnitude increased with increasing asphalt temperature, as expected. However, peak transverse strains did not show a strong correlation with temperature, even showing a weak negative trend in LFS-4N, as shown in Figure 24(d)

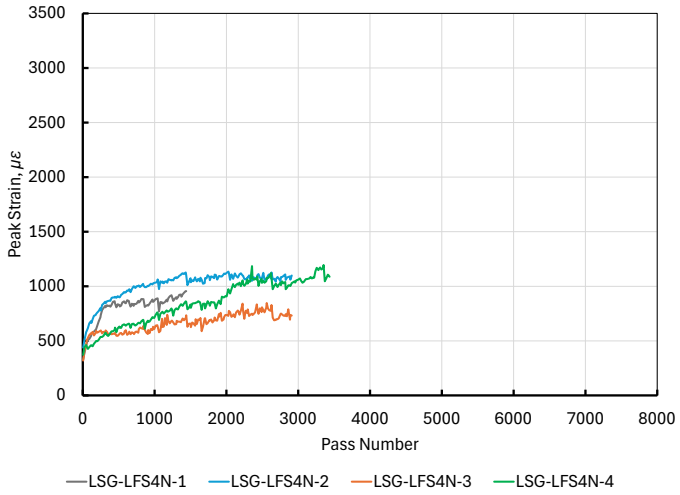

(a) Peak longitudinal strain versus passes

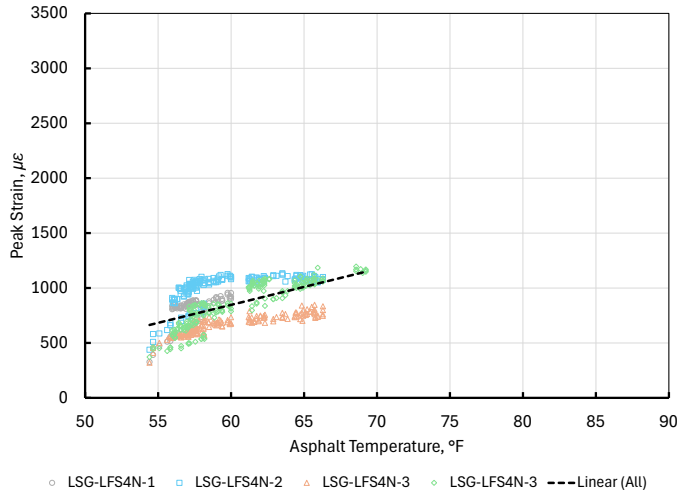

(b) Peak longitudinal strain versus asphalt temperature

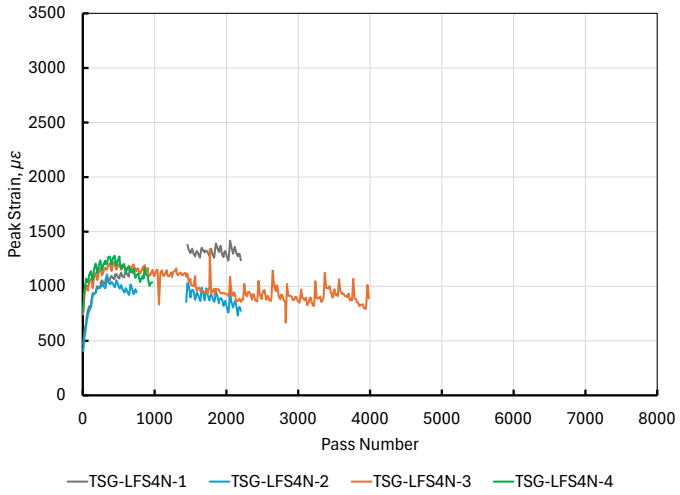

(c) Peak transverse strain versus passes

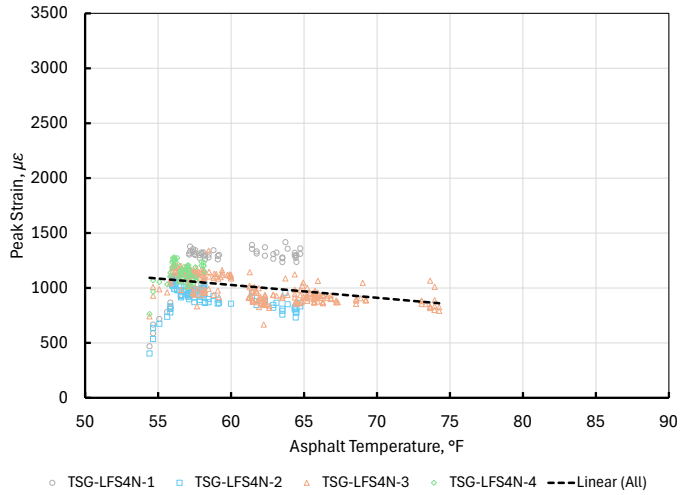

(d) Peak transverse strain versus asphalt temperature

Figure 24. Peak Tensile Strains at the Bottom of the Asphalt Layer, Test Item LFS-4N

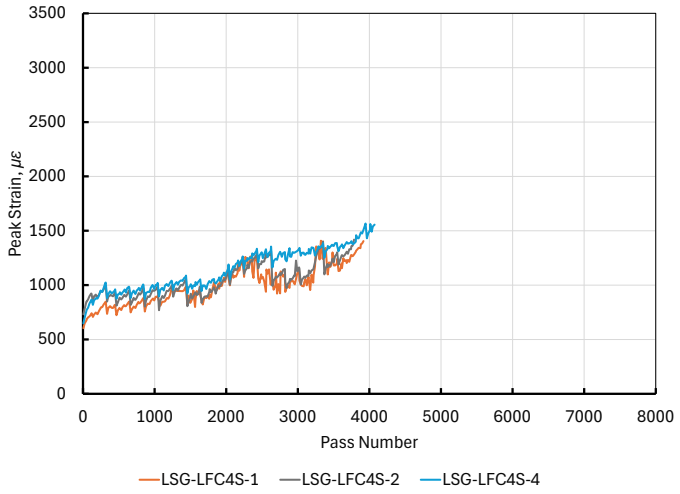

(a) Peak longitudinal strain versus passes

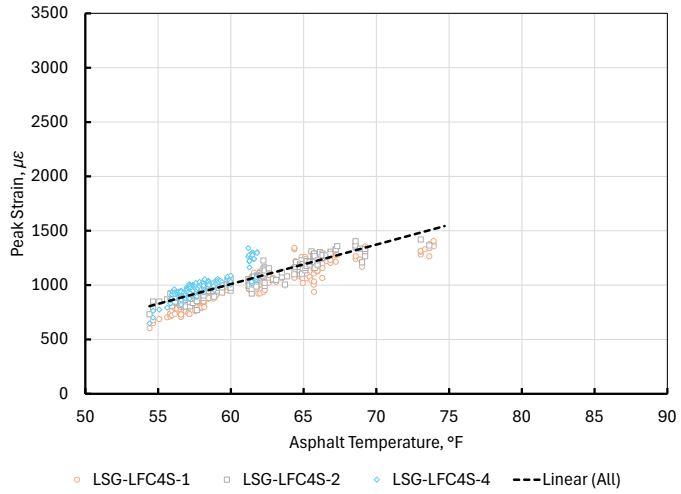

(b) Peak longitudinal strain versus asphalt temperature

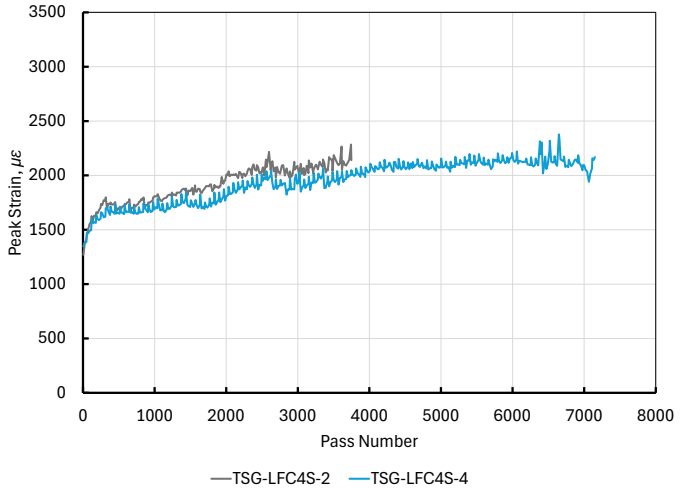

(c) Peak transverse strain versus passes

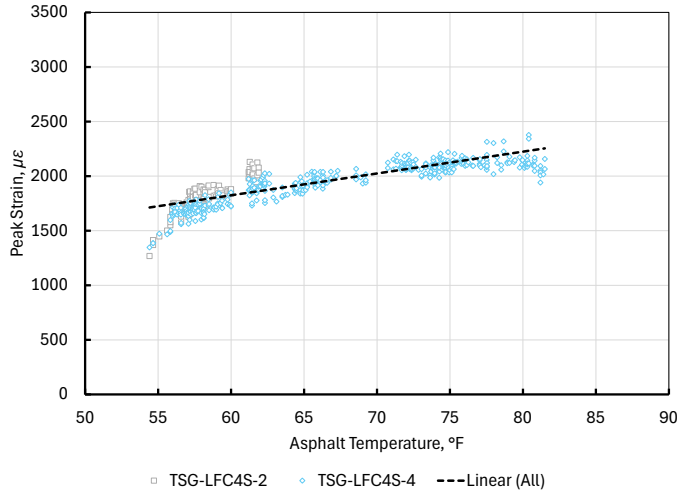

(d) Peak transverse strain versus asphalt temperature

Figure 25. Peak Tensile Strains at the Bottom of the Asphalt Layer, Test Item LFC-4S

5.2.2 Granular Subbase

Figure 26 and Figure 27 plot maximum vertical stress versus passes from PCs at the top of the granular subbase. Figure 26 compares responses from LFS-4N and LFC-4S over the duration of the CTPB test. Both PCs are located at 13 in. below the surface grade of the respective test items. For both test items, the maximum vertical pressure at the top of the subbase increased rapidly after the start of traffic. As shown in Section 4.2.3, at 12,610 passes there was an unplanned pause in traffic due to vehicle maintenance. When traffic resumed after this 5-month hiatus, PC readings returned to their initial levels but again increased rapidly under traffic.

PC-LFC4S-2 failed after 30,000 passes due to repeated stress above its rated limit. PCs had a standard rating of 58.0 psi but could read up to 1.5 times their rated pressure (87 psi) per the manufacturer's specification. Throughout the test, PC-LFS4-1 operated just at the limit of its real capacity. However, PC-LFC4S-2 repeatedly exceeded its capacity under load, with the result that peak stresses were repeatedly cut off (Figure 28). Hence, the maximum values shown in Figure 25 may be considered unreliable, and true peak pressures for LFC-4S are higher than those shown.

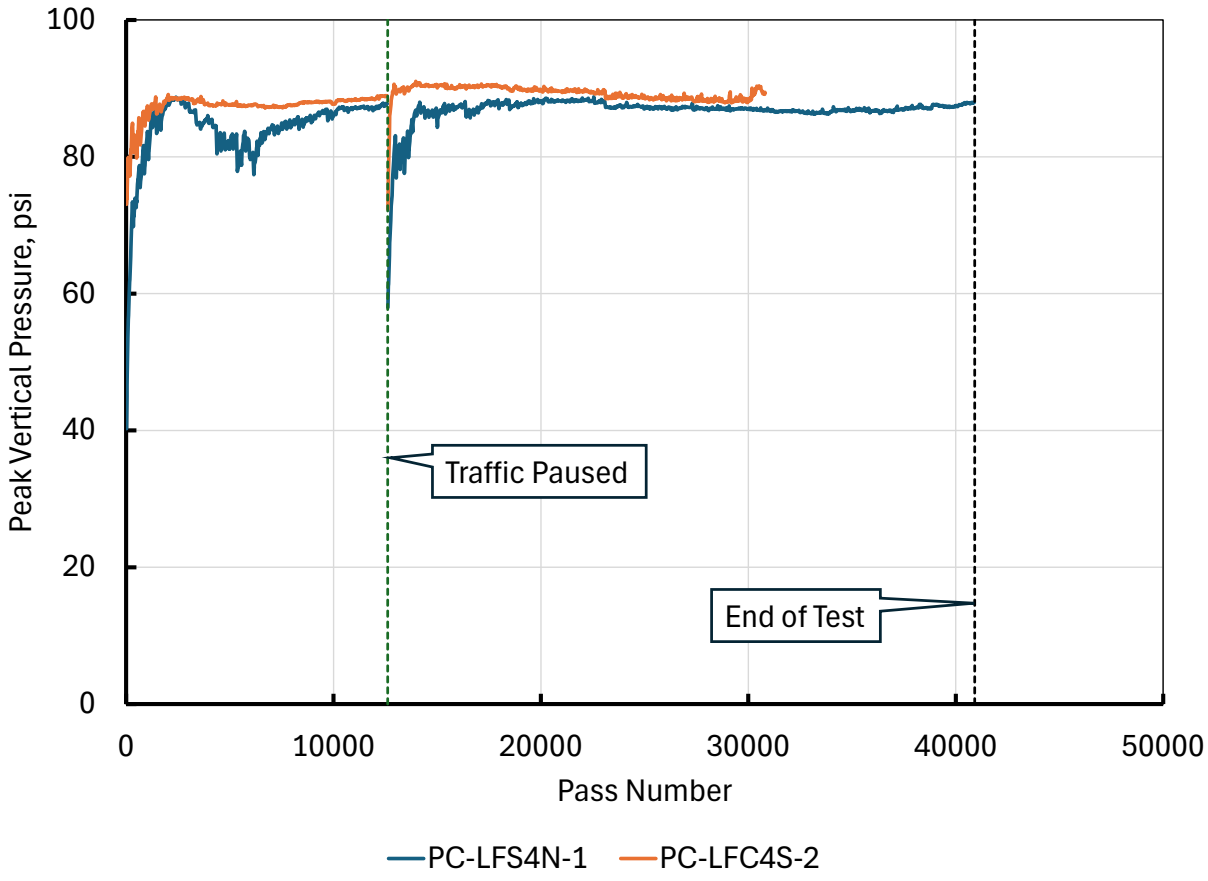

Figure 26. Pressure Cell Peak Response (top of P-154 granular subbase) for CTPB Test Items

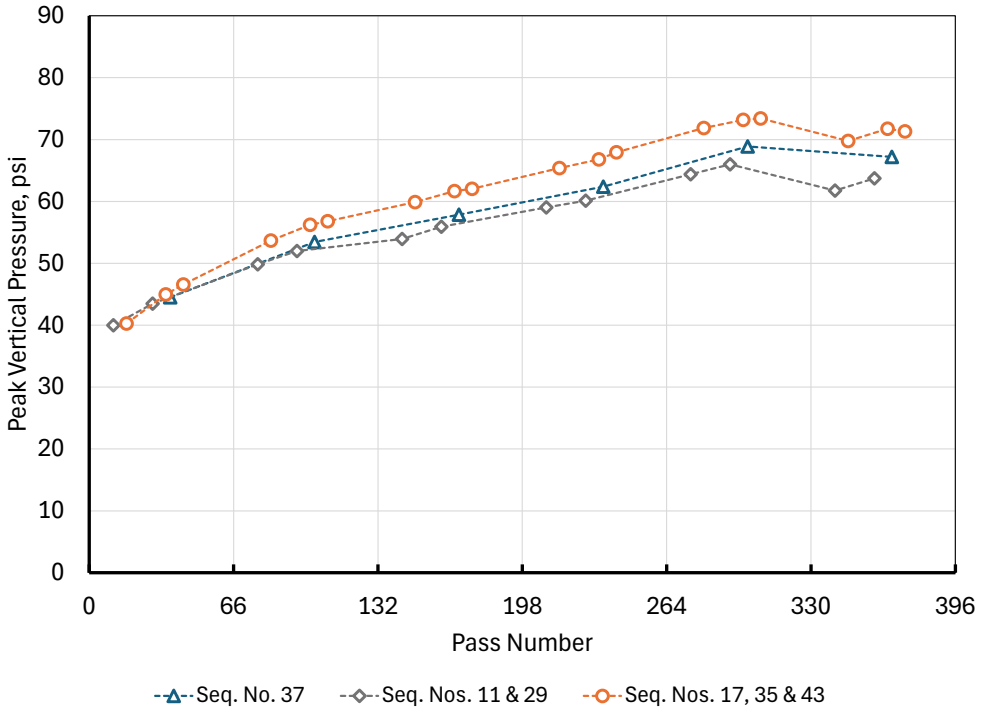

(a) PC-LFS-4N-1 (Test Item LFS-4N, top of subbase).

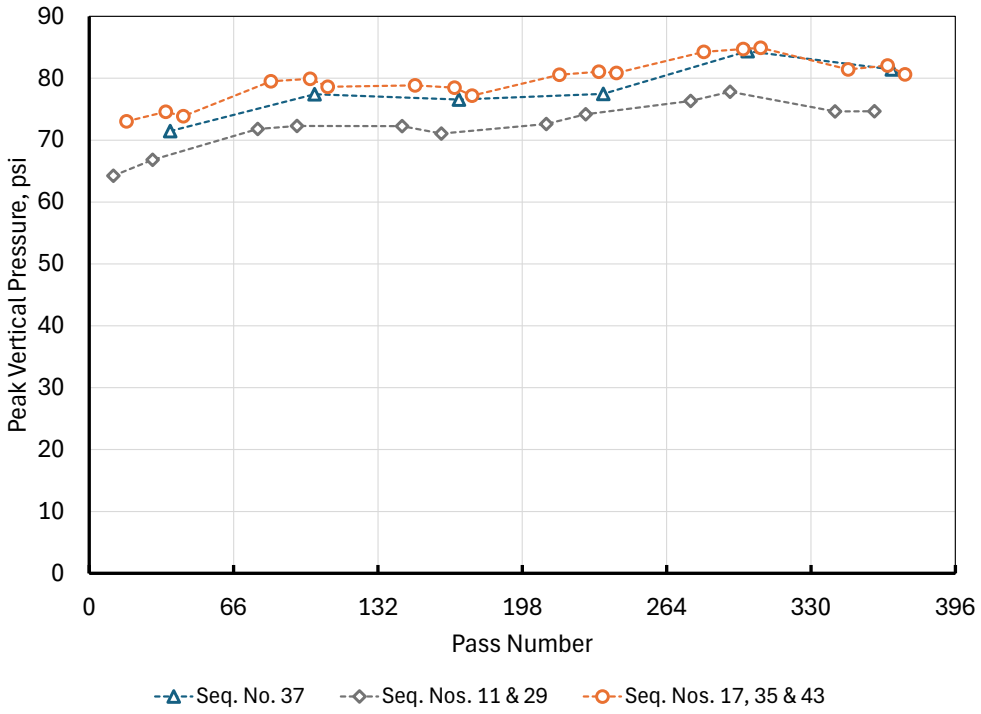

(b) PC-LFC-4S-1 (Test Item LFC-4S, top of subbase)

Figure 27. Pressure Cell Peak Response (top of P-154 subbase) for Critical Tracks +3 and -3, First 6 Wander Pattern Repetitions

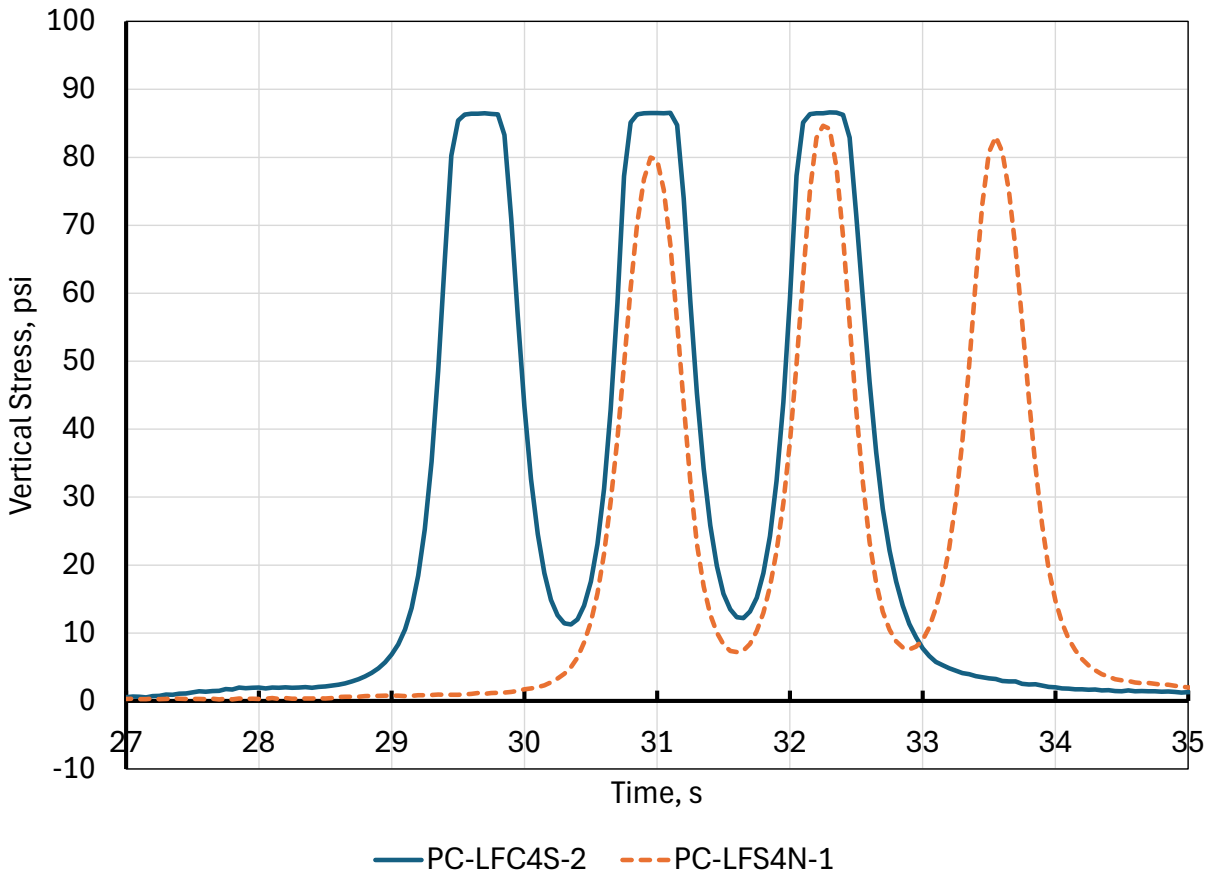

(b) PC-LFC4S-1 (Test Item LFC-4S, top of subbase)

Figure 28. Example of PC Response at Pass 14,093 Showing Signal Saturation at Approximately 87 psi
(The signal peak for PC-LFC4S-2 (but not PC-LFS4N-1) is cut off.)

Figure 28 shows the increase in peak vertical stress for the first six repetitions of the wander pattern (before the vertical pressure exceeded the PC capacity). The critical tracks for PCs (wheel directly on top of the sensor) were tracks +3 and -3. Analysis of the responses showed that the peak stress depended not only on the critical track, but also on the track number of the proceeding pass in the wander pattern. Hence, responses fell into three clusters, identified as (1) wander sequences 11 and 29, (2) wander sequences 17, 35, and 43, and (3) wander sequence 37. (Only the passes in the west-to-east direction were considered, not the return passes on the same track.) As illustrated in Figure 28, cluster 2, associated with wander sequences 17, 35, and 43, consistently gave the highest responses.

Figure 29 plots permanent vertical strain against passes, as measured by CS pairs near the top of the granular subbase. Permanent strain was determined by dividing the unloaded deformation in the CS pair at the end of each wander pattern by the nominal coil separation distance (75 mm, approximately 3 in.). The unloaded deformation was measured with the NAPTV powered down to eliminate electromagnetic interference from the vehicle motors. For both test items, the unloaded deformation increased rapidly up to about 7,500 passes, then leveled off. Throughout

the test, accumulated permanent strain in the CTPB test item subbase material was 20% to 30% higher than in the control test item.

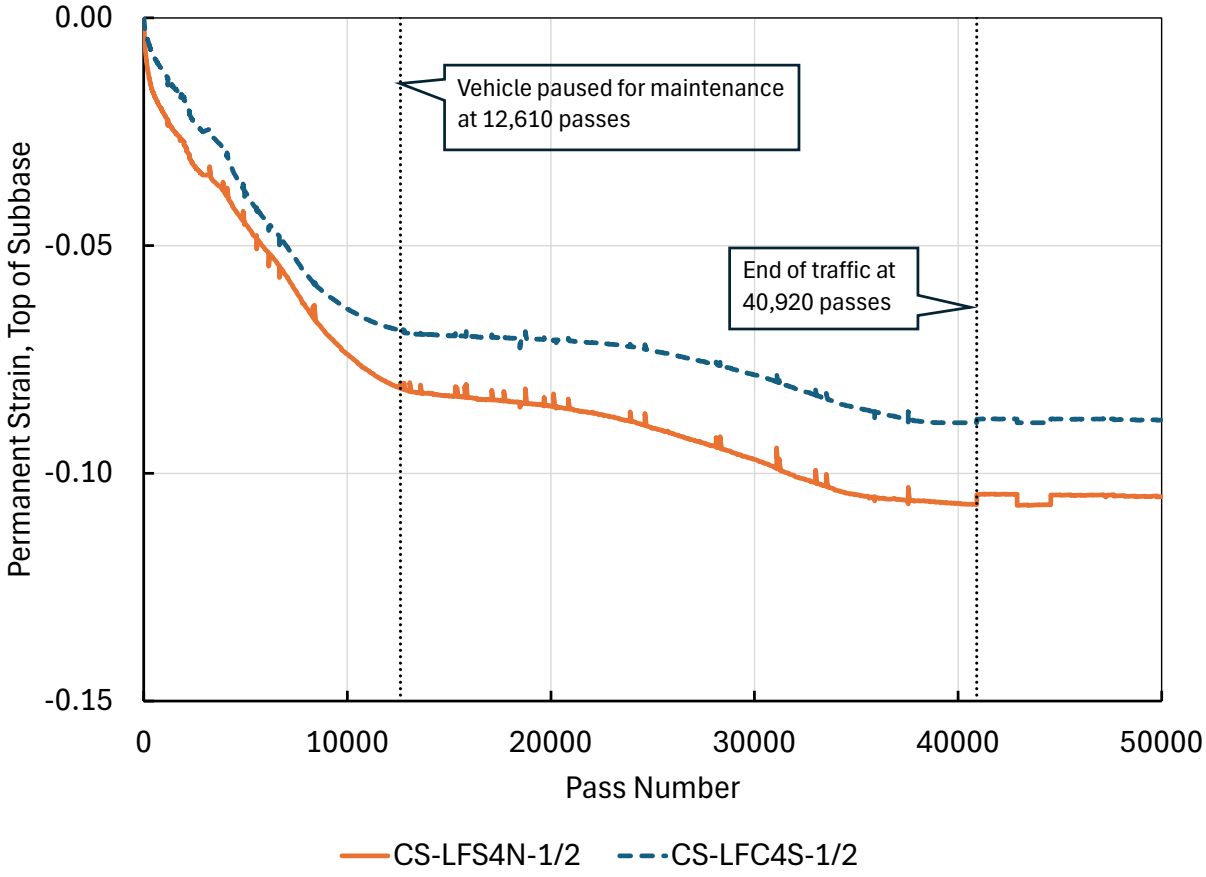

Figure 29. Permanent Strain at CS Location, top of P-154MR Subbase

Figure 30 plots peak vertical compressive strain at the top of the granular subbase against traffic. Similar to the trend for permanent (unloaded) strain, load-induced compressive strains in the LFS-4N subbase were higher than those in the LFC-4S. For CS pairs at the top of the subgrade, the critical track for peak strain was track 0. However, as described in Section 5.2.2, the peak response is also affected by the lateral position of the previous pass, due to particle rearrangement in the unbound layers. Referring to the wander pattern (Section 4.2.1), all W→E passes on track 0 were preceded by a pass on track -2, except for those in sequence number 65, which were preceded by track -1. This explains why the peak strain responses fell into two groups as shown in Figure 30.

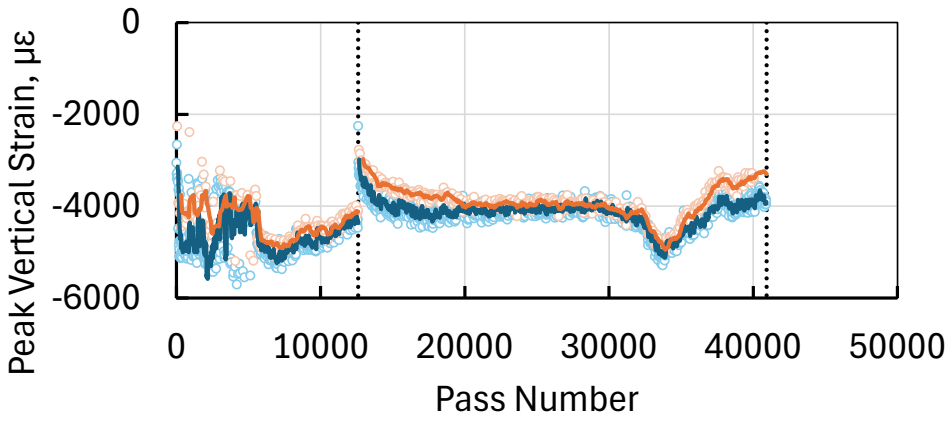

(a) CS-LFS4N-1/2

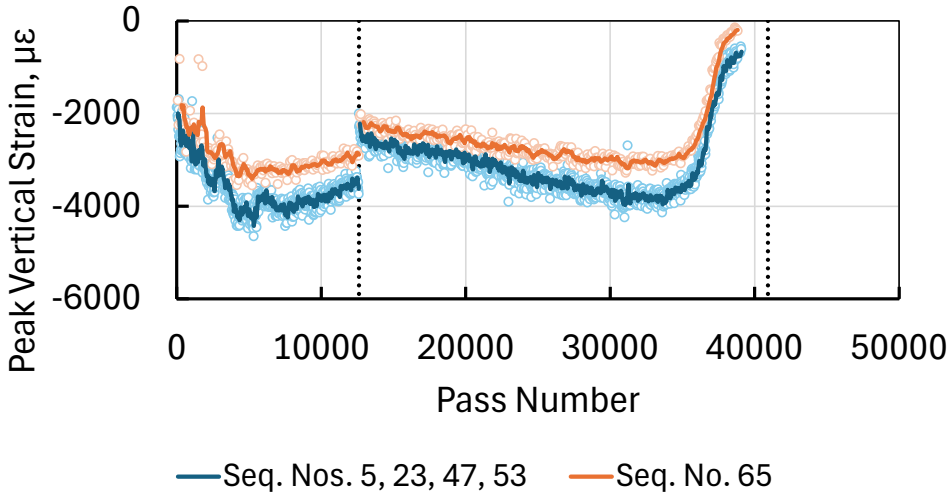

(b) CS-LFC4S-1/2

Figure 30. Compressive Strain at top of P-154MR Subbase
(Solid lines show 5-point moving average.)

5.2.3 Subgrade

5.2.3.1 Compressive Stresses from Pressure Cells

Figure 31 shows peak top-of-subgrade, load-induced vertical stress versus number of passes. Vertical stresses in the subgrade remained relatively stable throughout the test. Abrupt changes in the PC reading from LFC-4S in Figure 31 (at passes 1,452; 5,544; and following the pause at pass 12,610) were probably due to sensor malfunction.

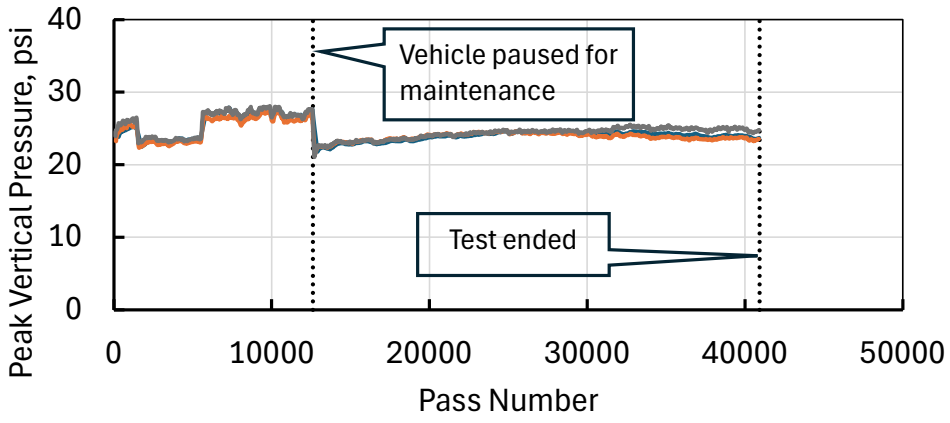

(a) PC-LFS-4N-2 (42 in. below grade)

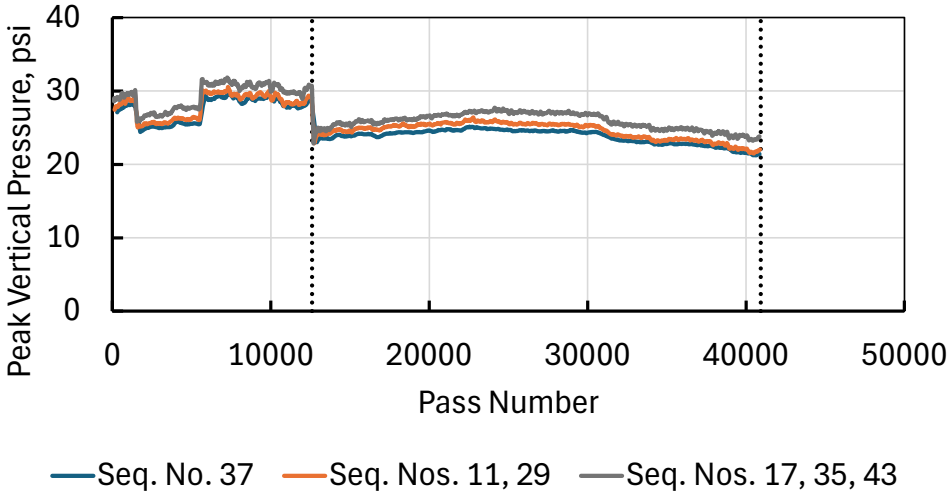

(b) PC-LFC-4S-4 (42 in. below grade)

Figure 31. Compressive Stress at top of Subgrade (5-point moving average)

5.2.3.2 Permanent and Load-Induced Compressive Strains from Coil Sensors

Figure 32 plots permanent vertical strain at the top of the subgrade against the number of passes. As with Figure 25, the permanent strain was computed as the ratio of unloaded deformation in the CS pair at the end of each completed wander pattern to the nominal coil separation distance (75 mm, approximately 3 in.).While both test items showed final permanent strain of the top of the subgrade of approximately 0.04, their paths to that point were clearly different. CS-LFC-4S-3/4 seems to show an initial large deformation under traffic, followed by a period of recovery after the pause in traffic. Some of this recovery may be only apparent, due to distortion or rotation of the CS pair. CS-LFS-4N-3/4 shows a significant increase in permanent deformation after approximately 23,500 passes, and no recovery.

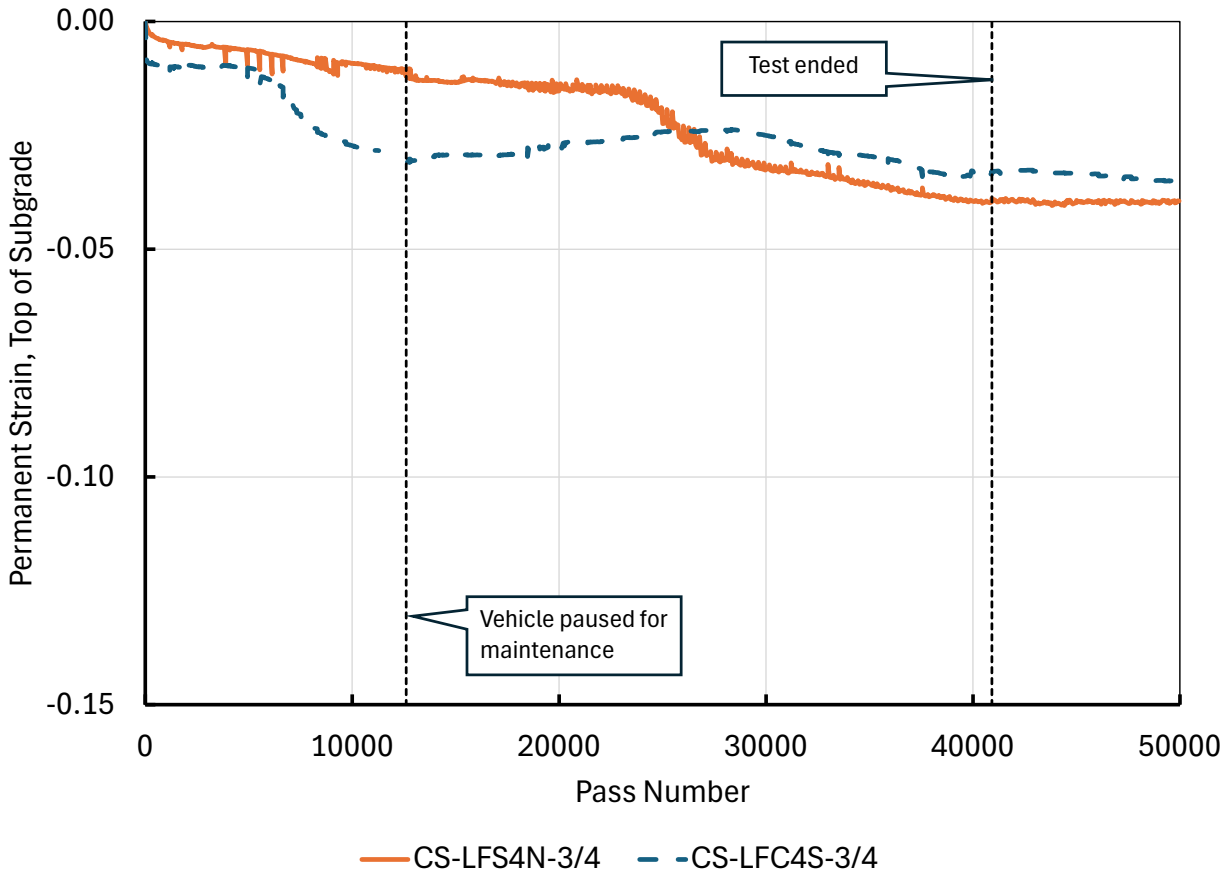

Figure 32. Permanent Strain at Coil Sensor Location, Top of Subgrade

Figure 33 shows subgrade peak compressive strain as a function of traffic passes. While there was considerable variability in the peak strain response (some of which is linked to temperature fluctuations in the asphalt, and some to errors in the filtering process for extracting peak values from the raw CS data), the overall trend was that the subgrade strain increased significantly with accumulated traffic. As shown in Figure 33, traffic was paused for an extended period at 12,610 passes. The peak strain response partially recovered after this extended pause but began to increase again with resumed traffic. After about 15,000 passes, CS-LFS-4N-3/4 failed to provide usable dynamic (load-induced strain) responses. However, CS-LFS-4N-3/4 continued to return static (permanent deformation) data when interrogated in static mode after the completion of each wander pattern repetition (Figure 29).

Because vertical strain at the top of the subgrade is the key response for FAA Rigid and Flexible Iterative Elastic Layered Design (FAARFIELD) flexible pavement design, it is useful to compare the strain response in Figure 33 with the FAA layered elastic analysis (LEAF) response for the same inputs. For the nominal LFC-4S structure (5-in. HMA, 8-in. P-209MR base, 29-in. P-154 subbase, CBR 5 subgrade) and assuming FAARFIELD standard properties and loading by the NAPTF three-dimensional test gear as discussed in Section 4.2.3, LEAF yields a vertical strain at the top of the subgrade of -1715 $\mu\varepsilon$. This is in fact reasonably close to in situ measured strains from CS pairs at the start of the test (Table 15). However, it is clear from Figure 33 that

the peak load-induced subgrade strain is not constant; rather, it rapidly increases from its initial static value under repeated traffic passes.

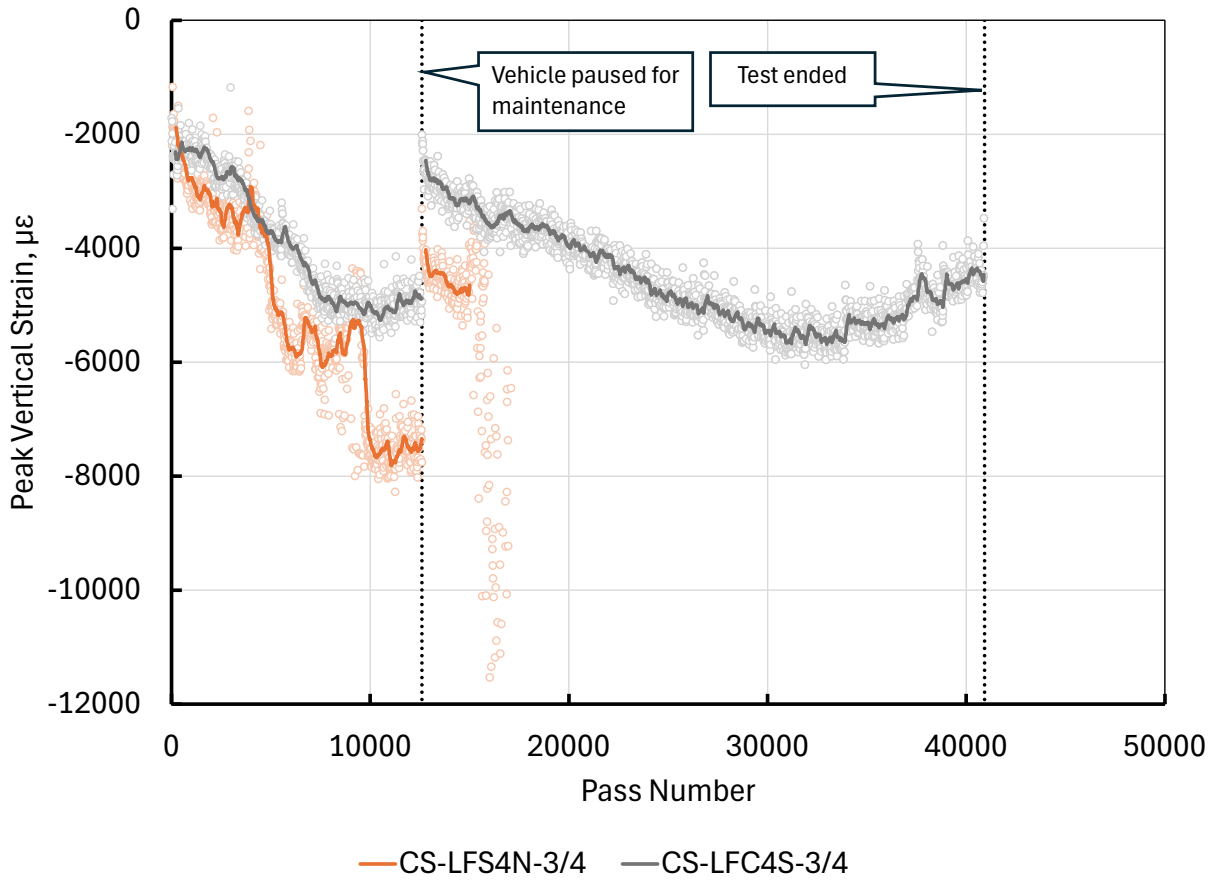

Figure 33. Compressive Strain at Top of Subgrade (Solid lines show a 15-point moving average.)

Table 15. Peak Vertical Strain at Top of Subgrade from CS Pairs at Start of Test (First wander repetition)

Pass Number*	Estimated in situ peak vertical strain, με	
	CS-LFS4N-3/4	CS-LFC4S-3/4
5	–	-1719
23	–	-2124
47	-2201	-1774
53	-1872	-1990
65	-1171	-3311

*Passes in west-to-east direction, on track 0

5.2.3.3 Volumetric Moisture Content

Subgrade moisture content θ_v was monitored closely during the test. Figure 34 plots subgrade θ_v against traffic for both test items. As shown in Figure 34, after about pass 18,500, MS-LFS-4N-1 started to behave erratically, and readings after that point were considered unreliable. In Figure 34, the value of θ_v associated with a pass number is the hourly value closest in time to the pass (nearest 30 minutes). Initially, θ_v increased with traffic for both test items. The LFS-4N subgrade exhibited a steep drop in θ_v during the 5-month pause when traffic was removed, behavior that was not reflected as strongly in LFC-4S.

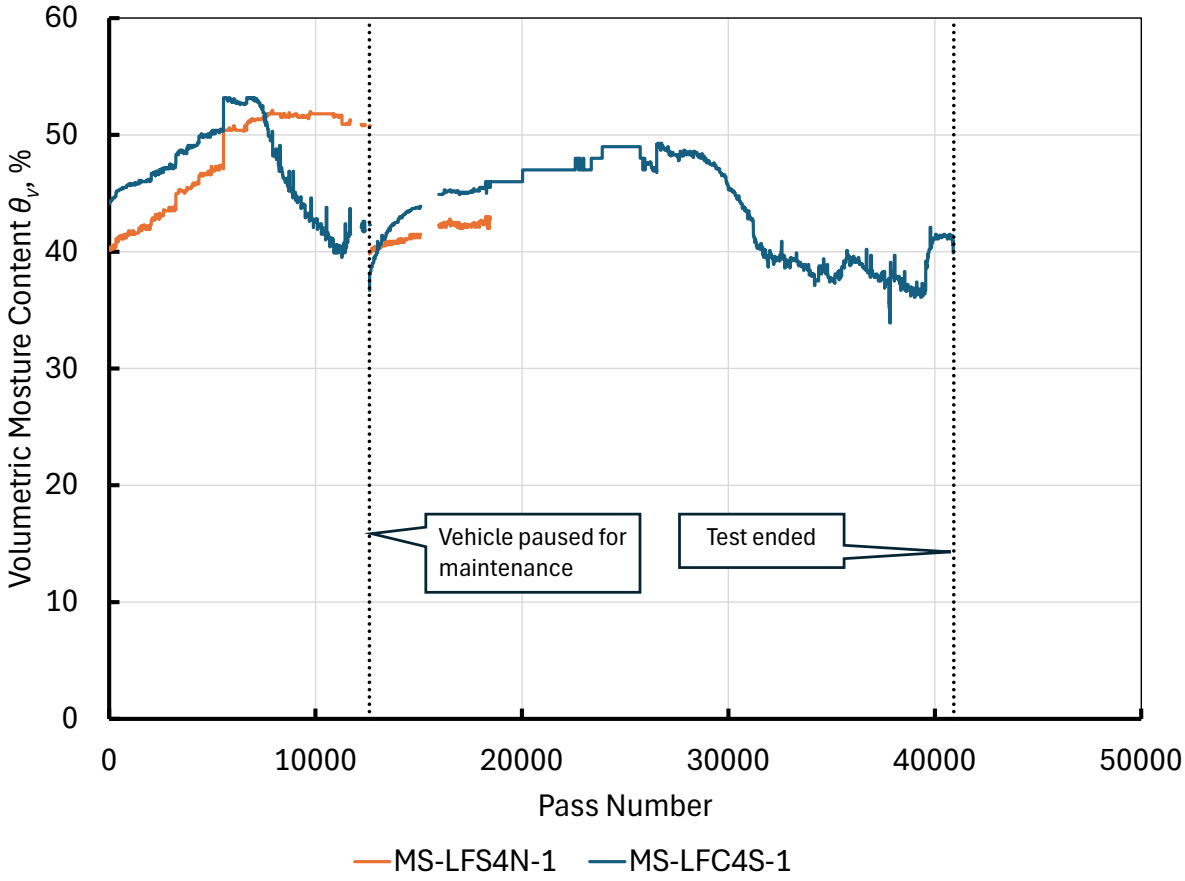

Figure 34. Change in Subgrade θ_v with Traffic

5.3 STRUCTURAL EVALUATION WITH NONDESTRUCTIVE TESTING

5.3.1 Heavy Weight Deflectometer Deflection Basin Evaluation

Area Under Pavement Profile (AUPP) is the area under the HWD deflection basin curve computed over a radial distance of 72 in. from the center of the load plate. This index is known to be an excellent indicator of tensile strain at the bottom of asphalt concrete. For the sensor arrangement in Figure 35, the AUPP equation is:

$$AUPP = {}^{1}/_{2} \times \{11D_0 - 2(D_{12} + D_{24} + D_{36} + D_{48} + D_{60}) - D_{72}\} \quad (4)$$

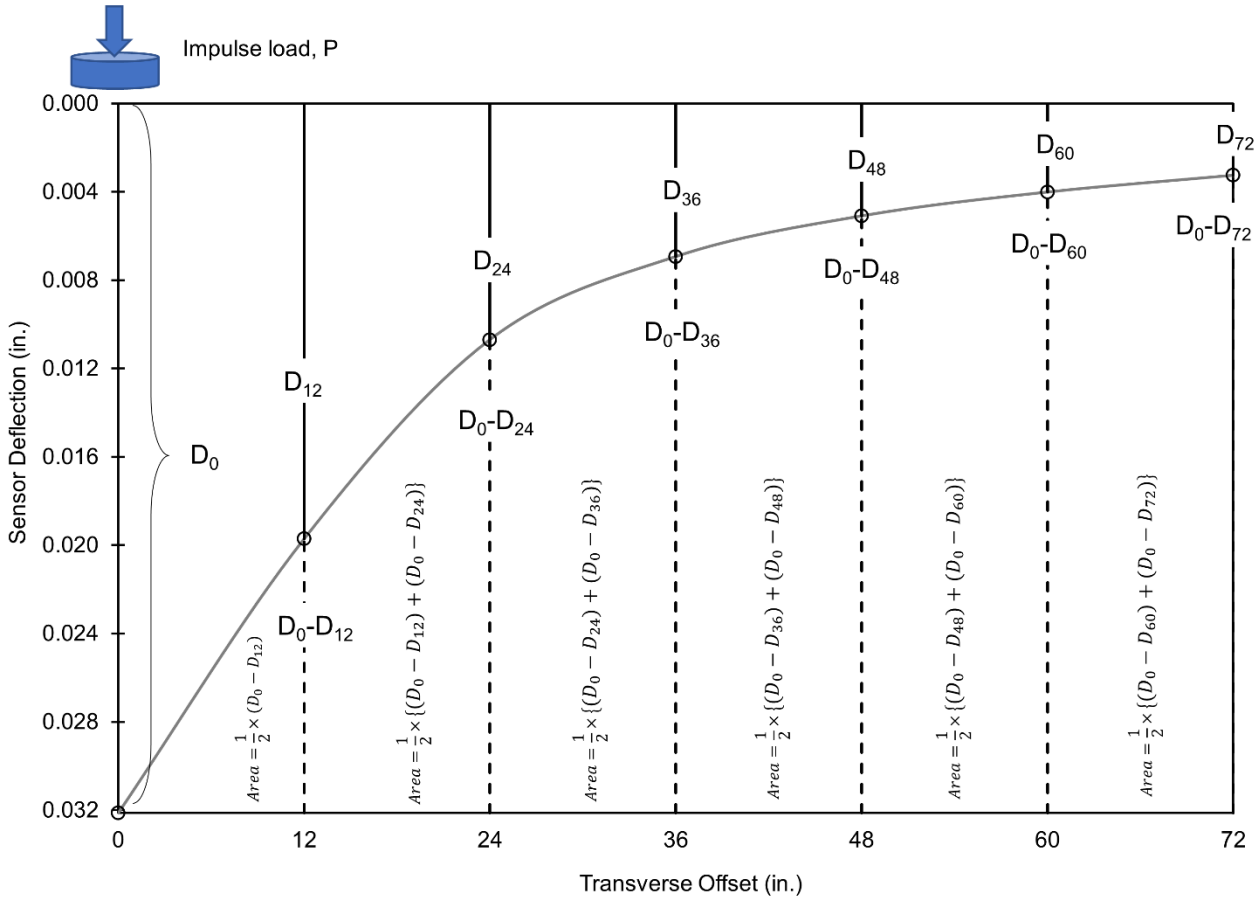

Figure 35. Sample HWD Deflection Basin

The ratio of AUPP for HWD drop locations within traffic lanes to AUPP for HWD drop locations outside of traffic lanes reveals the extent of load-induced damage. For CC9, HWD locations at ±15-ft offsets were within traffic lanes ($AUPP_{Trafficked}$), while those at ±5 ft and ±15 ft were outside of traffic lanes ($AUPP_{Untrafficked}$).

Figure 36 plots the ratio $AUPP_{Trafficked}/AUPP_{Untrafficked}$ versus pass number for the two CTPB test items. As expected, the AUPP ratios were consistently above one, but they did not consistently increase with traffic (as might have been expected). Rather, both test items saw a sharp increase in AUPP ratio after the start of traffic, which stabilized after several thousand passes. There was little correlation between AUPP ratio and additional traffic. AUPP ratios in test item LFS-4N (CTPB) were consistently much higher than those in LFC-4S (control).

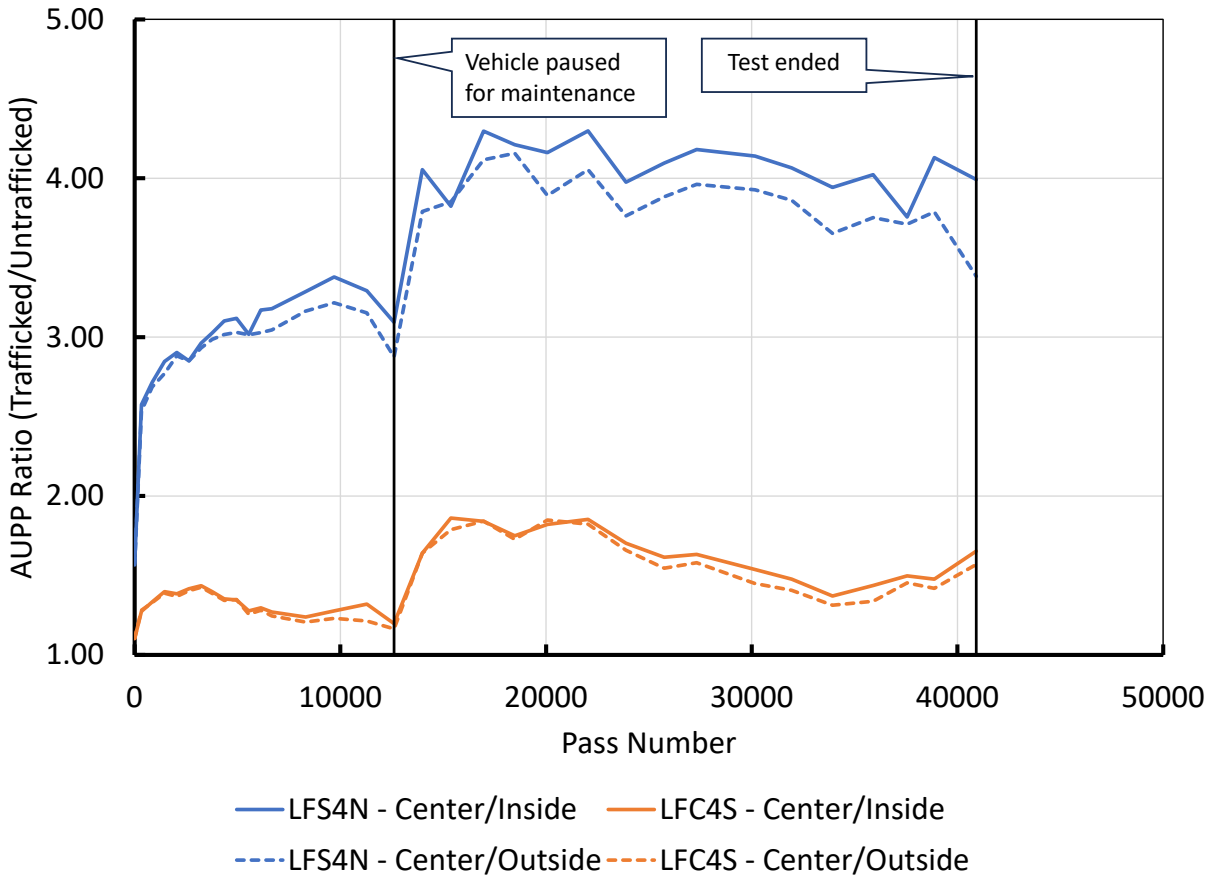

Figure 36. Variation of Area Under Pavement Profile Ratios Between Trafficked and Non-Trafficked Areas of CTPB Test Items
(Plotted values represent averages of the two drop locations (STA 1+95 and STA 2+10) within each test item.)

5.3.2 Ground-Penetrating Radar Deformation Profiles

Ground-penetrating radar (GPR) data were combined with surface laser scans to produce profiles of the deformed pavement layers. The GPR datasets analyzed for the CTPB test area are listed in Table 16. Detailed information on the data acquisition procedures can be found in Mazzotta et al. (2024). As discussed in Mazzotta et al. (2024), two sets of GPR apparatus were used: (1) a cart-mounted GPR with ground-coupled 900 MHz and 2.6 GHz antennas, and (b) a van-mounted GPR with ground-coupled 400 MHz and air-coupled 2.0 GHz antennas. Except as noted in Table 16, data were collected using both systems. However, only the cart-mounted system could be used for transverse profiles. On the other hand, only the van-mounted system with the low-frequency 400 MHz antenna could penetrate the subgrade surface. Hence, transverse profiles developed by GPR only include the upper pavement layers.

Table 16. Ground-Penetrating Radar Datasets for the CTPB Test Area

Dataset	Vehicle Passes	Notes
2020/09/09 Baseline Round 1	0	Baseline
2021/08/02 Weekly Set	6,138	Mid-summer
2022/06/13 Trafficking Set	27,324	Prior to large increase in surface rutting
2022/09/26 Trafficking Set	40,920	Cart-mounted GPR only
2022/11/07 Trafficking Set	40,920	Van-mounted GPR only

Figure 37 shows the evolution of the combined GPR/surface transverse profiles for the CTPB test area. Figure 38 shows the final GPR-based longitudinal centerline profiles (excluding the surface profile). Transverse profiles clearly show the progression of permanent deformation, with limited rutting occurring in upper structural layers for both test items. The asphalt layers in both test items, and the aggregate base (P-209MR) in LFC-4S, maintained their thickness throughout the test. The trafficked areas of the CTPB layer in LFS- 4N experienced some thinning, which could indicate material breakdown under traffic of the CTPB layer. However, from Figure 37 it can be inferred that most permanent deformation took place in the subbase and/or subgrade.

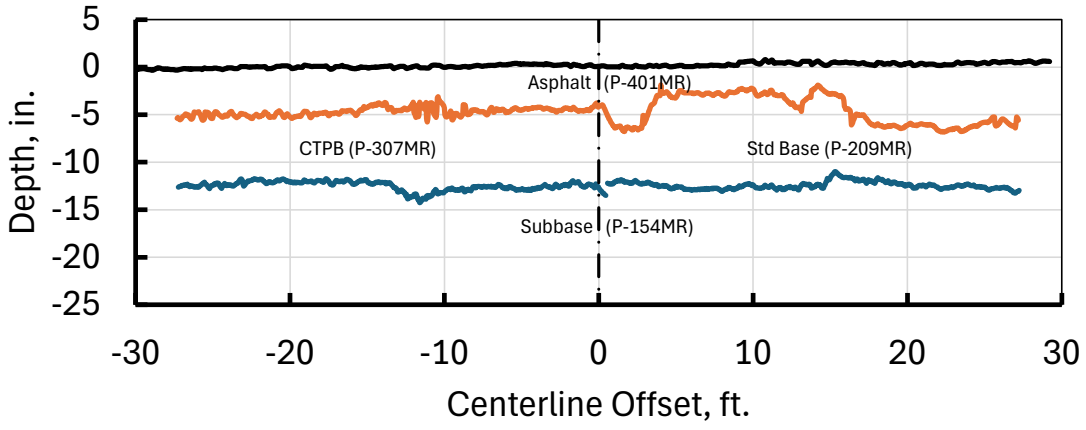

(a) September 9, 2020 (Baseline)

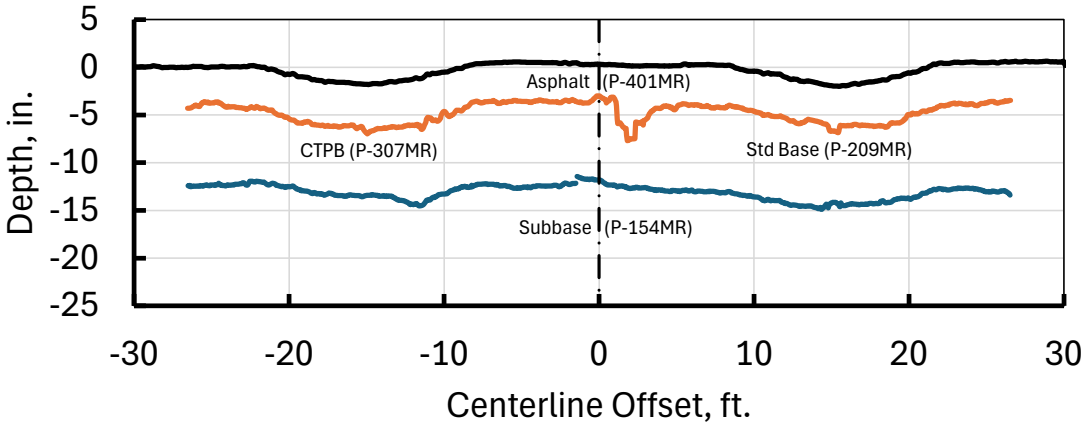

(b) June 13, 2022 (27,3324 passes)

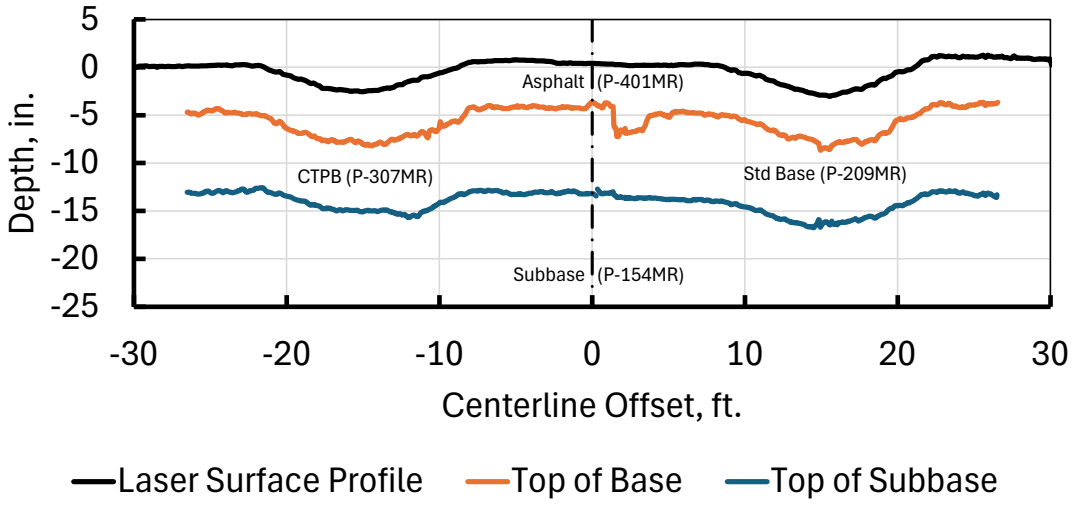

(c) September 26, 2022 (40,920 passes, end of test)

Figure 37. Transverse Profiles, STA 2+10, Laser Profile + GPR (900 MHz Antenna)

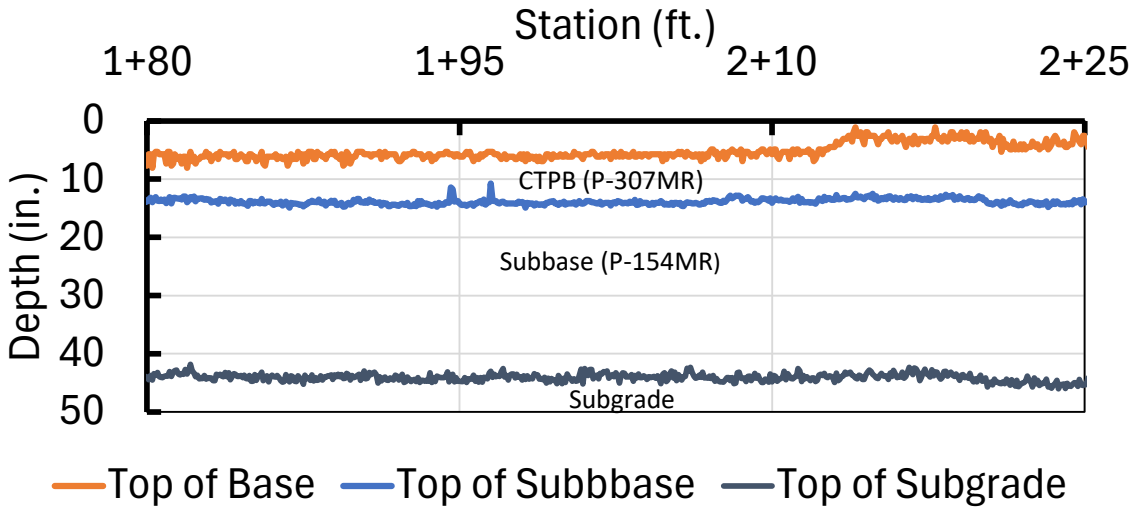

(a) LFS-4N Centerline

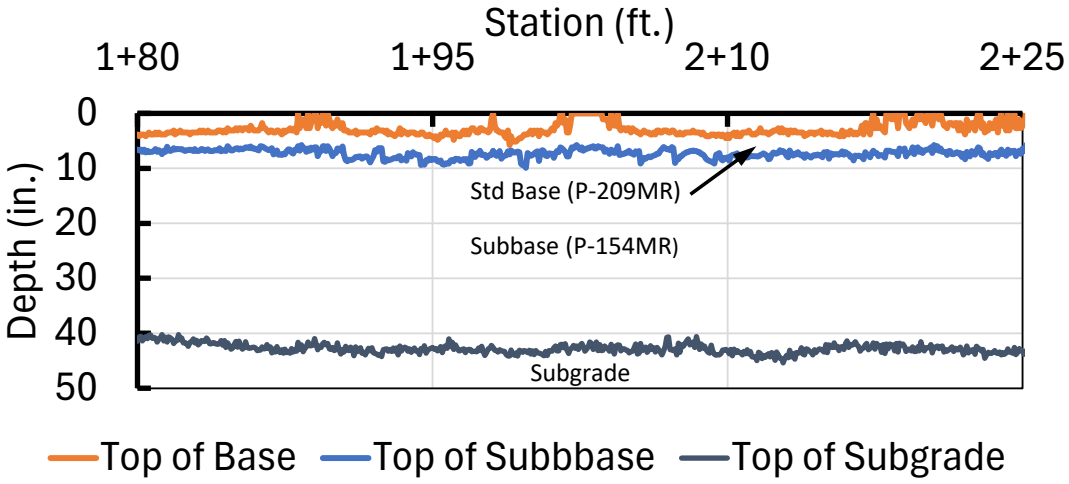

(b) LFC-4S Centerline

Figure 38. Longitudinal GPR Profiles, CTPB Test Area, November 7, 2022 (400 MHz Antenna)

Engineers used GPR data from tranverse profiles to estimate average layer thicknesses for asphalt and base layers at various stages of traffic, for trafficked and non-trafficked areas of the test items. These data are shown in Table 17 and Table 18. As-built thicknesses from the construction report (Figure 3) are provided for comparison. There were significant differences between the construction data and the GPR-estimated baseline (zero traffic) thickness values. These deviations are attributed to assumptions from GPR processing, including layer picking and dielectric constant values. Nevertheless, comparisons of trafficked and untrafficked areas are still valuable. Decreases in layer thickness in trafficked locations relative to untrafficked locations are evidence of traffic-related densification.

Disregarding the questionable baseline GPR asphalt thicknesses and considering the other datasets, some trends become apparent. In general, the asphalt layers did not experience significant thickness changes in thickness over more than 40,000 passes. Similarly, the crushed

aggregate base layer in LFC-4S exhibited little or no densification. However, the trafficked areas of the CTPB layer exhibited densification relative to the untrafficked areas. The CTPB layer densified in the initial phase of traffic, then stabilized after about 27,000 passes. The GPR data suggest that the CTPB layer lost more than 1 in. of thickness under repeated traffic. The relative disparity in AUPP indices between trafficked and untrafficked areas of test item LFS-4N (Figure 32) is corroborating evidence of traffic-related damage to the CTPB. Post-traffic physical investigations, including layer-by-layer exposure of damaged materials, will be performed in the future to varify the GPR estimates.

Table 17. Estimated Asphalt Layer Thicknesses from GPR Data

	Asphalt Thickness, in.			
	LFS-4N		**LFC-4S**	
Passes	**Trafficked**	**Non-trafficked**	**Trafficked**	**Non-trafficked**
As built	5.1	5.1	5.2	5.2
0	3.5	4.0	2.9	3.9
6,138	5.8	5.2	4.6	4.7
27,324	5.0	4.6	4.9	4.9
40,920	5.5	5.1	5.1	5.4

Table 18. Estimated Base Layer Thicknesses from GPR Data

	Base Layer Thickness, in.			
	LFS-4N (CTPB, P-307MR)		**LFC-4S (Agg. Base, P-209MR)**	
Passes	**Trafficked**	**Non-trafficked**	**Trafficked**	**Non-trafficked**
As built	7.8	7.8	7.8	7.8
0	8.5	8.9	9.6	9.1
6,138	7.4	8.2	8.9	9.2
27,324	6.7	8.3	7.9	8.1
40,920	6.7	8.2	8.2	8.2

6. COMPARISON TO CC7 ATPB TEST

The CC7 ATPB test lasted from September 5, 2014, to March 8, 2016. In that time, 23,364 passes were applied to CC7 ATPB test item LFS-6N (compared to total 40,920 passes on CC9 CTPB test items). Figure 24 shows the traffic timelines for both the CC9 CTPB and CC7 ATPB tests. As shown, a large share of the CC7 traffic was applied during the colder winter months, while CC9 traffic was more evenly distributed across the seasons. (CC7 LFS-6N traffic was purposely targeted for winter traffic because the north test lane also included the CC7 “perpetual pavement” test, which benefited from colder asphalt temperatures.) Therefore, a comparative analysis should take this seasonal difference into account. For example, except for a short period at the start of the test covering about 2,500 passes, internal asphalt temperatures for CC7 during the period of ATPB testing ranged from about 35 °F to 60 °F, much lower than the 55 °F to 80 °F range for CC9 shown in Figure 23 and Figure 24. Likewise, analyses of the moisture conditions in the NAPTF subgrade indicated higher moisture levels during spring due to the

interaction of thermal gradients (Jumikis, 1977). These higher seasonal soil moisture levels presumably had relatively little effect on the CC7 ATPB test (none of the traffic was during spring months) but certainly affected CC9 responses.

There were also significant differences in instrumentation between CC7 and CC9. CC7 test items did not include CS pairs. Instead, multi-depth deflectometers (MDDs) were used to monitor vertical deformations. The MDD in CC7 test item LFS-6N (MDD6) had sensors at two depths in the ATPB layer, three in the subbase layer, and one near the top of the subgrade. A report by Yin et al. (2020) found the data quality of MDD6 to be poor and cautioned that assessment of permanent deformation in the pavement layers of LFS-6N based on those MDD measurements could be erroneous. However, a new review of MDD6 showed that it is usable and aligns with other data.

A second significant difference was the method of monitoring surface deformations during the test. In CC9, this was done by means of a three-dimensional laser scanning device (Leica P20), with the transverse profiles extracted from the resulting point cloud surface. To determine transverse profiles in CC7, engineers primarily relied on a device called a "rail-to-rail profiler," which consisted of a Selcom laser riding on a metal truss spanning the width of the NAPTF between the rails. Measurements from the rail-to-rail profiler were sensitive to temperature changes and had to be corrected for the vertical deflection of the laser as it traveled along the truss, but the profiles could be collected and processed quickly. The Leica P20 device was also used occasionally in CC7 in conjunction with the rail-to-rail profiler, but not on a routine basis and mainly as a means of obtaining accurate data with which to correct the rail-to-rail profiles. (At the time of CC7 testing, processing the point cloud data from LiDAR scans to compute the profiles was very time-consuming, often requiring several weeks from the time a scan was performed, so it was not considered a practical tool for routine performance monitoring.)

Other CC9 monitoring procedures were paralleled in CC7. In both tests, one PC was placed at the top of the subgrade to monitor vertical load-induced stress. At regular intervals, engineers measured straightedge rut depth and conducted visual surveys following ASTM D5340 (ASTM, 2020).

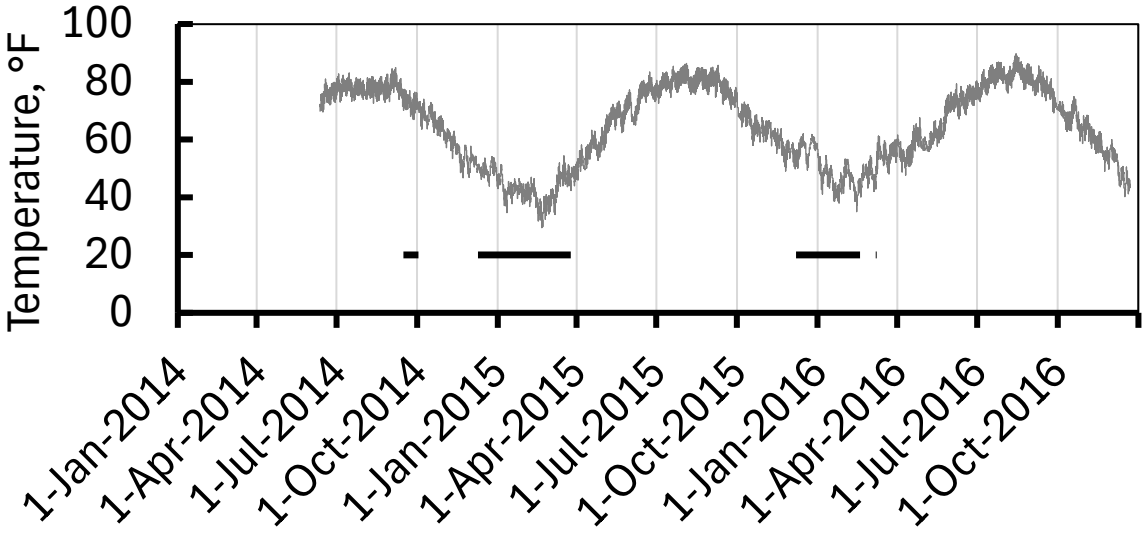

(a) CC7 ATPB Test Timeline

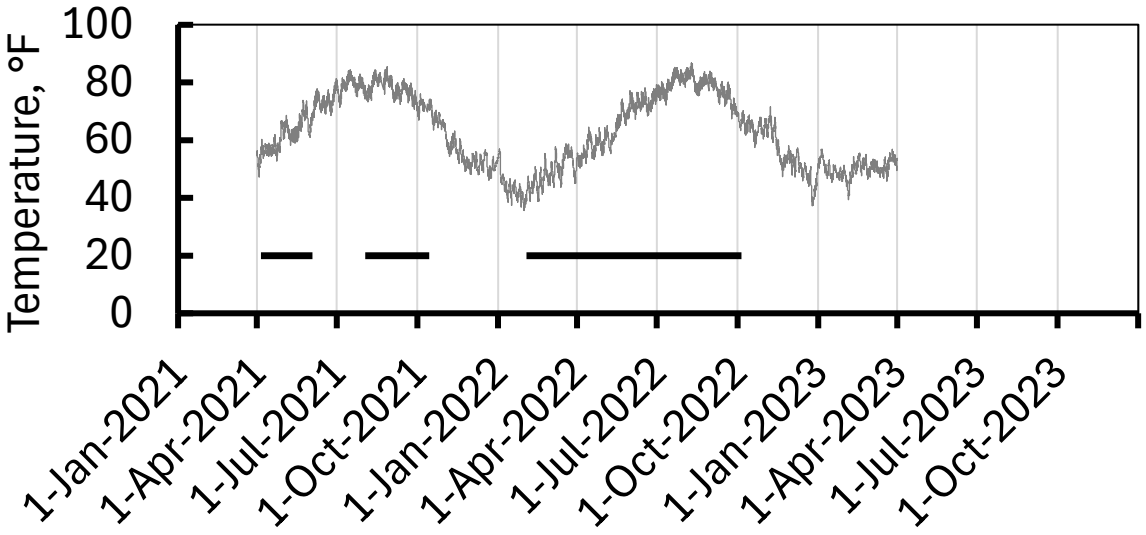

(b) CC9 CTPB Test Timeline

Figure 39. Seasonal Distribution of Traffic on Stabilized Permeable Base Test Items for (a) CC7 and (b) CC9, Plotted with Average Asphalt Temperature

Figure 40 compares the PSE rut depth for CC9 LFS-4N (CTPB) from Figure 22(a) with the corresponding rut depth for test item LFS-6N (ATPB) in CC7. Rutting rates were comparable, with both test items reaching a surface rut depth of approximately 2 in. after 23,000 passes, although the initial rate of rutting in the ATPB section (first 2,500 passes) was much higher. Figure 41 compares the CD trends for CC9 test items from Figure 23 with the CD trend for CC7 test item LFS-6N. Surface cracking in the ATPB test item was much more extensive than in either CC9 LFS-4N (CTPB) or LFC-4S (control). This result is explained by the much lower temperatures at which CC7 was tested, which increases the propensity for cracking (see above).

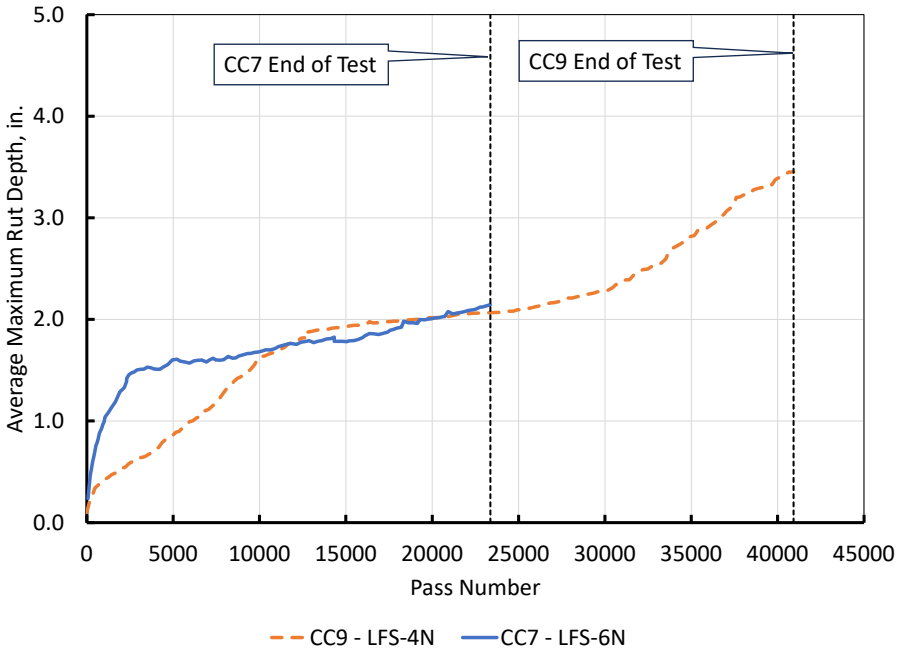

Figure 40. Physical Straightedge Maximum Rut Depth Versus Cumulative Passes for CC7 and CC9 Stabilized Permeable Base Test Items

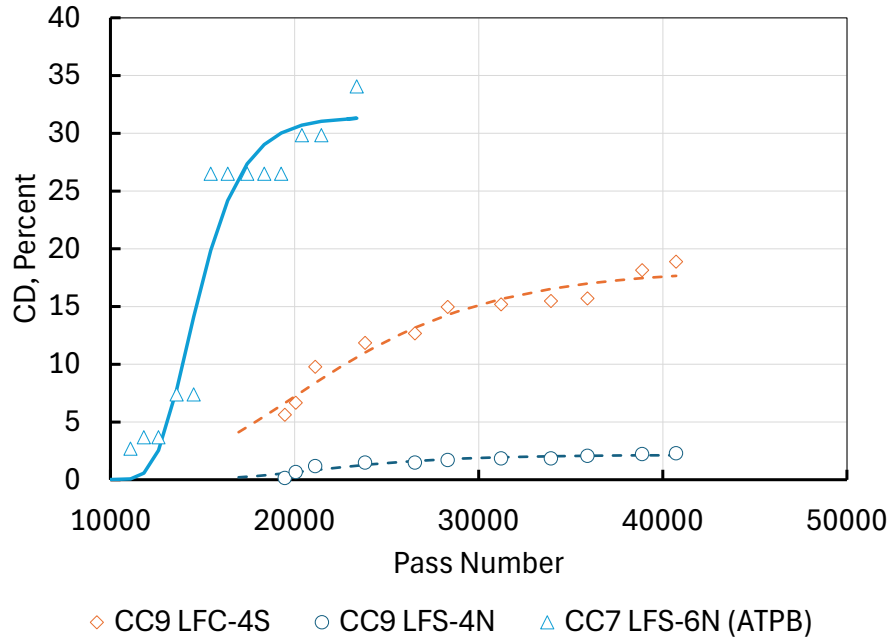

Figure 41. Crack Density Versus Cumulative Passes for CC7 and CC9 Stabilized Permeable Base Test Items

Figure 42 was developed from MDD data for CC7 test item LFS-6N. It shows the change in permanent deformation as a function of applied traffic at various depths within the structure. Lines indicate the total deformation above the indicated MDD component; hence, the contribution of a particular layer to the total deformation can be estimated as the difference between two components. Figure 43 shows the locations of the MDD components relative to the layer boundaries. For example, the difference between the readings of MDD-6C (top of subbase) and MDD-6A (top of ATPB) gives the contribution of the ATPB layer to the total deformation at the surface. Analysis of Figure 42 and Figure 43 shows that:

- There was little or no permanent deformation in the subgrade. This is clear from the fact that the lines for MDD-6E, MDD-6F, and MDD-6G nearly coincide. Nor was there significant rutting of the asphalt layer.

- The total deformation above the subgrade level from MDD data generally agrees with the measured surface (straightedge) rut depth in Figure 40. Figure 40 shows a slightly larger surface deformation magnitude (approximately 1.8 in. at 15,000 passes, versus 1.5 in. estimated from Figure 42) because the straightedge rut is measured from peak to trough of the transverse profile and, therefore, includes a significant upheaval component not captured by the MDD (see Figure 43).

- The ATPB layer contributed approximately 0.5 in., or about one-third, of total rutting.

Post-traffic investigations of CC7 LFS-6N conducted in 2017 included opening a transverse trench through the test item, which confirmed the above results. From physical inspection of the trench, the investigators concluded that that 27% of total rutting was contributed by the ATPB, 73% by the subbase, and zero by the asphalt or subgrade layers (Li & Yin, 2018). Comparing Figure 44 with the GPR deformation profiles for CC9 LFS-4N in Section 5.3.2, the rut contributed by ATPB appears to be somewhat less than that estimated for CTPB (Table 18). However, the results for CTPB are preliminary and must be confirmed by trench investigations.

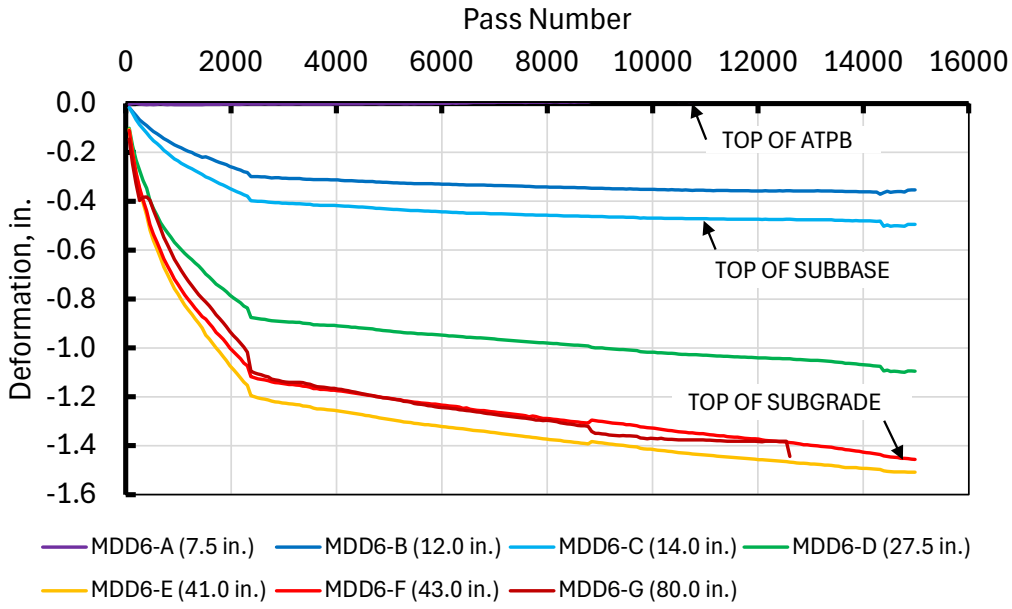

Figure 42. Permanent Deformation in CC7 ATPB Test Item LFS-6N from MDD
(The vertical axis shows the total deformation of the structure above the MDD component. Numbers in parentheses are the nominal depths below the surface elevation.)

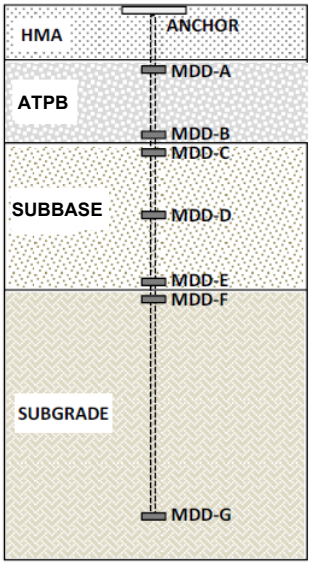

Figure 43. Locations of CC7 MDD Components Relative to Layer Boundaries (ATPB test item)

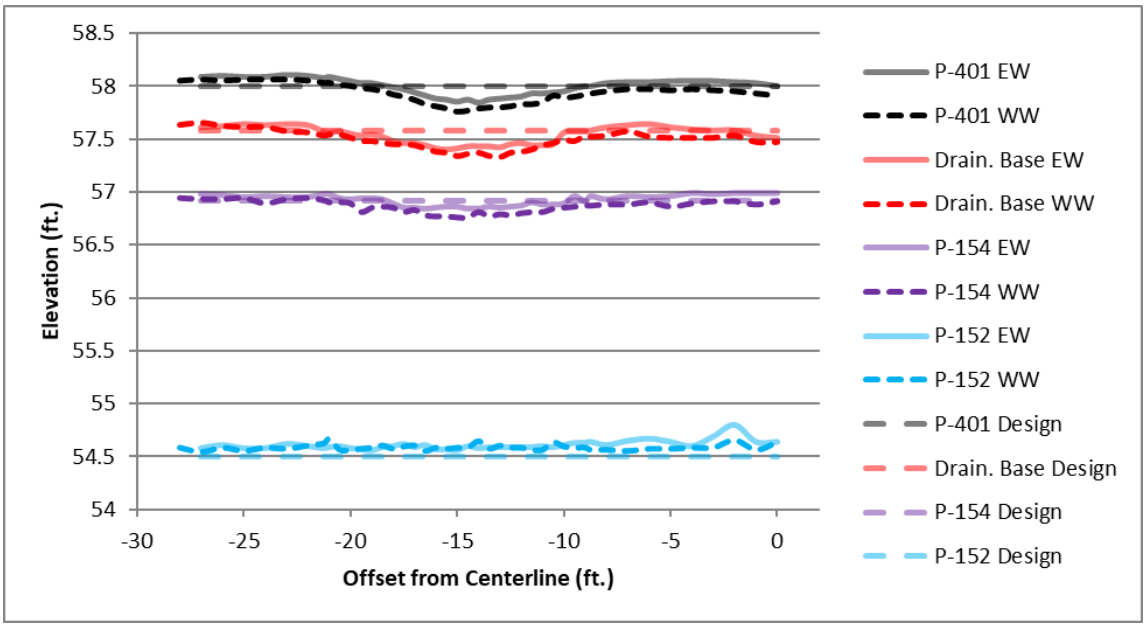

Figure 44. Pavement Layer Profiles from Post-Traffic Trench, CC7 Test Item LFS-6N (Li & Yin, 2018)
(EW and WW refer to the east wall and west wall of the trench, respectively.)

7. CONCLUSIONS

This report covered the construction, acceptance, material characterization, instrumentation, and traffic testing of CC9 CTPB test items. The following are key findings from the traffic tests on the CTPB test items:

1. Laboratory resilient modulus and in-place LWD data indicated the CTPB material had significantly higher stiffness than the traditional crushed aggregate base. A reasonable design modulus for CTPB is in the range of 200,000 to 400,000 psi, with a default value of 300,000 psi.

2. Both the CTPB and the control test item sustained more than 40,000 passes from the NAPTV three-dimensional gear at 58,000 lb per wheel. The control test item failed after about 38,000 passes by exhibiting a classic shear failure with upheaval exceeding one in. The CTPB test item was technically a non-failure, but final upheaval (~ 0.8 in.) was close to the failure criterion.

3. The CTPB did not improve rutting performance compared to the standard base.

4. Based on NDT analysis, permanent deformation under traffic in both the CTPB and control test items was largely confined to the base and subbase layers, with little to no permanent deformation of the asphalt surface or subgrade contributing to total rutting. These results must be confirmed by future physical investigations.

5. Densification of CTPB materials contributed to significant rutting over the service life of the flexible test pavements. NDT analysis suggested that thinning of up to 1 in. in the CTPB layer may have occurred in trafficked areas of the CTPB test item. Again, this result must be confirmed by future trench investigations.

6. Peak sensor responses in granular layers are primarily a function of the current wander position. However, they are also strongly affected by the track associated with the previous pass, demonstrating the rearrangement of aggregate particles that takes place during wandered traffic.

7. Total rutting was comparable between the CC7 ATPB and the CC9 CTPB test items. However, a direct comparison between them must consider the different trafficking seasons. CC7 LFS-6N was tested mainly in the winter, so it experienced much higher cracking than CC9 LFS-4N.

8. REFERENCES

Ahlvin, R. G., Turnbull, W. J., Sale, J. P., & Maxwell, A. A. (1971). *Multiple-wheel heavy gear load pavement tests, Volume 1* (Technical Report No. AFWL-TR-70-113). Defense Technical Information Center, Vicksburg, MS. https://archive.org/details/DTIC_AD0889705

ASTM. (2015). *Standard test method for measuring rut-depth of pavement surfaces using a straightedge* (ASTM E1703/E1703M-10(2015)). ASTM International, West Conshohocken, PA.

ASTM. (2020). *Standard test method for airport pavement condition index surveys* (ASTM D5340-20). ASTM International, West Conshohocken, PA.

Bilodeau, J. P., & Doré, G. (2014). Stress distribution experienced under a portable light-weight deflectometer loading plate. *International Journal of Pavement Engineering*, *15*(6), 564–575. https://doi.org/10.1080/10298436.2013.772612

Dawson, A. (1994) *The ε-mu System, User's Manual. Second Edition.* University of Nottingham.

Federal Aviation Administration (FAA). (2018, December 21), *Standards for Specifying Construction of Airports* (Advisory Circular (AC) 150/5370-10H*)*. https://www.faa.gov/airports/resources/advisory_circulars/index.cfm/go/document.current/documentnumber/150_5370-10

Garg, N., Li, Q., & Brill, D. (2020). Accelerated pavement testing of perpetual pavement test sections under heavy aircraft loading at FAA's National Airport Pavement Test Facility. *Journal of Testing and Evaluation*, *48*(1), 107–119. https://doi.org/10.1520/JTE20180906

Gemini Technologies & GDIT. (2019). *Resilient modulus testing of P-307MR cement-treated permeable base* (Contract No.: DTFACT-15-D-00007). U.S. Dept. of Transportation, Federal Aviation Administration.

Hall, J. (1998). *National Airport Pavement Test Facility Test Pavement, 100% Submittal* [Unpublished report]. Prepared by DMJM/Cornell, A Joint Venture, for U.S. Army Corps of Engineers, August 28, 1998.

Hall, J. W., Mallela, J., Smith, K. L., Evans, L. D., Feldman, D., & Gotlif, A. (2005). *Stabilized and drainable base for rigid pavement* (Research Report No. IPRF-01-G-002-02-1). Innovative Pavement Research Foundation, Airport Concrete Pavement Technology Program. https://www.acpa.org/wp-content/IPRF/Resources/iprf-01-g-002-02-1-final%20report.pdf

Jumikis, A. R. (1977). *Thermal Geotechnics.* Rutgers University Press.

Kazmee, H., Murrell, S., Ricalde, L., Parsons, T., Duah, E., & Brill, D.R. (2026a). *National Airport Pavement Test Facility Construction Cycle 9, Volume 1—Traffic test summary* (DOT/FAA/TC-26/11), U.S. Dept. of Transportation, Federal Aviation Administration. https://doi.org/10.21949/48sn-jq09

Kazmee, H., Murrell, S., Ricalde, L., Parsons, T., Duah, E., Brill, D. R. & Offenbacker, D. (2026b). *National Airport Pavement Test Facility Construction Cycle 9, Volume 3—Geosynthetic test* (DOT/FAA/TC-26/15), U.S. Dept. of Transportation, Federal Aviation Administration. https://rosap.ntl.bts.gov/view/dot/89588

Li, Q., & Yin, H. (2018). *Construction Cycle 7 post-traffic field testing report* [Unpublished internal report]. U.S. Department of Transportation, Federal Aviation Administration.

Liang, R. Y. (2007) *Evaluation of drainable bases under asphalt pavements* (Research Report No. FHWA/OH-2007/10). U.S. Department of Transportation, Federal Highway Administration. https://rosap.ntl.bts.gov/view/dot/39577

Mazzotta, C., Murrell, S., Evans, D., & Breder, E. (2024). *Exploring Construction Cycle 9 with nondestructive testing: Innovations and insights in full-scale airport pavement testing* (in publication). U.S. Department of Transportation, Federal Aviation Administration, Washington, DC.

Mooney, M. A., & Miller, P. K. (2009). Analysis of lightweight deflectometer test based on in situ stress and strain response. *Journal of Geotechnical and Geoenvironmental Engineering*, *135*(2), 199–208. https://doi.org/10.1061/(ASCE)1090-0241(2009)135:2(199)

Nazarian, S., Baker, M., & Crain, K. (1993). *Development and testing of a seismic pavement analyzer* (Research Report No. SHRP-H-375). Strategic Highway Research Program, National Research Council. https://onlinepubs.trb.org/onlinepubs/shrp/SHRP-H-375.pdf

Selig, E. T., & Grangaard, O. H. (1970). A new technique for soil strain measurement. *Materials Research and Standards*, *10*(11), 19–21.

Tomlinson, C, Traverso, D., Cary, C., & Brynick, M. (2022). *Construction cycle 9 (CC9) construction report* (DOT/FAA/TC-22/1) U.S. Department of Transportation, Federal Aviation Administration. https://www.airporttech.tc.faa.gov/Products/Airport-Pavement-Papers-Publications/Airport-Pavement-Detail/construction-cycle-9-cc9-construction-report

Yin, H., Cary, C., Li, Q., Augustyn, S., & Davis, J. (2020) *Partial fulfillment of deliverable 4.9.2 Construction cycle 7 test report—Perpetual Pavement and asphalt treated drainable base tests.* U.S. Department of Transportation, Federal Aviation Administration. FINAL_TO5_Del 4.9.2.1_CC7 North Traffic Report.pdf

APPENDIX A—LAYOUT OF SENSORS IN CEMENT-TREATED PERMEABLE BASE TEST ITEMS

Table A-1. Longitudinal Stations and Transverse Offsets of Embedded Sensors in Test Item LFS-4N

Sensor ID	Longitudinal Station (ft)	Transverse Offset (ft)	Embedment Depth (in.)
CS-LFC4N-1	202.5	-12.75	14
CS-LFC4N-2	202.5	-12.75	17
CS-LFC4N-3	202.5	-12.75	43
CS-LFC4N-4	202.5	-12.75	46
LSG-LFS4N-1	185	-17.25	5
LSG-LFS4N-2	187	-17.25	5
LSG-LFS4N-3	185	-12.75	5
LSG-LFS4N-4	187	-12.75	5
MS-LFS4N-1	202.5	-15	48
PC-LFS4N-1	202.5	-15	13
PC-LFS4N-2	202.5	-15	42
T-LFS4N-1	202.8	-28.71	0
T-LFS4N-2	202.8	-28.71	1
T-LFS4N-3	202.8	-28.71	2
T-LFS4N-4	202.8	-28.71	3
T-LFS4N-5	202.8	-28.71	4
T-LFS4N-6	202.8	-28.71	5
TSG-LFS4N-1	189	-17.25	5
TSG-LFS4N-2	191	-17.25	5
TSG-LFS4N-3	189	-12.75	5
TSG-LFS4N-4	191	-12.75	5

Table A-2. Longitudinal Stations and Transverse Offsets of Embedded Sensors in Test Item LFC-4S

Sensor ID	Longitudinal Station (ft)	Transverse Offset (ft)	Embedment Depth (in.)
CS-LFC4S-1	202.5	12.75	14
CS-LFC4S-2	202.5	12.75	17
CS-LFC4S-3	202.5	12.75	43
CS-LFC4S-4	202.5	12.75	46
CS-LFC4S-5	210	15	5.54
CS-LFC4S-6	210	15	8.54
CS-LFC4S-7	210	15	11.54
CS-LFC4S-8	210	15	14.54
LSG-LFC4S-1	185	12.75	5
LSG-LFC4S-2	187	12.75	5
LSG-LFC4S-3	185	17.25	5
LSG-LFC4S-4	187	17.25	5
MS-LFC4S-1	202.5	15	48
PC-LFC4S-1	202.5	15	5
PC-LFC4S-2	202.5	15	13
PC-LFC4S-3	202.5	15	19
PC-LFC4S-4	202.5	15	42
TSG-LFC4S-1	189	12.75	5
TSG-LFC4S-2	191	12.75	5
TSG-LFC4S-3	189	17.25	5
TSG-LFC4S-4	191	17.25	5

APPENDIX B—MAXIMUM SURFACE UPHEAVALS IN CONSTRUCTION CYCLE 9 CEMENT-TREATED PERMEABLE BASE TEST ITEMS

Table B-1. Test Item LFS-4N, Station 1+95 (upheaval computed from Virtual Upheaval Calculator)

Date	Pass Number	Left of Center		Right of Center		Maximum Upheaval, in.
		Offset, ft	Upheaval, in.	Offset, ft	Upheaval, in.	
04/02/2021	0	-29.9167	0.000000	-14.9167	0.000000	0.000000
04/09/2021	330	-28.5833	0.167824	-5.3333	0.132779	0.167824
04/16/2021	858	-28.5833	0.215824	-1.1667	0.152000	0.215824
04/23/2021	1452	-24.5000	0.140779	-5.5000	0.299221	0.299221
04/30/2021	2046	-24.4167	0.194145	-5.3333	0.148000	0.194145
05/07/2021	2640	-28.5000	0.291353	-5.3333	0.184000	0.291353
05/19/2021	3234	-28.5833	0.224296	-5.3333	0.172000	0.224296
06/04/2021	3762	-24.4167	0.254158	-5.3333	0.172000	0.254158
06/11/2021	4356	-28.6667	0.275553	-6.4167	0.218582	0.275553
06/18/2021	4950	-28.5000	0.243824	-5.4167	0.208000	0.243824
06/25/2021	5544	-28.5833	0.347824	-5.5000	0.212000	0.347824
08/06/2021	6138	-24.5000	0.224000	-6.5000	0.197822	0.224000
08/13/2021	6666	-28.5000	0.278720	-6.5000	0.271208	0.278720
09/17/2021	9702	-24.4167	0.338145	-4.5000	0.230364	0.338145
10/01/2021	11286	-28.6667	0.378099	-6.5000	0.262116	0.378099
10/20/2021	12610	-24.4167	0.409873	-4.2500	0.425462	0.425462
03/18/2022	15378	-24.4167	0.385436	-5.4167	0.581881	0.581881
04/01/2022	16962	-28.5000	0.488840	-5.3333	0.436000	0.488840
04/15/2022	18480	-24.4167	0.374145	-5.3333	0.396991	0.396991
04/27/2022	20064	-22.2500	0.385206	-5.3333	0.369475	0.385206
05/13/2022	22044	-23.5000	0.435548	-5.5000	0.415431	0.435548
05/26/2022	23892	-24.4167	0.406315	-5.3333	0.357159	0.406315
06/10/2022	25740	-28.5000	0.504829	-3.2500	0.412303	0.504829
06/24/2022	27324	-23.5000	0.393256	-5.5000	0.453055	0.453055
08/12/2022	33924	-28.5000	0.551623	-5.4167	0.745630	0.745630
08/26/2022	35904	-23.5000	0.686029	-4.3333	0.673851	0.686029
09/09/2022	37554	-24.3333	0.713639	-6.5000	0.869103	0.869103
09/23/2022	38874	-23.1667	0.690008	-5.3333	0.736000	0.736000
10/07/2022	40920	-24.4167	0.722139	-6.5833	0.720221	0.722139

Table B-2. Test Item LFS-4N, Station 2+10 (upheaval computed from Virtual Upheaval Calculator)

Date	Pass Number	Left of Center		Right of Center		Maximum Upheaval, in.
		Offset, ft	Upheaval, in.	Offset, ft	Upheaval, in.	
04/02/2021	0	-30.0000	0.000000	-15.0000	0.000000	0.000000
04/09/2021	330	-22.0000	0.185474	-3.8333	0.200570	0.200570
04/16/2021	858	-27.7500	0.178754	-7.9167	0.219532	0.219532
04/23/2021	1452	-23.0833	0.156000	-3.7500	0.228611	0.228611
04/30/2021	2046	-26.8333	0.123221	-6.0833	0.126726	0.126726
05/07/2021	2640	-29.4167	0.244998	-7.7500	0.165427	0.244998
05/19/2021	3234	-27.4167	0.168000	-6.0833	0.093622	0.168000
06/04/2021	3762	-24.3333	0.168000	-7.7500	0.140664	0.168000
06/11/2021	4356	-21.9167	0.258221	-6.0833	0.165622	0.258221
06/18/2021	4950	-29.5833	0.343386	-7.8333	0.128664	0.343386
06/25/2021	5544	-21.9167	0.302707	-7.8333	0.212647	0.302707
08/06/2021	6138	-22.9167	0.168000	-7.8333	0.128664	0.168000
08/13/2021	6666	-21.9167	0.267001	-7.8333	0.200652	0.267001
09/17/2021	9702	-24.3333	0.364000	-7.8333	0.293988	0.364000
10/01/2021	11286	-22.9167	0.345403	-7.7500	0.245096	0.345403
10/20/2021	12610	-21.9167	0.336324	-6.0833	0.393622	0.393622
03/18/2022	15378	-21.9167	0.266464	-4.0000	0.515572	0.515572
04/01/2022	16962	-21.8333	0.388734	-4.0000	0.371459	0.388734
04/15/2022	18480	-26.9167	0.331170	-7.4167	0.332823	0.332823
04/27/2022	20064	-29.5833	0.409343	-6.0833	0.286157	0.409343
05/13/2022	22044	-24.2500	0.367182	-6.0833	0.328133	0.367182
05/26/2022	23892	-23.7500	0.271272	-6.0833	0.296273	0.296273
06/10/2022	25740	-29.6667	0.392694	-6.0000	0.463912	0.463912
06/24/2022	27324	-24.2500	0.365000	-6.0833	0.346736	0.365000
08/12/2022	33924	-24.0833	0.341844	-5.9167	0.450796	0.450796
08/26/2022	35904	-22.0000	0.445586	-6.9167	0.647499	0.647499
09/09/2022	37554	-24.1667	0.527647	-6.0833	0.827328	0.827328
09/23/2022	38874	-22.8333	0.546612	-5.8333	0.683955	0.683955
10/07/2022	40920	-24.3333	0.492177	-6.0833	0.537622	0.537622

Table B-3. Test Item LFC-4S, Station 1+95 (upheaval computed from Virtual Upheaval Calculator)

Date	Pass Number	Left of Center		Right of Center		Maximum Upheaval, in.
		Offset, ft	Upheaval, in.	Offset, ft	Upheaval, in.	
04/02/2021	0	0.0833	0.000000	15.0833	0.000000	0.000000
04/09/2021	330	7.1667	0.250918	26.7500	0.246781	0.250918
04/16/2021	858	7.1667	0.202019	29.9167	0.204054	0.204054
04/23/2021	1452	6.4167	0.337806	24.5833	0.328277	0.337806
04/30/2021	2046	7.0833	0.143706	22.0000	0.173422	0.173422
05/07/2021	2640	7.1667	0.214019	25.5000	0.101919	0.214019
05/19/2021	3234	7.1667	0.190019	22.0833	0.075952	0.190019
06/04/2021	3762	7.1667	0.190019	29.1667	0.120000	0.190019
06/11/2021	4356	7.1667	0.262019	25.4167	0.202349	0.262019
06/18/2021	4950	7.1667	0.190019	29.5000	0.140730	0.190019
06/25/2021	5544	7.1667	0.262006	22.0000	0.170467	0.262006
08/06/2021	6138	7.16667	0.226019	29.8333	0.195516	0.226019
08/13/2021	6666	7.1667	0.246019	29.9167	0.189104	0.246019
09/17/2021	9702	6.3333	0.292956	23.3333	0.247220	0.292956
10/01/2021	11286	6.3333	0.280956	24.5833	0.204000	0.280956
10/20/2021	12610	7.2500	0.278997	22.0000	0.287343	0.287343
03/18/2022	15378	6.9167	0.397608	25.4167	0.234646	0.397608
04/01/2022	16962	7.0833	0.414079	22.0833	0.283780	0.414079
04/15/2022	18480	7.1667	0.348781	24.5000	0.268370	0.348781
04/27/2022	20064	7.1667	0.333127	22.0000	0.218815	0.333127
05/13/2022	22044	6.3333	0.366707	29.8333	0.304801	0.366707
05/26/2022	23892	7.3333	0.376877	21.8333	0.224863	0.376877
06/10/2022	25740	7.1667	0.370019	23.2500	0.337597	0.370019
06/24/2022	27324	6.4167	0.453333	27.1667	0.330386	0.453333
08/12/2022	33924	7.0833	0.531455	24.5000	0.486397	0.531455
08/26/2022	35904	6.3333	0.674943	23.3333	0.909238	0.909238
09/09/2022	37554	6.3333	0.616888	23.2500	0.951287	0.951287
09/23/2022	38874	6.3333	0.699606	24.5000	1.031350	1.031350
10/07/2022	40920	6.3333	0.544945	23.3333	1.395970	1.395970

Table B-4. Test Item LFC-4S, Station 2+10 (upheaval computed from Virtual Upheaval Calculator)

Date	Pass Number	Left of Center		Right of Center		Maximum Upheaval, in.
		Offset, ft	Upheaval, in.	Offset, ft	Upheaval, in.	
04/02/2021	0	0.0000	0.000000	15.0000	0.000000	0.000000
04/09/2021	330	1.5000	0.192000	21.9167	0.164471	0.192000
04/16/2021	858	4.5000	0.222400	22.0000	0.272186	0.272186
04/23/2021	1452	4.5000	0.107379	22.0000	0.152186	0.152186
04/30/2021	2046	1.4167	0.024000	24.7500	0.035678	0.035678
05/07/2021	2640	1.4167	0.096000	28.0833	0.144642	0.144642
05/19/2021	3234	2.5833	0.047442	28.1667	0.068307	0.068307
06/04/2021	3762	2.4167	0.044664	22.4167	0.060000	0.060000
06/11/2021	4356	3.7500	0.108000	28.0833	0.128642	0.128642
06/18/2021	4950	6.6667	0.027221	24.6667	0.036013	0.036013
06/25/2021	5544	5.2500	0.099336	24.6667	0.135234	0.135234
08/06/2021	6138	1.4167	0.024000	28.0833	0.053893	0.053893
08/13/2021	6666	2.7500	0.127288	28.0833	0.123862	0.127288
09/17/2021	9702	6.5833	0.134676	25.9167	0.127136	0.134676
10/01/2021	11286	1.3333	0.161646	24.7500	0.190498	0.190498
10/20/2021	12610	1.3333	0.137767	24.7500	0.250560	0.250560
03/18/2022	15378	7.9167	0.286417	23.1667	0.240688	0.286417
04/01/2022	16962	1.5000	0.221374	28.0000	0.250407	0.250407
04/15/2022	18480	1.4167	0.132252	22.3333	0.220138	0.220138
04/27/2022	20064	1.4167	0.126583	24.7500	0.181102	0.181102
05/13/2022	22044	1.7500	0.236807	24.6667	0.210789	0.236807
05/26/2022	23892	1.3333	0.300246	28.0833	0.279295	0.300246
06/10/2022	25740	1.3333	0.157665	28.0000	0.300195	0.300195
06/24/2022	27324	5.6667	0.204389	22.0000	0.208195	0.208195
08/12/2022	33924	5.6667	0.258784	22.6667	0.404224	0.404224
08/26/2022	35904	0.0000	0.295616	23.0000	0.761006	0.761006
09/09/2022	37554	1.6667	0.338179	22.8333	0.707116	0.707116
09/23/2022	38874	5.7500	0.231602	22.5833	0.682184	0.682184
10/07/2022	40920	1.4167	0.248375	22.8333	0.856815	0.856815

APPENDIX C—VISUAL DISTRESS LOG

Table C-1. Log of Cracks Observed in Cement=Treated Permeable Base Test Item LFS-4N

Crack Number	Date of Recording	Start		End		Length of Crack (ft)
		X (Offset from Centerline) (ft)	Y (Offset from Station) (ft)	X (Offset from Centerline) (ft)	Y (Offset from Station) (ft)	
176	7-Oct-22	230	10 from 1+80↑	233	14.5 from 1+80↑	5.4
177	7-Oct-22	228	12 from 1+80↑	225	15.5 from 1+80↑	4.6
178	7-Oct-22	224	15.5 from 1+80↑	223.5	16.5 from 1+80↑	1.1
179	7-Oct-22	207	16 from 1+80↑	204.5	14.5 from 1+80↑	2.9
180	7-Oct-22	224	46 from 1+80↑	223	53 from 1+80↑	7.1
181	7-Oct-22	193.5	65.5 from 1+95↑	194	64 from 1+95↑	1.6
182	7-Oct-22	133.5	50.5 from 2+25↓	134	51.5 from 2+25↓	1.1
183	7-Oct-22	170.5	22.5 from 2+25↓	170	25 from 2+25↓	2.5
184	7-Oct-22	175	13.5 from 2+25↓	174	21 from 2+25↓	7.6
185	7-Oct-22	216	47 from 2+25↓	215.5	50 from 2+25↓	3.0
186	7-Oct-22	151	92.5 from 2+10↑	150	99 from 2+10↑	6.6
187	7-Oct-22	153.5	95 from 2+10↑	171.5	94 from 2+10↑	18.0
188	7-Oct-22	216	22 from 2+10↑	215.5	8 from 2+10↑	14.0
189	7-Oct-22	146.5	52 from 2+10↓	166.5	51.5 from 2+10↓	20.0
190	7-Oct-22	127.5	71.5 from 2+10↓	127	74.5 from 2+10↓	3.0
191	7-Oct-22	128	83 from 2+10↓	128.5	85 from 2+10↓	2.1
192	7-Oct-22	107	70 from 2+10↓	107	72.5 from 2+10↓	2.5
193	7-Oct-22	132.5	23 from 1+95↑	132	26 from 1+95↑	3.0
194	7-Oct-22	197	6 from 1+95↓	211.5	10 from 1+95↓	15.0
195	7-Oct-22	225	24 from 1+95↓	228	24.5 from 1+95↓	3.0
196	7-Oct-22	131.5	34.5 from 1+95↓	132.5	32 from 1+95↓	2.7
197	7-Oct-22	176	67 from 1+80↑	171	64.5 from 1+80↑	5.6
198	7-Oct-22	173.5	2 from 1+80↑	175.5	9 from 1+80↑	7.3
199	7-Oct-22	109	32 from 1+80↑	108	25.5 from 1+80↑	6.6

Table C-2. Log of Cracks Observed in Control Test Item LFC-4S

Crack Number	Date of Recording	Start		End		Length of Crack (ft)
		X (Offset from Centerline) (ft)	Y (Offset from Station) (ft)	X (Offset from Centerline) (ft)	Y (Offset from Station) (ft)	
3	22-Apr-22	141	0 from 1+80↑	141	7 from 1+80↑	7.0
4	22-Apr-22	216	0 from 1+80↑	17.5	104 from 1+80↑	224.1
5	22-Apr-22	226.5	0 from 1+80↑	234.5	61 from 1+80↑	61.5

Crack Number	Date of Recording	Start		End		Length of Crack (ft)
		X (Offset from Centerline) (ft)	Y (Offset from Station) (ft)	X (Offset from Centerline) (ft)	Y (Offset from Station) (ft)	
6	22-Apr-22	248	0 from 1+80↑	250.5	129.5 from 1+80↑	129.5
7	22-Apr-22	110	71.5 from 1+95↓	112	69from 1+95↓	3.2
8	22-Apr-22	112	68 from 1+95↓	109	30 from 1+95↓	38.1
9	22-Apr-22	108	24 from 1+95↓	108	29.5 from 1+95↓	5.5
10	22-Apr-22	188.5	30 from 1+95↓	188.5	47 from 1+95↓	17.0
11	22-Apr-22	187.5	30 from 1+95↓	188.5	15 from 1+95↓	15.0
12	22-Apr-22	188	14 from 1+95↓	188.5	5 from 1+95↓	9.0
13	22-Apr-22	217	75 from 1+95↓	218	46 from 1+95↓	29.0
14	22-Apr-22	219	45 from 1+95↓	216	32.5 from 1+95↓	12.9
15	22-Apr-22	217	32 from 1+95↓	218	28 from 1+95↓	4.1
16	22-Apr-22	218.5	21.75 from 1+95↓	217	3.5 from 1+95↑	25.3
17	22-Apr-22	217.5	58.5 from 1+95↑	217.5	49 from 1+95↑	9.5
18	22-Apr-22	224.5	80 from 1+95↓	226	34.75 from 1+95↓	45.3
19	22-Apr-22	227	78.5 from 1+95↓	227.5	65 from 1+95↓	13.5
20	22-Apr-22	228.5	27.5 from 1+95↓	227.5	160.5 from 1+95↓	133.0
21	22-Apr-22	249.5	49 from 1+95↓	252	49 from 1+95↑	98.0
22	22-Apr-22	228.5	23.5 from 1+95↑	229.5	34.75 from 1+95↑	11.3
23	22-Apr-22	245.5	71 from 2+10↑	246	65 from 2+10↓	136.0
24	22-Apr-22	245.5	64.5 from 2+10↑	251	160.5 from 2+10↑	96.2
25	22-Apr-22	251	18.5 from 2+25↓	250.25	7.5 from 2+25↓	11.0
26	22-Apr-22	250	0 from 2+25↓	250	6 from 2+25↓	6.0
27	22-Apr-22	132	45 from 2+25↓	134	32 from 2+25↓	13.2
28	22-Apr-22	133	27 from 2+25↓	132.5	24 from 2+25↓	3.0
29	22-Apr-22	132.5	23 from 2+25↓	133.5	20.5 from 2+25↓	2.7
30	22-Apr-22	133	19.5 from 2+25↓	133	16 from 2+25↓	3.5
31	22-Apr-22	110	13 from 2+25↓	109	0 from 2+25↓	13.0
36	27-Apr-22	139	31.5 from 1+80↑	130	56.5 from 1+80↑	26.6
9	27-Apr-22	109.5	24.5 from 1+95↓	110	4 from 1+95↓	20.5
37	27-Apr-22	136.5	23 from 1+95↓	154	23.5 from 1+95↓	17.5
38	27-Apr-22	154	23 from 1+95↓	153	40 from 1+95↓	17.0
39	27-Apr-22	154	23 from 1+95↓	164	20.5 from 1+95↓	10.3
40	27-Apr-22	164	20.5 from 1+95↓	163.5	22 from 1+95↓	1.6
41	27-Apr-22	163.5	22 from 1+95↓	174	20.5 from 1+95↓	10.6
46	5-May-22	227	70 from 1+80↑	230	77.5 from 1+80↑	8.1
47	5-May-22	153	6.5 from 1+80↑	150.5	31.5 from 1+80↑	25.1
48	5-May-22	188.5	51.5 from 1+80↑	187	56 from 1+80↑	4.7
49	5-May-22	187.5	60.5 from 1+80↑	187	88 from 1+80↑	27.5
50	5-May-22	109	5 from 1+95↓	108	78 from 1+95↓	73.0
51	5-May-22	134	50 from 2+25↓	132	15 from 2+25↓	35.1
79	15-Jun-22	110.5	37 from 1+80↑	110.5	44 from 1+80↑	7.0
80	15-Jun-22	135.5	42.5 from 1+80↑	136.5	38.5 from 1+80↑	4.1
81	15-Jun-22	135.5	8 from 1+80↑	140	6 from 1+80↑	4.9
82	15-Jun-22	136	62 from 1+80↑	137	65.5 from 1+80↑	3.6
83	15-Jun-22	140.5	67.5 from 1+80↑	137	65.5 from 1+80↑	4.0
84	15-Jun-22	221.5	100.5 from 1+80↑	214.5	100.5 from 1+80↑	7.0
85	15-Jun-22	192	47.5 from 1+95↓	189.5	47 from 1+95↓	2.5
86	15-Jun-22	189	46 from 1+95↓	173	45.5 from 1+95↓	16.0
87	15-Jun-22	163.5	40.5 from 1+95↓	173	45.5 from 1+95↓	10.7
88	15-Jun-22	162.5	38.5 from 1+95↓	164.5	30.5 from 1+95↓	8.2

Crack Number	Date of Recording	Start		End		Length of Crack (ft)
		X (Offset from Centerline) (ft)	Y (Offset from Station) (ft)	X (Offset from Centerline) (ft)	Y (Offset from Station) (ft)	
89	15-Jun-22	216.5	65.5 from 1+95↑	218	0 from 1+95↑	65.5
90	15-Jun-22	108.5	78 from 1+95↑	106	105.5 from 1+95↑	27.6
91	15-Jun-22	249.5	109.5 from 1+95↑	249.5	106 from 1+95↑	3.5
92	15-Jun-22	109	13 from 2+25↓	110	16 from 2+25↓	3.2
93	15-Jun-22	122	16 from 2+25↓	126	15.5 from 2+25↓	4.0
94	15-Jun-22	133	50 from 2+25↓	136	50.5 from 2+25↓	3.0
95	15-Jun-22	173	12 from 2+25↓	176	14 from 2+25↓	3.6
96	15-Jun-22	183.5	12 from 2+25↓	176	14 from 2+25↓	7.8
100	1-Jul-22	171.5	14 from 1+80↑	169.5	8.5 from 1+80↑	5.9
101	1-Jul-22	160	7.5 from 1+80↑	169.5	8.5 from 1+80↑	9.6
102	1-Jul-22	157	9.5 from 1+80↑	160	7.5 from 1+80↑	3.6
103	1-Jul-22	162.5	0 from 1+80↑	186	2.5 from 1+80↑	23.6
104	1-Jul-22	168.5	17 from 1+80↑	171	19.5 from 1+80↑	3.5
105	1-Jul-22	173.5	67 from 1+80↑	186.5	67.5 from 1+80↑	13.0
106	1-Jul-22	162	65 from 1+80↑	165	63 from 1+80↑	3.6
107	1-Jul-22	165	63 from 1+80↑	171.5	65 from 1+80↑	6.8
108	1-Jul-22	110	36.5 from 1+80↑	109	35 from 1+80↑	1.8
109	1-Jul-22	159.5	83 from 1+80↑	161	87 from 1+80↑	4.3
110	1-Jul-22	153	67 from 1+95↓	157	68.5 from 1+95↓	4.3
111	1-Jul-22	196	73 from 1+95↓	200.5	73 from 1+95↓	4.5
112	1-Jul-22	109	56.5 from 1+95↓	109	46 from 1+95↓	10.5
113	1-Jul-22	122	17.5 from 1+95↓	123	18 from 1+95↓	1.1
114	1-Jul-22	164.5	27.5 from 1+95↓	165	31.5 from 1+95↓	4.0
115	1-Jul-22	163.5	38.5 from 1+95↓	164.5	39.5 from 1+95↓	1.4
116	1-Jul-22	200.5	21 from 1+95↓	203	21 from 1+95↓	2.5
117	1-Jul-22	170.5	0 from 1+95↓	193	2 from 1+95↓	22.6
118	1-Jul-22	170.5	0 from 1+95↑	166	4.5 from 1+95↑	6.4
119	1-Jul-22	155	19 from 1+95↑	173.5	19.5 from 1+95↑	18.5
120	1-Jul-22	170.5	22.5 from 1+95↑	171.5	21.5 from 1+95↑	1.4
121	1-Jul-22	169.5	37 from 1+95↑	172.5	35 from 1+95↑	3.6
122	1-Jul-22	171.5	34 from 1+95↑	172.5	35 from 1+95↑	1.4
123	1-Jul-22	172.5	35 from 1+95↑	179	34.5 from 1+95↑	6.5
124	1-Jul-22	228.5	33 from 1+95↑	229	34.5 from 1+95↑	1.6
125	1-Jul-22	229.5	34.5 from 1+95↑	229.5	37.5 from 1+95↑	3.0
126	1-Jul-22	106	73.5 from 2+10↓	106.5	72 from 2+10↓	1.6
127	1-Jul-22	109	16 from 2+25↓	109	17 from 2+10↓	181.0
128	1-Jul-22	122	15 from 2+25↓	123.5	16 from 2+25↓	1.8
129	1-Jul-22	182.5	11.5 from 2+25↓	185.5	11 from 2+25↓	3.0

APPENDIX D—DISTRESS MAP

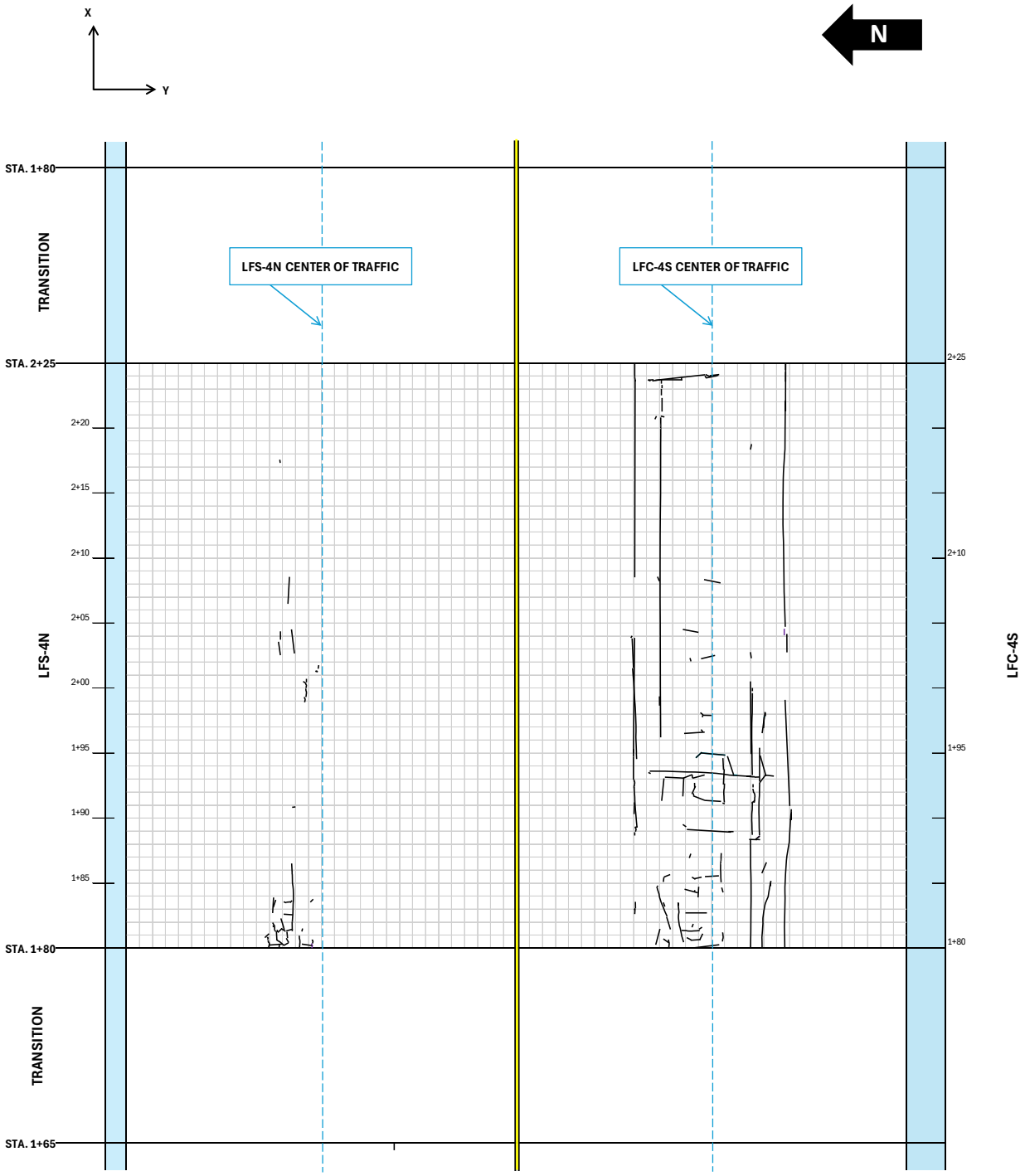

Figure D-1. Distribution of Cracks in Construction Cycle 9 Cement-Treated Permeable Base Test Items at the End of Trafficking

Item P-307MR Cement-Treated Permeable Base Course (CTPB)

DESCRIPTION

307MR-1.1 This item shall consist of an open-graded drainable base composed of mineral aggregate, cement and water mixed in a central mixing plant and placed on a prepared subgrade or subbase course in accordance with these specifications and shall conform to the lines, grades, thickness, and typical cross sections shown in the plans.

307MR-1.2 Submittals. At least 30 days prior to the placement of the CTPB, the Contractor shall submit certified test reports to the Engineer for those materials proposed for use during construction, as well as the mix design information for the material. The certification shall show the ASTM or AASHTO specifications or tests for the material, the name of the company performing the tests, the date of the tests, the test results, and a statement that the material did or did not comply with the applicable specifications. The submittal package shall be in accordance with Section 61MR Submittal Procedures and include the following:

a. **SD-02 Shop Drawings**
    1) **Proposed techniques.** Contractor shall provide a placement plan including the sequence of paving, forming and placing methods, consolidation methods, finishing methods, and curing methods.
b. **SD-03 Product Data**
    1) **Coarse aggregate.** Contractor shall provide the coarse aggregate source and physical properties as per Paragraph 307MR-2.1.
    2) **Fine aggregate.** Contractor shall provide the fine aggregate source and physical properties as per Paragraph 307MR-2.1.
    3) **Cement.** Contractor shall provide the cement source and physical properties as per Paragraph 307MR-2.3.
    4) **Admixtures.** Contractor shall provide the admixtures source and physical properties as per Paragraph 307MR-2.5.
    5) **Curing materials.** Contractor shall provide the curing materials source and physical properties as per Paragraph 307MR-2.6.
    6) **Construction equipment list.** Contractor shall provide to the Engineer the list of proposed equipment to be used in the performance of construction work, including descriptive data for approval.
c. **SD-05 Design Data**
    1) **Mix design.** Contractor shall provide the mix design containing the information identified in Paragraph 307MR-3.1. Mix design documentation must be complete, containing all items identified.
d. **SD-06 Test Reports**
    1) **Gradation (Pre-Construction).** Contractor shall provide the mix design gradation as per Paragraph 307MR-2.2a.
    2) **Gradation (In-Place).** Engineer shall provide in-place gradation results as per

Paragraph 307MR-2.2b.

3) **Compressive strength.** Engineer shall provide certified test reports that material complies with the requirements of Paragraph 307MR-3.1 and 307MR-5.2.
4) **Smoothness test results.** Engineer shall provide certified test reports that material complies with the requirements of Paragraph 307MR-5.3.
5) **Grade test results.** Engineer shall provide certified test reports that material complies with the requirements of Paragraph 307MR-5.4.
6) **Thickness test results.** Certified test reports shall be provided that material complies with the requirements of Paragraph 209MR-5.5.
7) **Coefficient of permeability.** Engineer shall provide certified test reports that material complies with the requirements of Paragraph 307MR-3.1 and 307MR-5.6.
8) **Survey.** Engineer shall provide a survey of the as-built surface after acceptance.

e. SD-07 Certificates

1) **Testing Laboratory Accreditation.** Contractor shall provide documentation that laboratories used for quality control and for acceptance testing are accredited in accordance with the requirements of this specification and Item C-100MR.

No drainable base course material shall be placed until the submittal is accepted in writing by the Engineer.

During production, the Contractor shall submit batch tickets for each delivered load.

MATERIALS

307MR-2.1 Aggregate. Coarse aggregate shall be crushed gravel or crushed stone and shall meet the gradation requirements of ASTM C33 Size 67. Fine aggregate shall consist of natural sand or manufactured sand meeting the requirements of ASTM C33. The aggregate shall meet the material requirements in the table below.

Aggregate Material Requirements

Coarse Aggregate Portion (retained on the No. 4 (4.75 mm) sieve)		
Material Test	**Requirement**	**Standard**
Resistance to Degradation	Loss: 40% maximum	ASTM C131
Soundness of Aggregates by Use of Sodium Sulfate **or** Magnesium Sulfate	Loss after 5 cycles: 10% maximum using Sodium sulfate - or - 15% maximum using magnesium sulfate	ASTM C88
Flat Particles, Elongated Particles, or Flat and Elongated Particles[1]	10% maximum, by weight, for fraction retained on the ½ inch (12.5mm) sieve and	ASTM D4791

Coarse Aggregate Portion (retained on the No. 4 (4.75 mm) sieve)		
Material Test	**Requirement**	**Standard**
	20% maximum, by weight, for the fraction passing the 1/2-inch (12.5 mm) sieve	
Clay lumps and friable particles	Less than or equal to 3 percent	ASTM C142
Fine Aggregate Portion (Passing the No. 40 (425µm) sieve)		
Clay lumps and friable particles	Less than or equal to 3 percent	ASTM C142
Soundness of Aggregates by Use of Sodium Sulfate **or** Magnesium Sulfate	Loss after 5 cycles: 10% maximum using Sodium sulfate - or - 15% maximum using magnesium sulfate	ASTM C88

[1] A flat particle is one having a ratio of width to thickness greater than three (3); an elongated particle is one having a ratio of length to width greater than three (3).

307MR-2.2 Sampling and testing.

a. **Aggregate base materials.** The Contractor shall take samples of the aggregate base in accordance with ASTM D75 to verify initial aggregate base requirements and gradation. Material shall meet the requirements in paragraphs 307MR-2.1. This sampling and testing will be the basis for approval of the aggregate base quality requirements.
b. **Gradation requirements.** The Engineer shall take at least two aggregate base samples per day to check the final gradation. Sampling shall be per ASTM D75. Material shall meet the requirements in paragraph 307MR-2.1. The samples shall be taken from the in-place, un-compacted material at sampling points and intervals designated by the Engineer.

307MR-2.3 Cement. Cement shall conform to the requirements of ASTM C150, Type I or II; ASTM C595, Type IP, IL, or IS.

The Contractor shall furnish vendor's certified test reports for cement shipped to the project.

307MR-2.4 Water. Water used in mixing or curing shall be from potable water sources. Other sources shall be tested in accordance with ASTM C1602 prior to use.

307MR-2.5 Admixtures. The use of any material to be added to the mixture shall be approved by the Engineer.

307MR-2.6 Curing Material. Curing materials shall conform to one of the following specifications:

- White burlap-polyethylene sheeting for curing concrete shall conform to the requirements of ASTM C171.

- Waterproof paper for curing concrete shall conform to the requirements of ASTM C171.

307-2.7 Separation Geotextile. Not used.

1) COMPOSITION OF MIXTURE

307MR-3.1 Mix design. The Mix Design shall be composed of a mixture of aggregate, cement, and water meeting the following requirements:

Mix Design Requirements

Material or Test	Requirements	Standard	
7-day Compressive strength, psi (kPa)	Between minimum 400 psi (2758 kPa) and maximum 800 psi (5516 kPa)	ASTM C31 and ASTM C39	Cylinders in accordance with ASTM C31 and test per ASTM C39
Coefficient of permeability (ft/day)	Between 500 to 1500 ft/day (150 to 450 m/day)	ASTM D2434.	
Water-Cement Ratio	Approx. 0.36		Cement content shall be adequate to hold the material together and meet strength requirements.
Coarse aggregate	Size #67	ASTM C33	
Fine aggregate	Approximately 300 to 400 pounds per cubic yard (178 to 237 kg/m3)		As necessary to meet stability while maintaining permeability

The mix design shall include a complete list of materials, including type, brand, source, and amount of cement, fine aggregate, coarse aggregate, water, and cementitious additives, if used. It shall also contain the 7 day compressive strength test results and the results of the permeability tests. Data shall be provided to the Engineer for 7-day breaks to serve as a basis for field testing requirements and comparison.

If the Contractor makes a change in aggregate sources or type of cement, or if cementitious additives are added or deleted from the mix, production of the drainable base course shall be stopped and a new mix design shall be submitted to the Engineer for approval at the Contractor's expense.

2) CONSTRUCTION METHODS

307MR-4.1 Control strip. Prior to construction, the Contractor shall place a quantity of CTPB according to the mix design at a location to be determined by the Contractor. The Contractor shall demonstrate, in the presence of the Engineer, that the materials, equipment, and construction processes meet the requirements of the specification. Control strips that do not meet specification requirements shall be removed and replaced at the Contractor's expense. Full operations shall not continue until the control strip has been accepted by the Engineer. Upon acceptance of the control

strip by the Engineer, the Contractor shall use the same equipment, materials, and construction methods for the remainder of construction, unless adjustments made by the Contractor are approved in advance by the Engineer. During placement of the CTPB test section, an additional "control strip" will be placed for field permeability testing, as to not introduce excess water into the test section.

When additional effort beyond that provided by the paver is required to seat the aggregate, additional compaction shall be initiated within 30 minutes following the placing and striking-off operations. The actual rolling pattern and sequence shall be established during placement of the control strip and approved by the Engineer. In areas inaccessible to the paver and roller, hand operated vibrator-plate compactors may be used to seat the aggregate.

The additional compaction, if required, shall be one to three passes of a self-propelled, steel-wheel static roller with weight between 5 and 12 tons (4.5 to 10.9 metric tons). The roller shall be in good condition and shall be capable of reversing without backlash and of compacting the CTPB without undue displacement or excessive crushing of the aggregate.

The control strip CTPB layer shall be considered acceptable when aggregate is completely coated with cement paste and shows no evidence of crushing; the surface is firm, unyielding and stable under construction traffic; and the layer meets the field permeability per paragraph 307MR-3.1.

307MR-4.2 Weather limitations. The CTPB material shall not be mixed or placed while the air temperature is below 40°F (4°C) or when conditions indicate that the temperature may fall below 35°F (2°C) within 24 hours. The CTPB shall not be placed on frozen underlying courses or mixed when aggregate is frozen. The CTPB may not be placed when rainfall is occurring or where rain is imminent. Any CTPB material that has become excessively wet by rain during transport and/or placement will be rejected.

307MR-4.3 Equipment. All equipment necessary to mix, transport, place, compact, and finish the CTDB material shall be furnished by the Contractor and approved by the Engineer. The equipment will be inspected by the Engineer prior to the start of construction operations.

307MR-4.4 Preparation of the underlying course. The underlying course shall be checked and accepted by the Engineer before placing operations begin. Prior to placing the material, the final grade should be firm, moist and free of frost. Use of chemicals to eliminate frost will not be

permitted. The underlying course shall be wetted in advance of placing the lean concrete base course.

307MR-4.5 Mixing. The batch plant site, layout, equipment, and provisions for transporting material shall assure a continuous supply of material to the work. Stockpiles shall be constructed in a manner that prevents segregation and intermixing of deleterious materials. Free access to the plant must be provided to the Engineer at all times for inspection of the plant's equipment and operation and for sampling the CTPB mixture and its components.

The mixers shall be examined daily by the Contractor and periodically by the Engineer for changes in condition due to accumulation of hard concrete or mortar or wear of blades. The pick-up and throw-over blades shall be replaced as necessary to provide adequate mixing. Aggregate and cement may be proportioned either by weight or volume, and shall be mixed sufficiently to prevent the forming of cement balls when water is added. Batching weights shall be within a tolerance of 1% for cement and 2% for aggregates. The mixing time shall be that required to produce a uniform mixture of aggregate, cement, and water.

307MR-4.6 Hauling. The CTPB mixture shall be transported from the plant to the job site in ready mix trucks, trucks, or other hauling equipment having beds that are smooth and clean. Truck bed covers shall be provided to protect the CTPB during transport from rain. CTPB material that becomes wet during transport will be rejected.

307MR-4.7 Placing. The CTPB material shall be placed using an asphalt paver. The CTPB shall be installed in a single 8 inch (200 mm) lift. The paver shall be capable of placing a uniform, full-depth layer of material across the full width of the base in one pass.

A secondary "control strip" shall be placed on the same day of placement for field permeability testing to limit the amount of water that is added to the test section.

307MR-4.8 Finishing. Shape the finished surface of the lean concrete base layer to the specified lines, grades, and cross-section.

307MR-4.9 Compaction. Immediately upon completion of the spreading operations, the CTPB material shall be compacted using the approved compaction equipment and roller pattern/sequence, as determined in the approved control strip. Sufficient rollers shall be furnished to handle the output of the plant. If the rolling pattern/sequence results in undue displacement of the surface, or causes crushing of the aggregate, work shall be stopped until the cause(s) can be determined and corrections are made.

Alternative compaction using a large asphalt paving machine with dual tamping bars may be used in lieu of the rolling.

In all places not accessible to the rollers (or the alternative paving machine), the CTPB material shall be compacted with approved mechanical hand-operated tampers.

When additional effort beyond that provided by the paver is required to seat the aggregate, additional compaction shall be initiated within 30 minutes following the placing and striking-off operations

307MR-4.10 Joints. The formation of all joints shall be made in such a manner as to ensure a continuous bond between old and new sections of the course. All joints shall present the same texture and smoothness as other sections of the course.

All contact surfaces of previously constructed courses shall be cleaned of all dirt or other objectionable material, thoroughly moistened with water prior to place the new material.

307MR-4.11 Curing. The completed drainage layer shall be moist cured for a period of seven days in accordance with paragraph 307MR-2.6.

307MR-4.12 Maintenance. The completed drainable base shall be maintained by the Contractor in a condition to meet all specification requirements until the pavement has been placed. Placement of the pavement shall be made within thirty (30) calendar days after placement of the drainage layer. The CTPB shall not be opened to traffic until specimens made in accordance with ASTM C31 and tested in accordance with ASTM C39 show that a 7-day compressive strength of 500 psi (35.2 kg/square cm) has been achieved.

3) MATERIAL ACCEPTANCE

307MR-5.1 Sampling and testing. All acceptance sampling and testing necessary to determine conformance with the requirements specified in this section will be performed by the Engineer for each day of production. Sampling locations will be determined by the Engineer on a random basis per ASTM D3665. The Contractor shall bear the cost of providing curing facilities for the strength specimens.

307MR-5.2 Acceptance Testing for Compressive Strength. One sample of CTPB will be taken for compressive strength for each day of production in accordance with ASTM C172. From the sample, three test cylinders will be made and cured per ASTM C31 and the 7-day compressive strength of each cylinder determined per ASTM C39. The compressive strength will be computed by averaging the three 7-day compressive strengths. The Contractor shall provide for the initial curing of cylinders in accordance with ASTM C31 during the 24 hours after molding.

307MR-5.3 Acceptance Testing for Smoothness. The Engineer shall perform smoothness checks daily. Any area not meeting smoothness and grade shall be corrected by the Contractor at the Contractor's expense.

The finished surface shall not vary more than ±3/8-inch (9 mm) when tested with a 12-foot (3.7-m) straightedge applied parallel with and at right angles to the centerline. The lot size shall consist of the entire length and width placed for each material. In the longitudinal direction, a smoothness reading shall be made along the centerline of each pull of material along the entire length of material. In the transverse direction, smoothness readings shall be made continuously across the full width of the testing area at 15 foot intervals and as determined by the Engineer (the outer 3ft may be excluded from testing). However, transverse smoothness readings shall not

be made across designed grade changes. The Contractor shall correct any high spots more than 3/8 inch (9 mm) in 12-foot (3.7-m) with a grinding machine or remove and replace the material at the Contractor's expense. The area will be considered accepted if less than 15% of the testing area is considered deficient.

307MR-5.4 Acceptance Testing for Grade. The Engineer shall perform grade checks daily. Any area not meeting grade shall be corrected by the Contractor at the Contractor's expense. The surface of the top layer in the testing area shall show no deviations in excess of 1/2 inch (13 mm) in the vertical direction from the target elevation when surveyed in a 5 foot by 5 foot grid, or equivalent method. When the surface is more than 1/2 inch (13 mm) above the grade shown in the plans, the surface shall be corrected at the Contractor's expense to an elevation that falls within a tolerance of 1/4 inch (6 mm).

307MR-5.5 Thickness Control. The thickness of the section shall be determined based on the before and after elevations of the finished surface. Prior to the first day of placement, the Engineer shall scan the surface using a LiDAR scanner. After placement, the Engineer shall scan the surface again using a LiDAR scanner. The difference in these two elevations shall not be more than 1/2 inch (12 mm) less than the thickness specified on the plans.

307MR-5.6 Acceptance Testing for Field Permeability. One test shall be limited to the control strips performed by the Engineer. The test location will be determined on a random basis in accordance with ASTM D3665. The permeability of the base will be determined in accordance with ASTM C1701.

4) METHOD OF MEASUREMENT

307MR-6.1 Measurement. The quantity of CTPB to be paid for shall be the number of square yards of material placed, and accepted in the completed base course.

5) BASIS OF PAYMENT

307MR-7.1 Payment. Payment will be made at the contract unit price per square yard for CTPB as measured by Engineer. This price shall be full compensation for furnishing all materials, for all preparation, mixing, placing, compacting, and curing; and for all labor, equipment, tools, and incidentals necessary to complete the item.

Payment will be made under:

Item P-307MR	Cement treated permeable base course (CTPB) - per square yard.

6) REFERENCES

The publications listed below form a part of this specification to the extent referenced. The publications are referred to within the text by the basic designation only.

ASTM International (ASTM)

ASTM C31	Standard Practice for Making and Curing Concrete Test Specimens in the Field
ASTM C33	Standard Specification for Concrete Aggregates
ASTM C39	Standard Test Method for Compressive Strength of Cylindrical Concrete Specimens
ASTM C94	Standard Specification for Ready-Mixed Concrete
ASTM C150	Standard Specification for Portland Cement
ASTM C172	Standard Practice for Sampling Freshly Mixed Concrete
ASTM C174	Standard Test Method for Measuring Thickness of Concrete Elements Using Drilled Concrete Cores
ASTM C309	Standard Specification for Liquid Membrane-Forming Compounds for Curing Concrete
ASTM C595	Standard Specification for Blended Hydraulic Cements
ASTM C1077	Standard Practice for Agencies Testing Concrete and Concrete Aggregates for Use in Construction and Criteria for Testing Agency Evaluation
ASTM D3665	Standard Practice for Random Sampling of Construction Materials

END OF SECTION P-307MR